2017-04-25

# Multi-Material Metal Casting: Metallurgically Bonding Aluminum to Ferrous Inserts

Carl Soderhjelm
*Worcester Polytechnic Institute*

# Multi-Material Metal Casting:
# Metallurgically Bonding Aluminum to Ferrous Inserts

by

Carl Soderhjelm

submitted to the Faculty in partial fulfillment of the requirements for the degree of

Doctor of Philosophy

in

Materials Science and Engineering

at the

Worcester Polytechnic Institute

April 2017

APPROVED:

_____
Diran Apelian
Alcoa-Howmet Professor of Engineering
Thesis Advisor

_____
Richard Sisson
George Fuller Professor of Mechanical Engineering
Materials Science and Engineering Program Director

# Table of Contents


Abstract ..... 3
Acknowledgements ..... 4
Executive Summary ..... 5
**1. Motivation** ..... 5
2. Bonding during Multi-Material Metal Casting ..... 5
2.1. Mechanical Bond ..... 5
2.2. Metallurgical Bond ..... 6
3. Why Metallurgical Bond? ..... 7
**4. Problem Statement** ..... 7
4.1. Challenges ..... 7
5. **Approach** ..... 8
**6. Experimental Work** ..... 9
6.1 Liquid-solid interaction between mild steel, A356 and 390 ..... 9
6.2 The influence of silicon during liquid-solid diffusion of aluminum and iron ..... 10
6.3 Effect of thermal treatments on the metallurgical bond ..... 10
6.4 Effect of coatings on the metallurgical bond formation ..... 11
**7. Conclusions** ..... 11
7.1. A Practical Guide to Multi-Material Metal Casting ..... 13
**8. Recommendations for Future Work** ..... 14
Appendix A – Literature Review ..... 15
Appendix B – Liquid-solid interaction between mild steel and A356 and 390 ..... 44
Appendix C – The influence of silicon during liquid-solid diffusion of aluminum and iron ..... 50
Appendix D – Effect of thermal treatments on the metallurgical bond ..... 75
Appendix E – Effect of coatings on the metallurgical bond formation ..... 94
Appendix F – A Practical Guide to Multi-Material Metal Casting ..... 112

# Abstract

Properties of cast aluminum components can be improved by strategically placing ferrous inserts to locally improve properties such as wear resistance and stiffness. A cost-effective production method is to cast-in the insert using the solidification of the molten aluminum as a joining method. Metallurgically bonding between the metals could potentially improve both load and heat transfer across the interface. The metallurgical bond between the steel and the aluminum has to be strong enough to withstand stresses related to solidification, residual stresses, thermal expansion stresses, and all other stresses coupled with the use of the component. Formation of a continuous defect free bond is inhibited by the wetting behavior of aluminum and is governed by a diffusion process which requires both energy and time. Due to the diffusional nature of the bond growth in combination with post manufacturing heat treatments defects such as Kirkendall voids can form.

The effect of aluminum alloying elements during liquid-solid bond formation in regards to microstructural changes and growth kinetics has been described. A timeframe for defect formation during heat treatments as well as microstructural changes has been established. The effect of low melting point coatings (zinc and tin) on the nucleation of the metallurgical bond has been studied as well the use of a titanium coating for microstructural modification. A set of guidelines for successful metallurgical bonding during multi-material metal casting has also been constructed.

# Acknowledgements

First and foremost, I want to express my sincere gratitude to my advisor Diran Apelian. His guidance kept me focused, his encouragement kept me persistent, his trust allowed me to learn from my mistakes, and his input inspired critical thinking which truly raised the quality of my work. As a friend, colleague, and advisee, I truly appreciate all our stimulating conversations during my time as a student at WPI, and they have been invaluable for the completion of this thesis.

I also wish to thank Prof. Sisson, Prof. Makhlouf, Prof. Brody, and Prof. Mishra for their help throughout this time, be it in the classroom or during conversations their eagerness to answers to questions or offer advise helped progress this thesis.

I want to thank the ACRC and its consortium members for the opportunity for me to work as a research assistant on the Multi-Material Metal Casting project. I specifically want to thank Lin Zhang, Adam Kopper, Kevin Anderson, and Jose Talamantes-Silva for their activity and many inputs during our focus group meetings. Thank you, Christof Heisser, Jim Lagrant, Brian Began, Vijay Alreja, Randy Beals, Tim Kaiser, and Doug Hamilton for your support during this project.

The Metal Processing Institute is an inspiring place which would not be what it is without Carol Garofoli, Renée Brodeur, Maureen Plunkett, and Libo Wang. Thank you for all of your help, assistance, and friendships. I would also like to thank Rita Shilansky for her assistance and help.

I have had much help during my time as a PhD student at WPI by students that have worked with me. The over 650 samples made, that has contributed to my understanding and knowledge in this thesis, in one way or another, was partly contributed by the following; the Masters' student Federico Canali, the MQP team Alino Te, Rachel Harrison, Scott Olson, and the Masters' student Chiara Bertuccioli. A thank you to all of you, I had a lot of fun working with you, and I made great friends.

I have a lot of great friends and colleagues here at MPI and WPI that have been great for endless discussions and much-appreciated distractions which made my time here unforgettable. Among others, thank you; Aaron, Inigo, Sean, Shaymus, Theo, Yangyang, Eunkyung, Danielle, Baillie, Anthony, and Yuwei! And of course all other friends I have met during my time as a student at WPI. I would also like to take the opportunity to thank all of my brothers back at home who made my vacations all the more enjoyable.

It should also be mentioned that I would not be here if it were not for the unconditional support of my parents and my sisters. My parent's hard work in making me who I am gave me the opportunity to work with something I love.

Lastly, but most importantly, I thank my wife, Pamela, for her love, patience, understanding, and encouragement in this endeavor. Without her support, help and confidence in me this would not be possible.

# Executive Summary

## 1. Motivation

The increasing temperatures in the atmosphere have sparked a race to reduce the carbon dioxide footprint of our way of life. To accomplish this in the required timeframe new regulations are pushing the automotive industry to reduce the $CO_2$ emissions of motor vehicles. To improve efficiency of a motor vehicle, three principal strategies can be employed;

- Weight Reduction
- Improving Powertrain Efficiency
- Reducing Friction

Reducing weight without compromising safety and comfort is generally achieved by moving from a heavier material to a lighter material to the extent for which it is both financially and technically viable. The Carnot cycle states that to improve the efficiency of the engine, it need to operate at higher temperatures and pressures. The friction of the car towards the environment can be improved by optimizing the aerodynamics as well as reducing the friction between the tires and the ground.

For many of the metal components, weight reduction can be achieved by switching from ferrous alloys to aluminum. It is lightweight, corrosion resistant, superior specific strength, and cheap relative to other lightweight metals. However, aluminum does not have the necessary stiffness for certain components, and its strength properties deteriorate at elevated temperatures. This means that two strategies for decreasing the carbon footprint of the car collides. To increase the efficiency of the powertrain requires higher temperatures and pressures, and we want the engine lightweight to reduce its fuel consumption even more.

A powerful technique is to create hybrid or bimetallic structures, so the majority of the component is manufactured out of aluminum and locally reinforce a crucial section of the component using steel. The component will act as a bimetallic composite which allows for a lightweight component with the required strength at the necessary locations. An efficient production method to produce this bimetallic structure for cast components is to place the reinforcing insert in the mold and cast the aluminum around it creating a multi material metal cast component.

## 2. Bonding during Multi-Material Metal Casting

A chain is only as strong as its weakest link which means that the integrity of the dissimilar metal component is dependent on the bond between the two metals. If the bond is weak, the load cannot be transferred between the two metals which will result in failure of the component. There are two types of bonds that can form during multi-material metal casting, a mechanical bond, and a metallurgical bond.

### 2.1. Mechanical Bond

Mechanical bond forms after and during solidification of the liquid aluminum as the casting starts to cool. The difference in thermal expansion causes the aluminum to shrink at a faster rate compared which creates pressure on the insert holding it in place. This type of bond is common and necessary for the structural integrity of the bimetallic component. The mechanical bond is commonly referred to as interference fit or shrink fit.

## 2.2. Metallurgical Bond

Metallurgical bond forms when diffusion between the metals occur and chemically interact. The interaction between the insert and the casting creates a material bridge across the interface, and the type of bond formed will depend on the material used. If the metals have solid solubility, a solid solution metallic bond can form but the case of aluminum and iron the solid solubility, see Figure 1, is very low and brittle intermetallic compounds (IMCs) will form at the interface, see Figure 2.

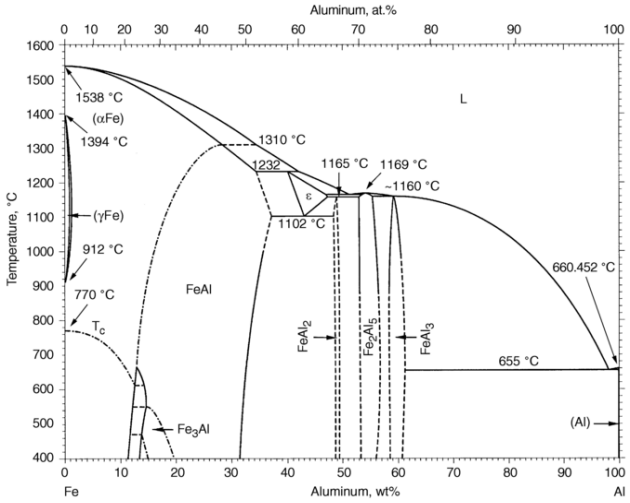


*Figure 1: Binary phase diagram for iron and aluminum.*

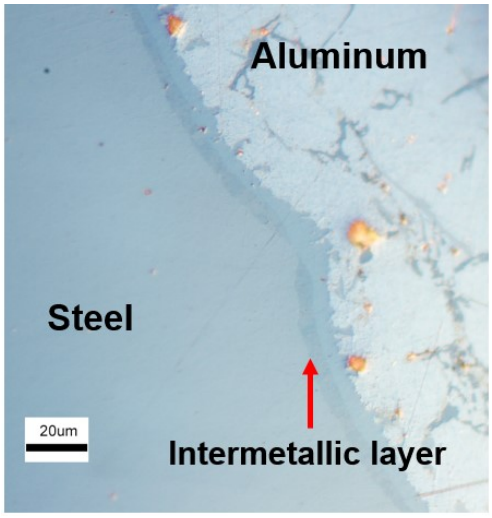


*Figure 2: Metallurgical bond between A356 and a 1015 mild steel.*

This thesis is focused on the formation of a metallurgical bond during the liquid-solid interaction of aluminum and steel. The growth of the bond is in broad terms considered to be reactive diffusion and and can be either diffusion or reaction controlled. During the former the transport of atoms by diffusion is slow and thus determines the growth rate. If the growth is reaction controlled the formation of the intermetallic compounds is the rate determining step. The nucleation of the intermetallic compounds at the interface of a Al-Fe liquid-solid diffusion couple is considered to be reaction controlled with fast reaction rates so it is considered to be instantaneous while the overall growth of the reaction layer tends to be diffusion controlled. In the case of Al-Fe, according to the phase diagram, see Figure 1, the

following phases should be present during reactive interdiffusion at 675°C between aluminum and iron; Al/$Al_3Fe$/$Al_5Fe_2$/$Al_2Fe$/AlFe. However, only $Al_3Fe$ and $Al_5Fe_2$ forms which is due to the fast growth the $Al_5Fe_2$ phase and slow formation and growth rate of the $Al_2Fe$ phase.

There are certain characteristics of the Al-Fe system that allows for the formation and growth of the reaction layer. The solid solubility of aluminum is low in iron which initiates the formation of the intermetallic compounds. The second characteristic is that the solubility of iron in the liquid aluminum is relatively low which prevents excessive dissolution of iron from the intermetallic compounds to the liquid aluminum. For which large difference in melting point is generally a requirement.

The following steps were identified as mechanisms that influence the bond formation:

- Wetting – The melt comes in contact with the aluminum and needs to wet the surface to provide an intimate contact for any bond to form.
- Heat transfer – (If the insert is at a lower temperature) Once the aluminum is in contact with the steel heat will be transferred from the hot melt to the cold steel.
- Nucleation – Once the steel reaches a certain temperature intermetallic compounds starts to nucleate on the surface. This step is reaction controlled(fast).
- Growth – As the intermetallic nuclei thicken they start to grow by aluminum diffusing in and iron out. This step is diffusion controlled(slow).

# 3. Why Metallurgical Bond?

***A continuous metallurgical bond will provide very close and intimate contact between the two metals.*** This continuous contact the two metals improves the load transfer between the two metals and the complexity of the ferrous insert can be reduced. Viala et al. [Viala 2002] managed to reduce the weight of a steel insert in a suspension part by 36% by metallurgically bonding it to the aluminum.

The absence of any space between the steel and aluminum also allows for all thermal conductivity to proceed through conduction through a solid instead of conduction and radiation through a gas. This could substantially improve the overall thermal conductivity of the component.

# 4. Problem Statement

Casting aluminum around a solid ferrous alloy insert achieving a continuous metallurgical bond across the bimetallic interface. A metallurgical bond without gaps and cracks will improve bond properties such as mechanical strength and heat transfer. The bond has to be robust enough to withstand stresses related to solidification, residual stresses, thermal expansion stresses, and all other stresses coupled with the use of the component.

## 4.1. Challenges

Using casting as a joining method is different from the traditional methods. There is a limited amount of energy and time available for bond formation to occur. To yield a defect free continuous bond, it is necessary for the melt to completely wet the surface of the insert and for the reaction to start occurring immediately. The formation of iron aluminides is an exothermic reaction, but several studies have shown that a continuous bond without any surface engineering is not easy to form during the solidification of the cast component. For insert casting to be a competitive and viable option for the automotive industry, there is a need to be able to form this bond using casting processes, like permanent

mold and high pressure die casting, which have a very high solidification rates. This restricts the time available for the bond to form.

The strength of the bond generally decreases with the thickness of the brittle layer and the poor thermal conductivity of intermetallic compounds requires careful control of their growth kinetics. During heat treatments of these components, there is a tendency to form Kirkendall voids in and around the interface which results in poor performance of the final component.

Aluminum and iron have different coefficients of thermal expansion which causes residual stresses during cooling or subsequent heat treating that are required for most aluminum casting alloys.

# 5. Approach

Understanding the limitations and possibilities of this technique is crucial for its implementation. It is important to know the suitability of each casting process for metallurgically bonding the insert to the aluminum casting. For the design of a casting procedure and process to allow for a continuous metallurgical bond to be formed the following needs to be understood and determined:

- Thermodynamics
- Kinetics
- Energetics

The thermodynamics describe what will form, whereas the kinetics dictate how fast it is formed, and the energetics inform us as to how much can be formed during the casting procedure. It is also imperative to understand the entire lifecycle of the metallurgical bond, from manufacturing, heat treatment, and end use of the component.

Initial exploratory experiments, a literature review, see **Appendix A**, and industrial applicability indicated a couple of restrictions that had to be considered:

- Metallurgical bond formation needs to be initiated during the casting procedure when liquid aluminum is in contact with the ferrous alloy. The difference in thermal expansion causes the aluminum to expand faster, and during post heat treatment steps this could cause the surface to separate and prevent diffusion. The cause of this is likely due to the difference in cooling and heating rates during processing. If cooling rates are faster after casting the internal residual stress will be higher, and if the heating rate upon subsequent heat treating is slower there will be a relaxation of residual stress, and the expansion will cause the interface to separate.
- Die soldering during high-pressure die- and permanent mold casting is a big concern due to expensive repairs of the dies and tools which add limitations to the techniques that can be applied to initiate the bond.

There can be significant residual stresses within a bimetallic casting due to the difference in thermal expansion of the two metals. The influence and formation of these stresses have not been the focus of this thesis while they seem to influence the results in certain experiments, see **Appendix D**.

Several experiments were carried out to learn and characterize the system in the form of thermodynamics, kinetics, and energetics which will be described in the next section.

# 6. Experimental Work

## 6.1 Liquid-solid interaction between mild steel and A356 and 390

The purpose of this experiment was to measure the kinetics of the reaction layer that forms between A356 and 390, and to try to relate the characteristics of the microstructure to the kinetics of the bond growth. Mild steel rods were dipped in liquid aluminum alloy for times between 10 and 300 seconds at three different temperatures to allow for a reaction to form and grow. It is also known that the surface roughness of a substrate can affect the wetting so three different surface roughness of the steel were used for the experiments.

The results show that the growth of the metallurgical bond follows a parabolic curve and that it is diffusion controlled which is consistent with the literature, see the section on kinetics in **Appendix A**. Activation energies for the growth of the bond was measured and the values for A356 corresponds well with literature while 390 indicated a negative activation energy (slower growth at higher temperatures). The results also indicated that the surface roughness could affect the results, for example for A356 surface roughness changed the calculated activation energy. Microstructural characterization of the bond formed between A356 and the mild steel also corresponded well with literature while experiments with 390 have previously not been published the formed bond was characterized using electron backscatter diffraction. The results also indicated that the microstructure changes depending on the cooling rate which also corresponds well with what has been shown previously in the literature.

A more detailed summary of these experiments can be seen in **Appendix B** which was published in La Metallurgia Italiana, see "Soderhjelm, C., Apelian, D., (2016) "Metallurgical bonding between cast-in ferrous inserts and aluminum," La Metallurgia Italiana, 6, 93-100.", and presented at High Tech Die Casting 2016 conference in Venice Italy.

Several conclusions can be drawn from the results of these experiments.

- The growth curves for the high silicon content alloy indicate diffusion controlled process, but negative activation energies show slower growth at elevated temperatures. This is contradictory since diffusion speeds up with temperature. It was suggested that this behavior is due to increased dissolution of iron to the melt.
- The microstructure that is characterized is necessarily not the microstructure that grows during liquid-solid reactive diffusion. This can influence kinetics data since the reported time does not correspond to that specific temperature as well as the phases that are considered to be in equilibrium during growth. It also suggests that there can be significant growth and microstructural change at solid-state temperatures.
- Initiation of a continuous metallurgical bond is slow and will take up to 2 minutes.

Based on this experiment three new experiments were designed to further investigate the basic mechanisms behind the conclusions and to answer the following questions:

- How does the silicon concentration in the liquid influence of silicon on growth kinetics and the effect of silicon on dissolution? See Appendix C.
- What microstructural changes are accompanied by heat treatment of bimetallic castings? How does solid-state diffusion affect growth rate? See *Appendix D.*
- Why is the nucleation of the metallurgical bond is slow? Is it due to slow reaction rates or poor wetting of the substrate? See Appendix E

## 6.2 The influence of silicon during liquid-solid diffusion of aluminum and iron

It is well known that additions of silicon reduce the thickness of the reaction layer formed with iron. However, the mechanism behind the behavior is still being discussed in the literature for a more detailed explanation please see the literature review in **Appendix A**.

The purpose of this experiment was to investigate the effect of Si on the liquid-solid interaction of aluminum and iron, more specifically bridging the gap between microstructure and kinetics of the intermetallic layer growth. Liquid-solid diffusion couples were prepared by dipping a mild steel in liquid aluminum alloy with a silicon concentration ranging from 0 – 15 wt.% for diffusion times ranging between 5 – 180 minutes. Although the diffusion time is not representative of a casting process it is necessary for theoretical considerations and the formed microstructure may also depend on time.

The results show that Si reduces the growth rate of the reaction layer by two major mechanisms; there is change in diffusion rates within $Fe_2Al_5$ layer due to a change in crystal cell size and the Si increases the saturation limit of Fe in the liquid aluminum causing an increase in dissolution. The diffusion couples form a stationary growth microstructure that corresponds to diffusion paths within the ternary Al-Fe-Si phase diagram.

The details of the experiments can be seen in **Appendix C** and are in preparation for submission for publication.

## 6.3 Effect of thermal treatments on the metallurgical bond

It is well known that joints of dissimilar metals experience Kirkendall voids due to the difference in the diffusion coefficient of the atomic species. Joints between aluminum and iron are no different, and solid-solid diffusion tends to create a different microstructure compared to liquid-solid diffusion. In literature, the most investigated Al-Fe joint of interest is mild steel bonded to A356. The fast diffusion of aluminum creates voids at the bond/aluminum interface.

The purpose of this experiment was to investigate the behavior two different alloys in the form of castings with the intent to investigate microstructural changes, growth kinetics, and Kirkendall porosity formation during isothermal holding. Two alloys were chosen, 390 and an Al-Mg-Zn alloy with high magnesium to zinc ratio that is being developed by the Advanced Casting Research Center. The intent was to try to slow down the diffusion of aluminum by changing the microstructure. It was shown in **Appendix B** that 390 exhibits a different microstructure with multiple ternary Al-Fe-Si intermetallic phases and Al-Mg alloys are known for their tendency for die soldering.

The growth kinetics of the liquid-solid interaction was measured and characterized by hot-dip experiments. Small bimetallic castings were made by dipping the insert in the liquid alloy for 2 minutes and then quickly transferring it to the mold and casting aluminum around it. The bimetallic castings were then placed in a furnace for two types of heat treating. A high-temperature heat treatment at the alloys solutionizing temperature and a low-temperature heat treatment to simulate either use at elevated temperatures or the aging temperature.

The results show that there are changes to the microstructure after high-temperature thermal treatment while low temperature indicated no significant change for the 390 alloy but only minor changes for the Al-Mg-Zn alloy. There is significant damage to the metallurgical bond due to porosity formation for the Al-Mg-Zn alloy after less than 8 hours of isothermal holding at 430°C. While minor porosity at the aluminum/bond interface started to form between 4 – 8 hours of holding for the 390 samples. The Al-

Mg-Zn samples started to show porosity formation after 24 hours of heat treating at 180°C while no noticeable change was discovered for 390 after 870 hours.

The details of the experiments are documented and given in **Appendix D** and are being prepared for publication.

### 6.4 Effect of coatings on the metallurgical bond formation

The metallurgical bond can be hard to form during the casting procedure. In fact, there is no source in literature that managed to induce a continuous metallurgical bond without any form of insert interface engineering. The cause for this is often considered to be due to poor wetting of liquid aluminum on steel, but the wetting angle of an Al-Si alloy on steel has been measured to be 59° which is considered a partially wetted substrate. The presence of oxides is known to reduce this angle and can also act as diffusion barriers.

The purpose of this experiment was to investigate the efficiency of three metallic (Zn, Sn, and Ti) coatings on the metallurgical bond formation between a coated mild steel and liquid aluminum alloy. A metallic coating such as Zn or Sn is interesting due to that it is sacrificial nature and that there is a relatively high tolerance for these in the aluminum alloy specifications. While a titanium coating is of interest due to the stability of the titanium aluminides which could prove to be more stable compared to the ternary Al-Fe-Si phases that tend to form Kirkendall porosity during subsequent heat treatment of the bimetallic casting.

Hot-dip zinc and tin coated steel samples were prepared and characterized. The coated samples were submerged into liquid A356 at 700°C for aluminum for 1, 3, 5 seconds and carefully removed and quickly quenched in water to investigate the wetting and metallurgical bond formation for short reaction times. Cold-sprayed Ti coated steel was cleaned from titanium oxide and submerged in pure liquid aluminum and A356 alloy at 700°C for different periods of times ranging from 30 seconds to 15 minutes to map the progression of the metallurgical bond.

Zinc and tin coatings show a very fast initiation of the metallurgical bond. The zinc coating shows that a continuous metallurgical bond has formed after 5 seconds of reaction time while the tin coating exhibits a similar bond after 1 second of reaction time. The progression of the reaction seems to be as follows; as the liquid aluminum comes in contact with the coating, it melts and mixes in and instantly reacts with the steel. The titanium coating shows a very slow initiation for the formation of the metallurgical bond and the results suggests that this is mainly due to the presence of oxide films. There are also indications that titanium efficiently slows down the diffusion of aluminum.

The details of the experiments are given in **Appendix E** and are to be submitted for publication.

## 7. Conclusions

The formation of the metallurgical bond during multi-material metal casting as previously mentioned requires four steps; wetting, heat transfer, nucleation, and growth. The conclusions of this work will be presented with respect to these steps.

**Wetting**

Consistently hot-dip experiments of steel into liquid aluminum indicate poor and only partial wetting for short reaction times. Wetting in systems like Al-Fe are under the label reactive wetting in literature

and one of their characteristics is that the wetting angle changes with time as the reaction progresses. The wetting is also strongly influenced by the presence of contaminates like oxides, iron and aluminum. This means that to optimize wetting both the presence of iron and aluminum oxide needs to be minimized.

The iron oxides are relatively easy to manage at low temperature but the aluminum melt front will always be covered in an oxide. Zinc and tin proved efficient in initiating a metallurgical bond by removing the need for wetting the steel. Aluminum melted the coating, mixing occurred, and the strong affinity of aluminum and iron initiated a reaction. For many reasons, there is a need to preheat the ferrous insert. The low melting point coating does not allow for high temperature preheating due to their low melting points. If these are preheated the process becomes time dependent due to oxide formation on the coated sample which could significantly change their effectiveness.

The results show that without proper flow of aluminum around the insert there is a tendency for macro segregation of the coating material around the insert. Segregation of the low melting point metals could cause insipient melting in regions around the insert.

**Heat transfer**
The heat transfer between the liquid aluminum and steel was not actively studied here there are no indications that the heat transfer is a rate limiting step in the formation of the metallurgical bond. There are however other considerations necessary in more complicated castings than what has been produced during these studies. The metallurgical bond could change the heat transfer coefficient between the steel and the aluminum which could affect solidification patterns in castings.

**Nucleation of the metallurgical bond**
The nucleation of the bond is instant upon contact with the steel which was shown using the tin coating. This indicates that there is not a lack of energy for the initiation of the metallurgical bond, it is a problem of wetting.

**Growth of the intermetallic layer**
The growth rate of the metallurgical bond depends on the composition and temperature. Liquid-solid diffusion couples between aluminum alloys and steel tend to form a stationary microstructure that are related to diffusion paths within the phase diagram. This can be utilized to predict a microstructure that forms for metallurgical bonds between ferrous alloys and different aluminum alloys. The stationary microstructure is time dependent and can take time to form. The microstructure of the metallurgical bond can and is likely to change during cooling.

There seems to be a distinct difference between solid-solid and liquid-solid diffusion due to different rate controlling mechanisms. During liquid-solid diffusion the diffusion of iron out of the steel determines the growth rate while during solid-solid diffusion the diffusion across the aluminum/bond interface appears to be rate controlling.

The results show that the growth rate will be determined by the diffusion of iron out from the steel through the intermetallic layer and the dissolution rate. This has certain implications for engineering applications. For example, the thickness of the reaction layer could be reduced by changing the diffusivity of iron in the steel. It will also prevent and reduce bond formation but by for example the steel surface could be decarburized to allow for the initiation of the bond but later restrict its growth.

Silicon reduces the growth rate of metallurgical bond by two mechanisms. It changes the cell parameters of the $Fe_2Al_5$ phase and increases the dissolution rate. There is a desire to keep the dissolution rate low and the intermetallic layer thin which could be important considerations during alloy selection.

A timeline for the formation of Kirkendall porosity was established and aluminum the faster diffuser. There is therefore a need to interracially engineer the metallurgical bond to reduce the diffusion rates of aluminum. Titanium seems to be a suitable element for slowing down diffusion of aluminum but the coating design needs to be optimized. There is also a difference in the location of the formed porosity in the solid-solid diffusion couples depending on shape and volume. This is likely due to the difference in thermal expansion which makes this process dependent on the system size. There is also damage due to oxidation along the metallurgical bond which would require engineering solution before being applied industrially.

### 7.1. A Practical Guide to Multi-Material Metal Casting

As part of the "Multi-Material Metal Casting" project for the Advanced Casting Research Center (ACRC) new testing methods for the metallurgical bond strength molds were designed for producing these specimens. The design of the samples and molds were revealing in the sense that many practical issues were faced and had to be attended to. **Appendix F** outlines the different challenges and also describes the pitfalls that could be of practical value for successful metallurgical bonding during multi-material metal casting. A summary of the practical guidelines are as follows:

1. *Component and Casting Design* – The metallurgical bond should in the extent possible be cast-in so it is surrounded by aluminum to prevent failure along the brittle intermetallic layer.

2. *Mold Design* –
    - Melt flow – Generally, higher flow rate is better around the insert to promote bond formation and to remove any eventual coating residues.
    - Heat transfer – The volume ratio of insert to mold cavity will determine the amount of heat available for bond formation and thus should rather be lower than higher. There can be only one solidification front to avoid formation of counterproductive residual stresses.

3. *Insert Design* – Large complex insert could be difficult to predict the behavior during heat treatment in manners of both diffusion within the metallurgical bond and distortions due to difference in thermal expansion. The edges of the insert need to have a curvature to prevent crack initiation and propagation.

4. *Materials Selection* –
    - Aluminum alloy – Should be selected to have a higher ductility than the ferrous alloy and should preferably not require extensive heat treatments. Composition of the aluminum alloy can change the thermal stability of the bond.
    - Ferrous alloy – Should have greater stiffness and strength than aluminum to maximize the benefits of the bimetallic component. The composition of the ferrous alloy can change the growth of the metallurgical bond.

5. *Coatings* – The coating is necessary to form a defect free continuous metallurgical bond and needs to be selected based on the casting process.

6. *Machining* – The metallurgical bond is brittle and it is not recommended to machine the components in a manner where it is completely exposed.

## 8. Recommendations for Future Work

The biggest challenge for industrial deployment is that the process of metallurgical bonding during casting that it is dependent on the size of the system it forms in. Variables that differ from casting to casting are and can impact the formation of the bond are:

- *Casting process* – Casting processes have very different solidification time which can affect both the thickness and microstructure of the bond.
- *Cavity size* – Similar to the previous point, a bigger cavity has longer solidification times.
- *Melt flow patterns* – More flow generally implies more heat input for the bond to grow. If there is excessive flow around the insert dissolution can increase which changes both the dimension of the insert and iron impurities are introduced in the casting.
- *Solidification patterns* – Depending on the preheating temperature of the insert the solidification patterns can change in a casting and if not designed properly can deteriorate the properties.

A robust method for designing for multi-material metal casting is required.

# Appendix A

# Literature Review

# Table of Contents

1. Kinetics and Microstructure of Liquid Aluminum and Iron ..... 17
1.1 Aluminum – Iron ..... 17
1.1.1 Intermetallic layer constituents ..... 17
1.1.2 Growth rate ..... 19
2. Kinetics and Microstructure of Liquid Aluminum and Iron ..... 25
2.1. Aluminum-Silicon alloys – Steel ..... 25
2.1.1. Intermetallic layer constituents ..... 26
2.1.2. Growth rate ..... 27
3. Conclusive Remarks on Kinetics and Microstructure ..... 28
4. Effect of other aluminum alloying elements ..... 29
4.1. Cu content ..... 29
4.2. Mn content ..... 29
5. Effect of insert type ..... 29
5.1. Steel ..... 29
5.2. Cast Iron ..... 31
5.3. PM Insert ..... 32
5.4. Insert preheating ..... 33
5.5. Alloying element content ..... 34
6. Coatings ..... 34
6.1. Aluminum coating ..... 34
6.2. Zinc coating ..... 35
6.3. Ni/Cu coating ..... 35
6.4. Titanium coating ..... 36
7. Patent Search for Bonding Techniques ..... 36
8. Interface strength ..... 37
References ..... 39

## 1. Kinetics and Microstructure of Liquid Aluminum and Iron

### *1.1 Aluminum – Iron*

The interest of the liquid aluminum-iron reactions system is largely due to the hot dip aluminizing steel (HDA steel) process. The surface of the steel can be covered in a thin layer of aluminum by submerging it in liquid aluminum. It will make the surface of the steel very resilient to corrosion due to excellent corrosion resistance of the surface layer of aluminum. The adherence of the aluminum layer is however dependent on how well it bonds to the steel and the bond similar to processes like hot dip galvanizing and hot dip tinning depends on the metallurgical bond that forms between the two metals. For these three processes, there is an intermetallic layer forming which determines the properties like coating adherence. Therefore, a lot of the knowledge from HDA process can be extracted and applied to the dissimilar metal casting between steel and aluminum.

#### *1.1.1 Intermetallic layer constituents*

The major constituent in the intermetallic compound layer is the η-phase ($Fe_2Al_5$) which was identified by Gebhardt and Obrowski in 1953 [1]. It was later shown that there was a thinner additional θ-phase ($FeAl_3$) layer forming close to the aluminum discovered using TEM by Eggeler et al. [2]. After the identifications, there has been numerous articles regarding the crystal structure and orientation of the intermetallic constituents. The $Fe_2Al_5$ is easly identified in light optical microscopy due to its characteristic tongue (saw-tooth morphology) like appearance, see Figure 3.

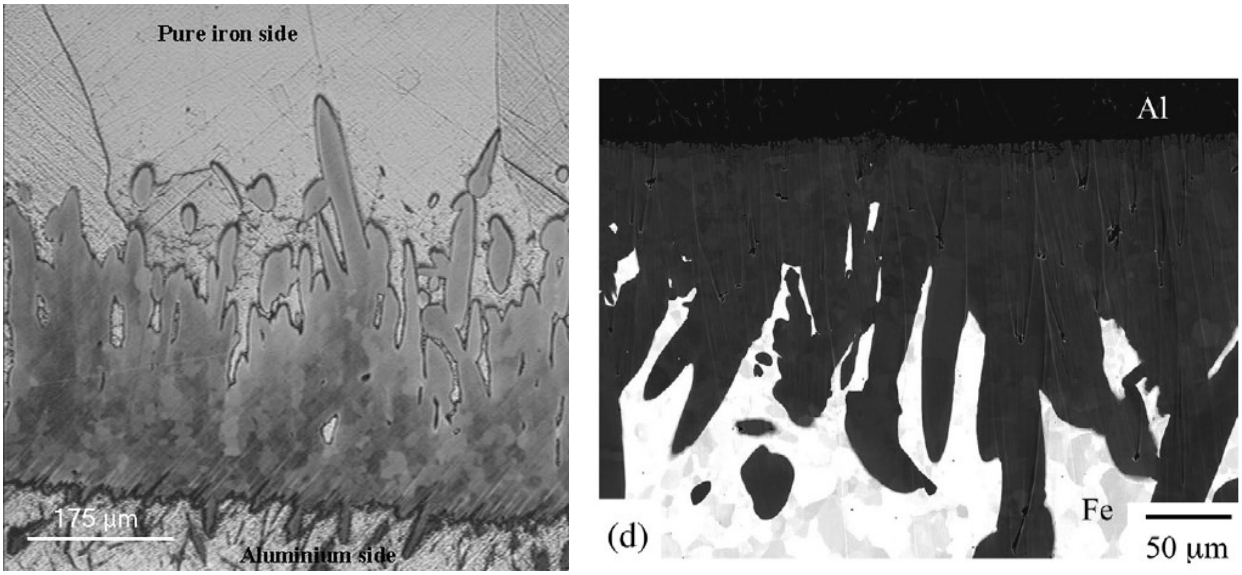


*Figure 3: Left: optical micrograph of the intermetallic layer[3]. Right: SEM micrograph of the intermetallic layer[4].*

There has been many attempts to explain the characteristic tongue like appearance of the $Fe_2Al_5$ layer. Heumann and Dittrich [5, 6] suggested that due to structural vacancies along the C-axis of the $Fe_2Al_5$ crystal paved was for accelerated diffusion in these directions [7, 8]. This theory is what has been accepted by many authors as an explanation to the tongue like morphology [3, 9-11].

Kwon and Lee [12] argued that the $Fe_2Al_5$ layer is unaffected by the orientation or structure of the iron and that the tongue like morphology is due to a preferred nucleation rate for certain crystallographic orientations of the $Fe_2Al_5$ crystal. It should however be noted that they did not have the proper tools to identify the $FeAl_3$ layer which could have changed their reasoning.

Based on studies of electron backscatter patterns maps Takata et al. [4] argued that the morphology of the $Fe_2Al_5$ layer is due to strains introduced in the $Fe_2Al_5$-phase during growth due to a difference in volume between the BCC iron and the orthogonal $Fe_2Al_5$-phase. If the volume expansion is anisotropic then a stress field shown in Figure 4, is possible. These strains introduce stresses at the surface of the $Fe_2Al_5$-phase which induces a vacancy flow which allows for Al atoms to preferentially diffuse fast to the tip of the tongues.

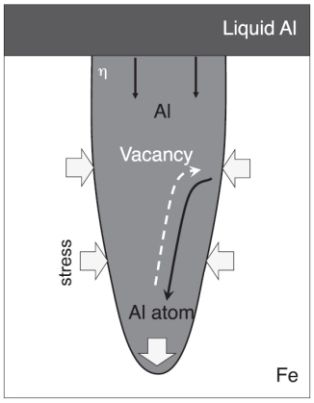


*Figure 4: Sketch of the vacancy and aluminum atom flux giving rise to the elongated structure of the Fe2Al5 phase according to Takata et al.[4].*

There has been multiple studies of the microstructure of pure aluminum reacting with either a mild alloy steel or pure iron. The typical microstructure can be seen in Figure 5 and Figure 6.

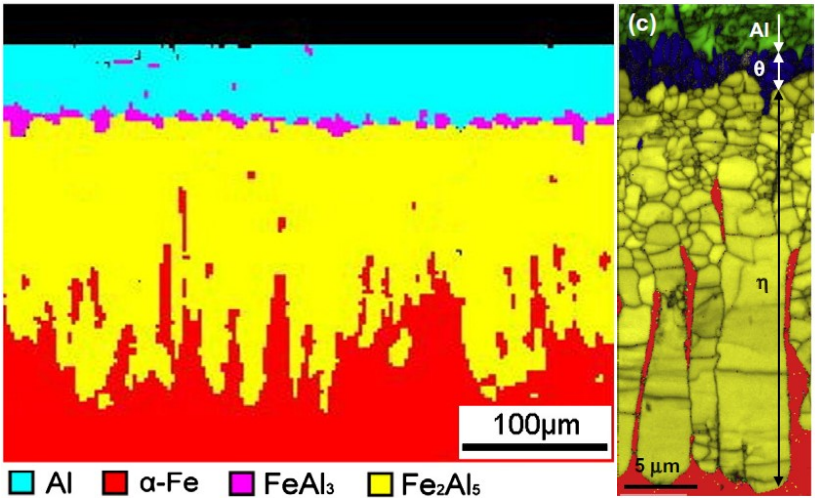


*Figure 5: Electron backscatter diffraction images of the intermetallic layer[7, 13].*

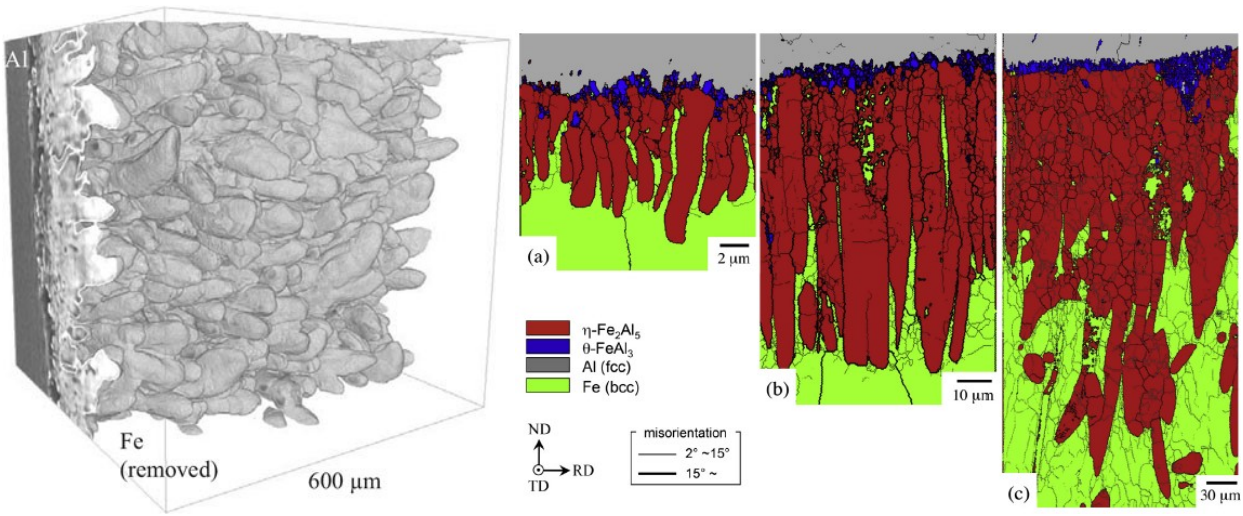


*Figure 6: Left: x-ray tomography image of the intermetallic layer showing the characteristic tongue like appearance [14]. Right: Electron backscatter diffraction image of the intermetallic layer for various dipping times[4].*

*1.1.2 Growth rate*

The first systematic study on the liquid aluminum-iron system was as mentioned earlier by Gebhardt and Obrowski [1]. Their measurements of the showed a linear relationship between the layer thickness and the reaction time. Heumann and Dittrich [5] performed similar experiments and got a linear relationship between the thickness and the square root of the reaction time which was to be expected if it is a volume diffusion controlled process.

$$d = k\sqrt{t}$$

They explained that the difference was that they measured the maximum diffusion distance while the measurements performed by Gebhardt and Obrowski only measure the mean diffusion distance.

Heumann and Dittrich also came to the conclusion that the constant k had an Arrhenius type temperature dependence.

$$k \sim e^{\frac{-\Delta H}{RT}}$$

Denner and Jones [15] did similar experiments and found that the mean thickness of the intermetallic layer has a linear relationship to the square root of time. This discrepancy they believed could be stresses introduced in the intermetallics once a certain thickness was achieved and this caused spallation of intermetallic pieces into the melt. This could explain that they noticed a deviation from the parabolic relationship at longer reaction times. In a later study, Denner and Jones [16] analyzed the growth kinetics while correcting for the dissolution of iron using the Nernst-Brunner equation and following the work by Eremenko [17-19]:

$$\frac{dc}{dt} = \frac{KS}{V}(C^S - C)$$

where C is the solute concentration at time t and S the surface area, V the melt volume, and CS the saturation concentration. K is the dissolution constant. The equation can be rewritten using the boundary at x = 0 and t= 0:

$$x = \frac{\rho_{Al} C^S}{\rho_\eta \theta} \frac{V}{S} \left[1 - exp\left(-\frac{KSt}{V}\right)\right]$$

X is the thickness of the intermetallic layer, ρ is the density for aluminum and $Fe_2Al_5$, θ is the iron concentration in the $Fe_2Al_5$ layer. Even with the dissolution correction they noticed that for longer reaction times there was a negative deviation from the dissolution corrected parabolic growth equation. They believed that this could be due to either a change in dissolution rate or spalling of the intermetallic layer. They also noticed that for higher reaction temperatures (826 °C) the $Fe_2Al_5$ layer can be thinner than for shorter times.

Yeremenko et al. [20] published a study on the effect that dissolution of iron to the aluminum melt has on the growth of $Fe_2Al_5$. With a very similar approach as Denner and Jones [16] they managed to get a good approximation of the layer thickness. Their model slightly overestimates the thickness for short reaction times and underestimates it for longer times. They claim this is due to the assumption that the rate of dissolution is assumed to be linear while more likely it is higher in the beginning and slower as the melt becomes more saturated. They suggest that the growth rate is slower for shorter time due to the random crystallite orientation of the $Fe_2Al_5$ intermetallic grows into each other and impinges the growth. Only grains with the preferred (c-axis) orientation normal to the surface can grow at maximum rate.

Eggeler et al. [9] studied the growth of the intermetallic layer in pure aluminum and iron saturated melts. They discovered that they would similarly like Denner and Jones [16] would get negative deviations from the parabolic growth curve when the steel was dipped in pure aluminum. However, they also discovered that if the steel is dipped in an iron saturated melt it followed the parabolic growth curve. So they came to the conclusion it is dissolution of iron into the aluminum melt that causes the negative deviation from the parabolic growth curve.

In 1986 Dybkov published three papers on the reaction diffusion in heterogeneous binary systems. The papers deal with systems that form one [21], two [22], and multiple [23] compound layers at the interface. The model proposed in [21] is similar to the work of Yeremenko [20] and Denner and Jones [16] but with adjustments to consider if the growth is either reaction rate controlled or diffusion controlled. For the liquid aluminum-solid iron interaction the model proposed in [22] is more suitable since there are evidently two layers forming. The model incorporates both if the growth is either diffusion limited or reaction limited, meaning that it can also take into account for different formation rates of the different intermetallics. Forming the intermetallic layers like in Figure 7 can occur by the following reactions:

$$qB + pA = A_pB_q$$

$$(sp - qr)A + qA_rB_s = A_pB_q$$

and

$$(sp - qr)B + rA_pB_q = A_rB_s$$

$$rA + sB = A_rB_s$$

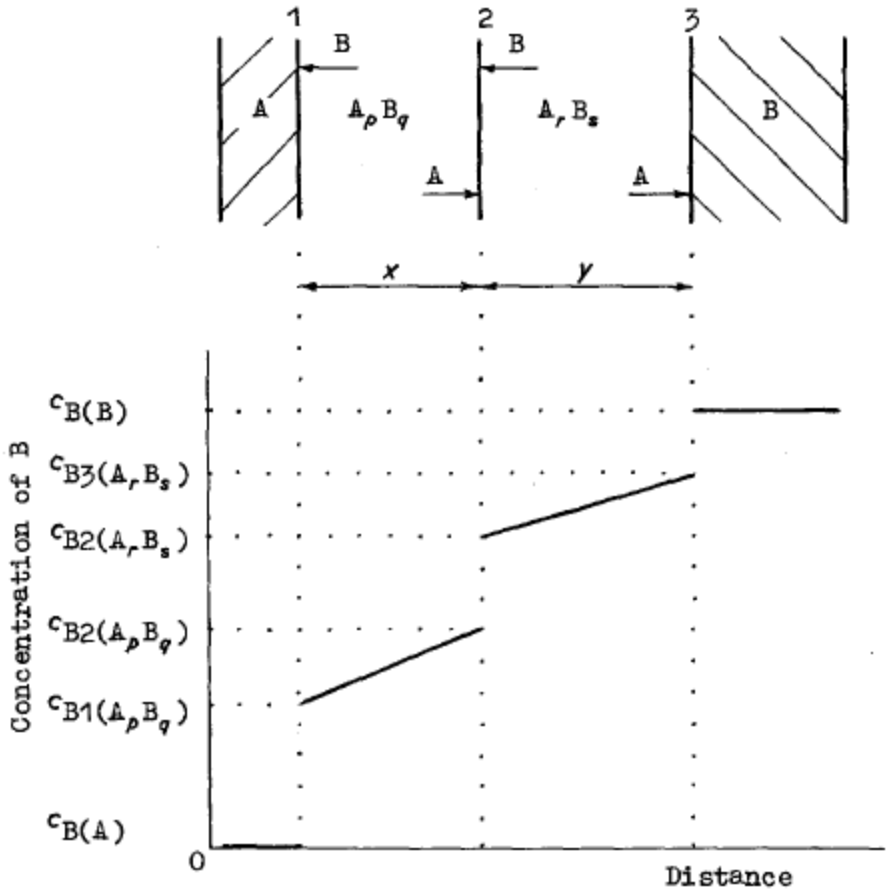


*Figure 7: Sketch of the diffusion couple[22].*

Thus each layer can be produced by two reactions and dissolved by one. So the total growth of the $A_pB_q$ for a short period of time dt can be described by:

$$dx_+ = dx_{B1} + dx_{A2}$$

Where $dx_{B1}$ is due to the reaction at interface 1 and $dx_{A2}$ due to the reaction at interface 2. From Dybkovs paper on one growth layer the following equation is derived:

$$dx_{B1} = \frac{k_{0B1}}{1 + k_{0B1}/k_{1B1}}dt$$

$k_{1B1}$ is the rate constant for reaction controlled conditions and $k_{1B1}$ for diffusion controlled and can be expressed as:

$$k_{1B1} = \frac{D_{B(A_pB_q)}(C_{B2(A_pB_q)} - C_{B1(A_pB_q)})}{C_{B1(A_pB_q)}}$$

Similarly:

$$dx_{A2} = \frac{k_{0A2}}{1 + k_{0A2}/k_{1A2}} dt$$

and

$$k_{1A2} = \frac{D_{A(A_pB_q)}(C_{A1(A_pB_q)} - C_{A2(A_pB_q)})}{C_{A2(A_pB_q)}}$$

D is the diffusion coefficient and C the concentration at the specific locations indicated by the subscript. With a similar procedure $dy_+$ and its components can be derived to these equations:

$$dy_+ = dy_{B2} + dy_{A3}$$

$$dy_{B2} = \frac{k_{0B2}}{1 + k_{0B2}/k_{1B2}} dt$$

$$dy_{A3} = \frac{k_{0A3}}{1 + k_{0A3}/k_{1A3}} dt$$

$$k_{1B2} = \frac{D_{B(A_rB_s)}(C_{B3(A_rB_s)} - C_{B2(A_rB_s)})}{C_{B2(A_rB_s)}}$$

$$k_{1A3} = \frac{D_{A(A_rB_s)}(C_{A2(A_rB_s)} - C_{A3(A_rB_s)})}{C_{A3(A_rB_s)}}$$

At the same time as growth is occurring there is also loss of thickness due to dissolution, $dx_-$ and $dy_-$ is simply the loss for the growth of the other layer:

$$\frac{m_{A_pB_q}}{m_{A_rB_s}} = \frac{rM_{A_pB_q}}{pM_{A_rB_s}} \rightarrow \frac{\rho_{A_pB_q} dx_-}{\rho_{A_rB_s} dy_{B2}} = \frac{rV_{A_pB_q}}{pV_{A_rB_s}}$$

Where M is the molecular mass and V the unit cell volume which can be rearranged to

$$dx_- = \frac{rV_{A_pB_q}}{pV_{A_rB_s}} dy_{B2}$$

And for $dy_-$

$$dy_- = \frac{qV_{A_rB_s}}{sV_{A_pB_q}} dx_{A2}$$

So the change overall thickness with respect to time of the two different compound layers can be described by

$$dx = dx_{B1} + dx_{A2} - dx_-$$

$$dy = dy_{B2} + dy_{A3} - dy_-$$

So the equations for the growth of intermetallic in two compound layers are described by:

$$\frac{dx}{dt} = \frac{k_{0B1}}{1 + k_{0B1}/k_{1B1}} + \frac{k_{0A2}}{1 + k_{0A2}/k_{1A2}} - \frac{rV_{A_pB_q}}{pV_{A_rB_s}}\left(\frac{k_{0B2}}{1 + k_{0B2}/k_{1B2}}\right)$$

$$\frac{dy}{dx} = \frac{k_{0B2}}{1 + k_{0B2}/k_{1B2}} + \frac{k_{0A3}}{1 + k_{0A3}/k_{1A3}} - \frac{qV_{A_rB_s}}{sV_{A_pB_q}}\left(\frac{k_{0A2}}{1 + k_{0A2}/k_{1A2}}\right)$$

The combination of reaction controlled and diffusion controlled growth rate that Dybkov [22] developed explains certain particularities of the liquid aluminum- iron system that cannot be explained by the diffusion theory by itself. If the process is considered to be purely diffusion controlled the phases present in the binary iron-aluminum phase diagram, see Figure 8, are expected.

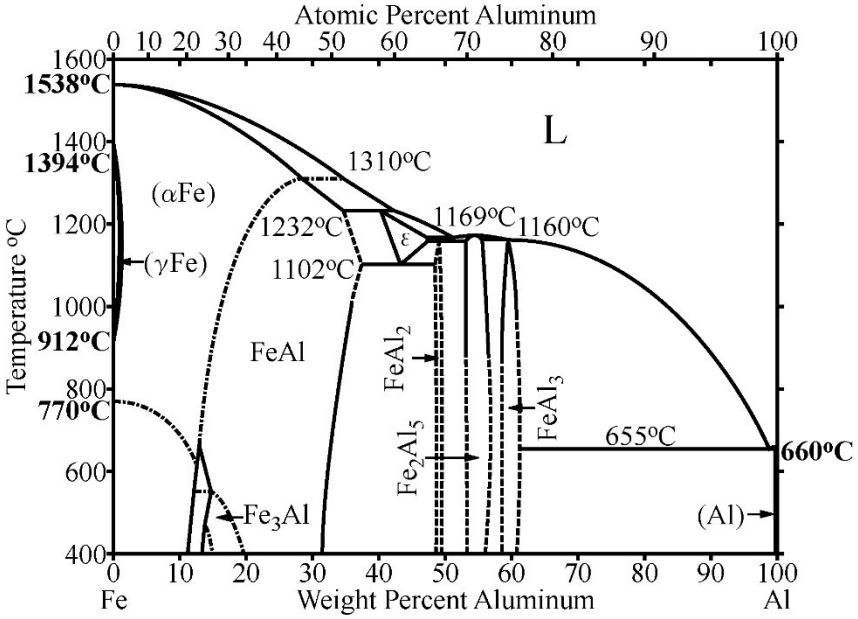


*Figure 8: Binary phase diagram for Iron and Aluminum.*

However, due to other controlling factors such as the chemical reaction rate can inhibit the formation. There are certain predictions that can be made using this theory that is of practical importance. During the very early stages of growth it can be argued that the diffusion is very fast due to the thin layers and thus the growth is predicted to be linear. The change from one diffusion to reaction controlled growth can cause deviations from what is expected to be a parabolic growth curve. For example, consider growth after relatively long periods of time, one of the layers could follow diffusion controlled growth, due to the existing concentration gradient in the intermetallic compounds, the other layer can be experiencing a reaction controlled growth, this combinations can result in a paralinear growth behavior, see Figure 9. Where line 1 is diffusion controlled and line 2 is reaction controlled. This will give the total compound layer growth a paralinear behavior.

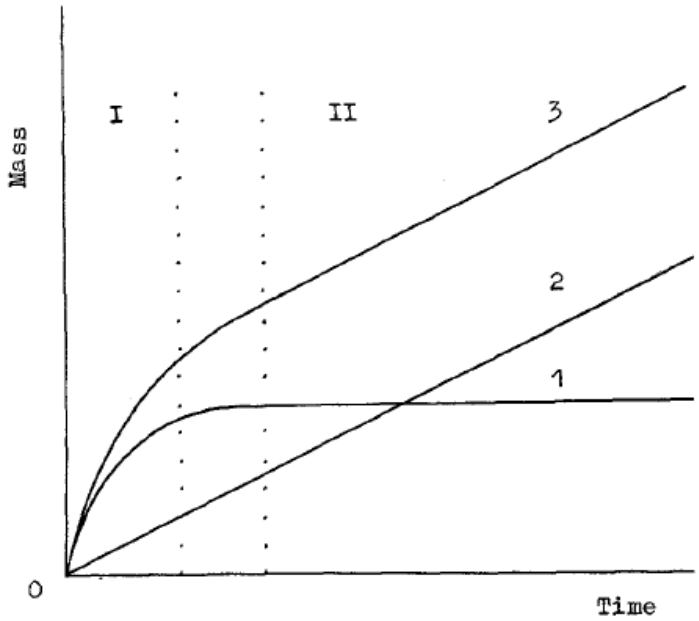

*Figure 9: Plot of the components that can form paralinear growth kinetics[22].*

In a later paper published by Dybkov [24] on the interaction between a stainless steel and molten aluminum in which the dissolution of iron, chromium, and nickel as well as the intermetallic growth rate was studied. He found that the dissolution was non-selective so they dissolve in ratios similar to the ratio in the steel meaning that the stainless steel can be considered a single element. The growth rate also supported his previous theory on the paralinear growth behavior, see Figure 9, the behavior changes from parabolic to linear. From this he makes the conclusion that these results cannot be explained, quantitatively or qualitatively, by the more simple diffusion control theory, indicating that the growth kinetics in fact are of a more complicated nature.

Bouche et al. [10] studied the growth of pure iron in contact with static pure liquid aluminum. They concluded that for short reaction times the intermetallic compound layer grows with little to no dissolution out from the initial interface at lower temperatures (700°C). While at higher temperatures (800 - 900°C) they did not find dissolution at shorter times (15s) but for longer reaction times (15 min) there was significant dissolution. The growth rate of the two intermetallic layers were of parabolic nature which is consistent with a diffusion controlled process with an exception of an initial transient period.

Shahverdi et al. [25] performed a systematic investigation similar to what Bouche et al. [10] did. Their results also showed a parabolic growth behavior but they got a better fit using 0.4 as a time exponent meaning a slight negative deviation from the parabolic growth rate. They also noticed the deviation from parabolic growth for short reaction times which they noted was likely due to the effects reaction and dissolution at the early stage of intermetallic compound formation. However, in contradiction to the paper by Bouche et al. [10] they noticed a large decrease in reaction layer thickness for samples at high temperature (900°C) for long reaction times(375s and up).

Bouayad et al. [3] performed a similar study and found that $Fe_2Al_5$ layer grows following the parabolic rate law while the outer FeAl3 layer shows a linear dependency to time. They were able to characterize the growth rate using the theories presented by Dybkov [22].

A compilation of the rate constants and activation energies from Heumann and Dittrich [5], Denner and Jones [16], Eggeler et al. [9], and Bouayad et al. [3] can be seen Table 1: Rate constants for selected temperatures and activation energies.

*Table 1: Rate constants for selected temperatures and activation energies.*

| | HEUMANN AND DITTRICH[5] | DENNER AND JONES[16] | EGGELER ET AL.[9] | BOUAYAD ET AL.[3] |
|---|---|---|---|---|
| Temperature (°C) | 700 | 771 | 800 | 800 |
| Iron purity | 99.99% | 99.78% | Mild Steel | 99.999% |
| Aluminum purity | Iron sat. | 99.99% | Iron sat. | 99.9% |
| Time exponent, n | 0.5 | 0.49 | 0.49 | 0.5 |
| Rate constant $k_1$ ($m^2/s$) | $10^{-10}$ | $5.64*10^{-11}$ | $1.394*10^{-10}$ | $9.05*10^{-11}$ |
| Activation energy, q (kJ/mol) | 155 | 76 | 134 | 74 |

*Effect of Carbon Content in Steels*

Niinomi and Ueda [26] studied the effect of different alloying elements on the intermetallic layer formation. They looked at pure Fe, Fe-3Si, Fe-3C, Fe-2C, Fe-3Cr, Fe-3Ni, Fe-3Cu, Fe-3Mn, and Fe-2Mn. They say that Cu, Ni, and Si had the greatest effect on growth rate and slowed down the growth considerably. Although both Mn and C showed a significant decrease in growth rate. While Cr were more inefficient in decreasing the growth rate it showed a greater decrease for longer reaction times.

El-Malhallaway et al. [27] performed a study on four different types of steel with varying alloying element content. If nickel, chromium, or a high carbon content is present the intermetallic layer thickness is decreased. A higher carbon content also shows a decrease in growth rate compared to a similar steel grade with lower carbon content.

Sasaki et al. [28] compared the growth rate of intermetallic layer between pure aluminum and steels with different amounts of carbon content. They were able to show that the parabolic rate constant decreased as the carbon content increased. For a low carbon steel (0.05 wt%) they noticed negative deviations from the parabolic growth at higher temperatures (800-850 °C) as well for their medium carbon steel (0.45 wt%). For their high carbon steel (0.88 wt%) there was no noticeable deviation. They also noticed less dissolution of iron with an increase in carbon content and that the rate constant k showed no decrease at carbon concentrations above 0.8%.

## 2. Kinetics and Microstructure of Liquid Aluminum and Iron

### *2.1 Aluminum-Silicon alloys – Steel*

Additions of silicon to the aluminum alloy is known to slow down the growth rate of the intermetallic layer. The intermetallic phases formed between steel and aluminum are very hard and brittle and therefore controlling the size during manufacturing of the bimetallic component can prove to be crucial. If the layer grows to thick it can have detrimental effects on the final properties of the component. It is also important to impede the growth of the intermetallic compounds if the component is used at elevated temperatures.

Intermetallic layer constituents

Eggeler et al. [29] carried out hot dipping experiments using a low alloy steels in liquid Al-2%Si alloy at temperatures of 780-792°C. They identified two binary phases the $FeAl_3$ (close to aluminum) and $Fe_2Al_5$ (close to iron) with 2% silicon in solution which is the solubility limit of silicon in the binary phases.

El-Mahallaway et al. [30] performed hot dip experiments on mild steel sheets in aluminum melts containing up to 12% Si. For a melt with 8% Si there is an outer layer (close to aluminum) of $Al_7Fe_2Si$ and with an inner layer of $Al_{20}Fe_7Si$ and $Al_{19}Fe_8Si$ containing percipitates of $Al_3Fe_2Si$.

Awan and Hasan [31] identified two intermetallic layer when studying hot dipped steels of different carbon content in melts containing up to 7% Si. They identified the $Fe_2Al_5$ phase close to the steel substrate and $Fe_3Al_{0.7}Si_{0.3}$ close to the aluminum. They explain that the $Fe_3Al_{0.7}Si_{0.3}$ phase has the same crystal structure as FeAl3 but Si takes the place of some of the Al atoms.

Cheng and Wang [32] analyzed the intermetallic layer formed between a mild steel reacting at 700°C for 3 minutes using electron backscatter diffraction. They identified an outer layer of $Al_7Fe_2Si$ with an inner layer of mostly of $Fe_2Al_5$ and some $FeAl_3$ with dispersed $(Al,Si)_5Fe_3$, see Figure 10.

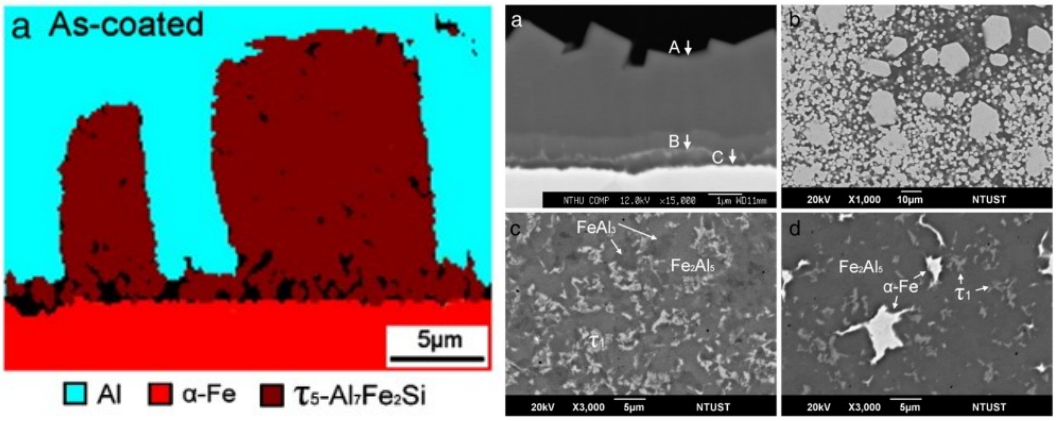


*Figure 10: Left: Figure showing the phase distrubution for the intermetallic compound layer for a silicon containing aluminum coating[32]. Right: Disperesed $(Al,Si)_5Fe_3$ in the $Fe_2Al_5$ layer[32].*

Zhe et al. [33] looked at a low carbon steel hot dip coated in A356 at 680°C for 40 seconds and then quenched. They also prepared samples that were allowed to cool inside the melt. The quenched samples consisted of a very thing intermetallic layer of $Al_{7.4}Fe_2Si$. The samples that experienced a slower cooling rate had a thin inner intermetallic layer consisting of $Fe_2Al_5$ close to the steel surface with and intermediate layer of $Al_{7.4}Fe_2Si$ and an outer layer of $Al_{4.5}FeSi$.

Springer et al. [13] analyzed the reaction layer using TEM of a mild steel coupon that was hot dipped in a 5% Si aluminum melt at 675°C for 30 seconds and air cooled. They concluded that there was an inner layer (close to steel) of $Fe_2Al_5$ with dispersed $Al_2Fe_3Si_3$, an intermediary layer of $FeAl_3$, and an outer layer of $Al_8Fe_2Si$, see Figure 11.

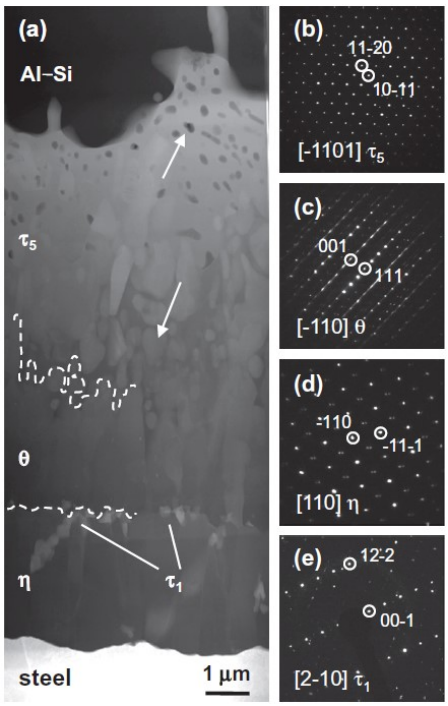


*Figure 11: TEM image with corresponding diffraction patterns for Al-5%Si alloy interacting with a low carbon steel[34].*

*2.1.1 Growth rate*

As mentioned in the above paragraph adding silicon to the aluminum melt impedes the growth of the intermetallic layer. Evaluation in literature of quantifying growth rate in aluminum-silicon alloys and ferrous substrates are the same as for pure aluminum which is discussed in section. The mechanism behind the retardation of the metallurgical bond growth rate has been debated and a few theories will be presented.

It was established by Gittings et al. [35] that alloying the aluminum with silicon reduces the reaction layer in hot dipping experiments and it has been confirmed by many others [13, 29-33, 36-46]. The literature on the mechanism behind the slow growth of the reaction layer due to the silicon in the melt is diverse. While Nicholls [36] suggests that silicon occupies structural vacancies in the formed η-($Al_5Fe_2$)-phase and thus slows down the diffusion through this layer. Lainer et al. [37] explained the slow growth by considering the ternary intermetallic compounds ($Al_xSi_yFe_z$) that form during the reaction forms much slower and thus lowers the build rate of the of the reactive layer. Komatsu et al. [38] suggested that the silicon in the melt improves the rate of iron dissolution in the aluminum melt which would explain the slower growth rate.

Eggeler et al. [29] were able to reach the conclusion that the decrease in growth rate is due to the behavioral change in the solid state, rather than the liquid. They compared the concentration iron in a melt with and without silicon and there was no difference in the dissolution rate between pure aluminum melts and melts containing silicon.

Springer et al. [47] measured the silicon concentration in the η-phase and it was expected that if the reduction in atomic mobility is due to the occupation of structural differences, then there would be a silicon concentration difference for layers grown at different rates. However, they measured the

concentration of silicon in the η-phase for intermetallics grown at different rates and could not measure a concentration difference.

## 3. Conclusive Remarks on Kinetics and Microstructure

The growth rate of metallurgical bond formation between steel and aluminum is relatively well known. Qualitatively there are several different theories on the high growth rate of Fe2Al5 during reaction between pure liquid aluminum and a solid iron substrate. However, quantitatively the results are fairly similar. The addition of silicon to the aluminum melt retards the growth rate while again the mechanism behind the retardation is argued, quantitatively the results are similar.

The initial steps during reaction is in most cases not described or are considered to have minor effects on the experiments. For example, Yeremenko et al. [20] measured the growth after 1 second interaction between the steel and the melt and concluded that nucleation is extremely fast and will have minor effects on the results. During their experiments they preheated the iron to the melt temperature by keeping it in molten flux on top of the aluminum melt.

It can also be seen for the results that there is much faster growth very early in the reaction process. This is clearly visible in the parabolic growth curves since the straight lines does not intersect with zero instead at a positive value. This could be due to that the very initial stages are not controlled by diffusion (very short distances) but instead are controlled by the for example the reaction rate [21].

If the initial nucleation and growth is either reaction or diffusion controlled they will both be dependent on temperature of both the aluminum melt and the ferrous substrate. For the reaction to proceed a certain critical temperature must be reached. During insertion of a ferrous substrate in an aluminum melt the surface will heat up relatively quickly and allow for the reaction to start.

If the wetting of the substrate is effective, then the heat transfer will be more effective, and the reaction is allowed to progress for a longer period of time. The wetting is not only crucial for the heat transfer it is also a requirement for any chemical interaction between the two metals.

The temperature in the reaction zone will determine the kinetics of the controlling processes, nucleation, growth, and dissolution. Therefore, parameters that directly controls the temperature surrounding the insert have an effect on the kinetics of formation. As a result, every casting will interact differently with the insert. The size and shape of the melt will together with melt flow will determine the energy distribution around the insert. If the insert is large relative to the surrounding melt it will absorb more energy and less can be used for bond formation. The initial temperature of the insert can also have major effects on the final results. If it acts as a chill and solidification is premature then a gap can form between the ferrous insert and the aluminum.

The bond formation can be seen to follow some steps. Once the melt is in contact with the insert it needs to wet the surface. Upon contact with the surface there is a heat transfer step where the heat flows from the hot melt to the cold insert. At the required reaction temperature, the intermetallic compounds will start to form. Once the first compounds are formed diffusion is needed to continue the growth of the metallurgical bond, see Figure 12.


*Figure 12: Steps in the metallurgical bond formation.*

**4. Effect of other aluminum alloying elements**

*4.1 Cu content*

Yousaf et al [48] studied the aluminizing process of steel in an aluminum 11% copper alloy. They came to the conclusion that the addition of 11% copper reduces and changes the morphology of the intermetallic layer. The reduction in thickness is attributed to the formation of intermetallic phases, $Al_2Cu$ and $Al_7CuFe$ on the outer coating of the steel. Figure 13 shows the change of morphology of the intermetallic layer for alloys with copper.

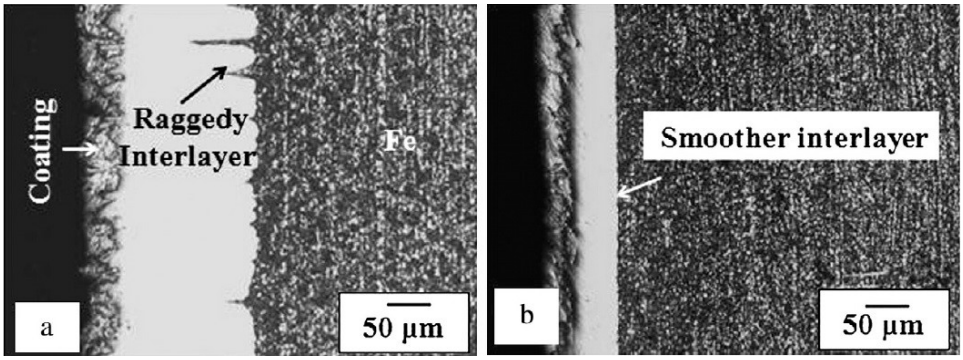


*Figure 13: Effect of copper on the reaction layer between steel and a) pure aluminum b) addition of 11 wt% copper[48].*

The wetting angle experiments carried out by Fragner et al [40] did not reveal any change in the wetting angle due to the addition of 7 wt% copper but a decrease in the intermetallic layer thickness was confirmed.

4.2Mn content

Liu et al [44] studied the metallurgical bond between grey iron and aluminum-silicon alloy with different manganese content. The addition of manganese prevented the formation of needle like intermetallic phases that can be formed at the matrix transition layer when iron is present. This was explained by the formation of $\alpha$-$Al_{15}(Fe_xMn_{1-x})_3Si_2$ phases. Their results also indicated that a slightly thicker intermetallic layer formed with alloys that had a manganese concentration higher than 2%.

**5. Effect of insert type**

*5.1 Steel*

There have been several studies on bimetallic castings using a solid mild steel insert and casting aluminum around it, see [49-53] These studies show that a metallurgical bond can form between the insert and the aluminum although some form of bonding technique was used. They all measured the shear strength using a push-out test method, see Evaluation methods, of the samples prepared but due

to differences in preparation methods and testing methods it is very hard to quantitatively compare the results between the studies.

Aguado et al. [51] compare sand cast bimetallic samples using several cleaning and bonding techniques. All of the samples were also exposed to the thermal treatment T6. The sample with the best performance in the shear testing was an uncoated sample without signs of a metallurgical bond. The sample had been sand blasted so they suggest that the strength is strongly related to the surface morphology of the insert which in the case for the sand blasted sample is rougher. During shear strength testing samples with a metallurgical bond tend to fail at the interface which contains the brittle intermetallic compounds.

Dezellus et al [52] cast steel/aluminum-silicon hot dipped samples in lab crucibles and studied the behavior during mechanical testing using the push-out test. The hot dipping allowed for a continuous metallurgical bond to form. They were able to determine that crack initiation occurs at the bottom surface in the intermetallic reaction layer but with no brittle failure of the component, see Figure 14.

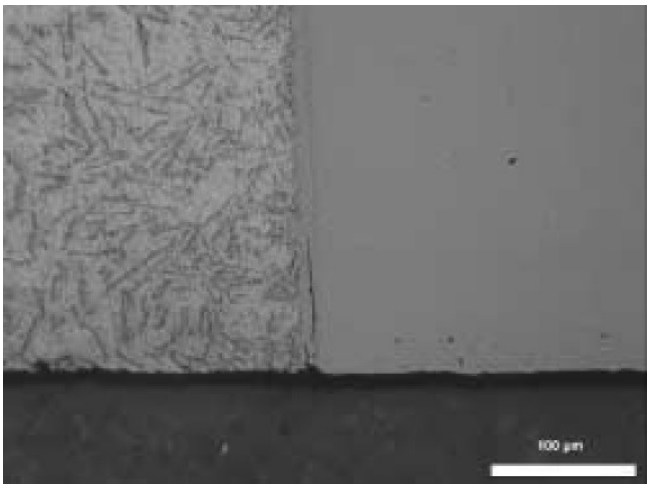

*Figure 14: Crack initiation in the metallurgical bond between the steel insert and aluminum matrix. The pushout test was interrupted at 50% of previously measured maximum force for failure[52].*

Durrant et al [53] squeeze cast steel inserts with and without coatings. By hot dipping steel inserts in aluminum they were able to show that a metallurgical bond greatly increases the interface shear strength. They also concluded that preheating the uncoated insert before casting does not show any significant improvement in the formation of a metallurgical bond. Durrant et al could also establish relationship between the surface roughness and very high strengths of the bond.

Choe et al [49] studied expandable pattern casting process with different pressures and also tested different preparation techniques. Using a zinc coating they successfully metallurgically bonded steel with aluminum alloy A356. They also observed improved bonding with a higher pouring temperature of the aluminum.

Pan et al [50] managed to metallugically bond a steel pipe with aluminum using ultrasonic vibration during casting. They concluded that the vibrations break down the oxide layer on the insert which improves wettability and reactivity of the surface.

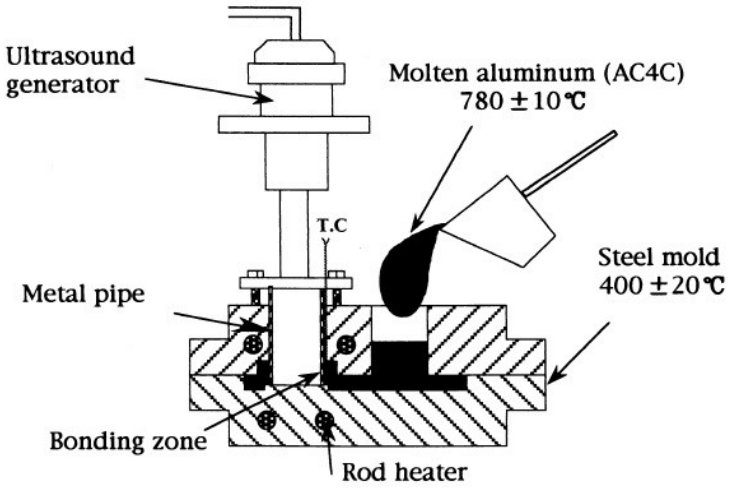


*Figure 15: Setup for casting aided by ultrasound vibrations[50].*

*3.2 Cast Iron*

There have been a few studies focusing on casting aluminum that reinforced with cast iron, see [44, 54-56]. Although in all of the mentioned studies they hot dipped the inserts in aluminum before casting to ensure a metallurgical bond between the insert and the aluminum. Attention in these articles is focused on finding and identifying the intermetallic compounds that are formed during the reaction.

Viala et al. [54] used a spheroidal graphite cast iron insert and bonded it with a silicon containing aluminum alloy by first hot dipping the insert and immediately after the aluminum was gravity cast. They were able to identify three intermetallic compound layers forming at the interface, η-($Al_5Fe_2$) contacting the iron, $\tau_5$-($Al_{7.4}Fe_2Si$) intermediate, and $\tau_6$-(Al4.5FeSi). During heat treatment two new ternary intermetallic compounds, $\tau_2$-(Al5Fe2Si2) and $\tau_{10}$, are formed at the expense of \tau5 and \tau6.

Bouayad et al. [55] tried to cast spheroid graphite cast iron using the high pressure die casting process but were unable to achieve a metallurgical bond. They were also unable to bond the insert with the aluminum using a gravity sand casting procedure. However, after hot dipping the inserts in aluminum they managed to successfully create a bond to the insert. Identified binary intermetallics were $Fe_2Al_5$, and $FeAl_3$ and two ternary intermetallic compounds $\tau_5$ and $\tau_6$.

Li et al. [44] investigated the effect of the silicon content on the reaction layer during hot dipping a cast iron ring in aluminum and then die casting aluminum around it. The effects of Si on the bonding layer will be discussed more in detail in the Aluminum alloy section. They also identified ternary intermetallic Al-Fe-Si compounds at the interface.

Liu et al. [56] successfully bonded a gray cast iron to aluminum by hot dipping the inserts in an aluminum-silicon melt containing different concentrations of Mn and then transferring it to a mold a gravity cast aluminum around it. They identified some quaternary Al-Fe-Mn-Si intermetallic phases at the boundary. The effect of Mn on the bond layer growth will be discussed more in more detail in the Aluminum alloy section.

*5.3 PM Insert*

Powder metallurgy (PM) techniques can produce parts with a relatively low density that has a continuous network of porosity. The open structure of the PM parts can allow for infiltration of aluminum if cast under pressure. If the pressure and velocity of the melt during the casting is high enough it is possible to produce a fully dense component. The aluminum will form a matrix around the PM part and it will be fully integrated in the part [57, 58]. Compared to a solid steel insert the area interacting with the melt is much higher which allows for much more reactive phase to form.

Baron et al [57] used PM insert of a steel and a stainless steel with a relative density of 0.6 and 0.7 and squeeze cast aluminum A380 around them. By optimizing the cast condition they were able to produce composite samples that were completely infiltrated. As can be shown in Figure 16 and Figure 17, comparing the location, side or center, in samples and also materials, steel and stainless steel. There is a significant difference in the reaction layer thickness comparing the plain steel with the stainless steel. They were also able to determine that the melt temperature has a strong effect on the mechanical properties of the composite part. They also correlated the volume fraction of reaction phase formed during processing to the mechanical properties of the part. A higher volume fraction indicated deleterious effects on the properties especially there was a decrease in ductility.

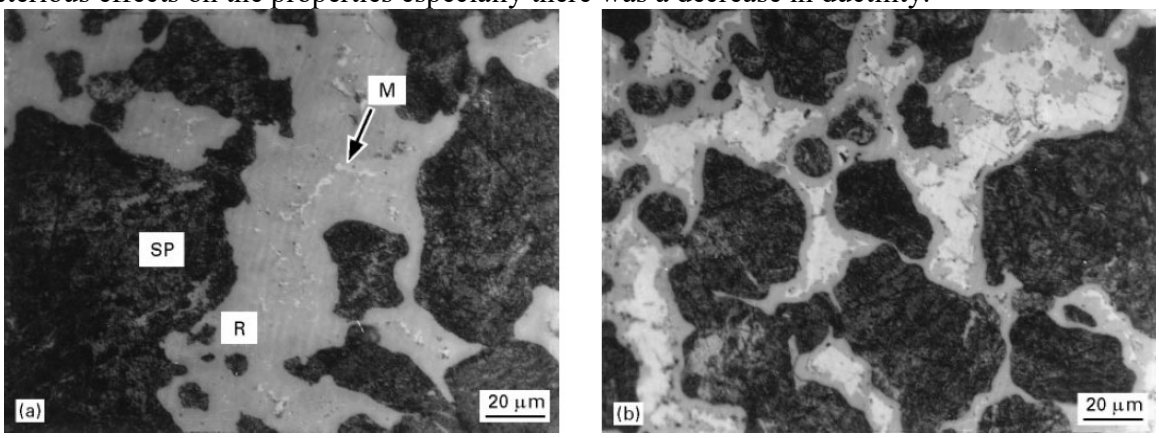


*Figure 16: PM steel insert infiltrated with aluminum. M-Al-matrix, SP-Steel insert, R-Reaction phase. (a) The midde of insert. (b) The edge of the insert[57].*

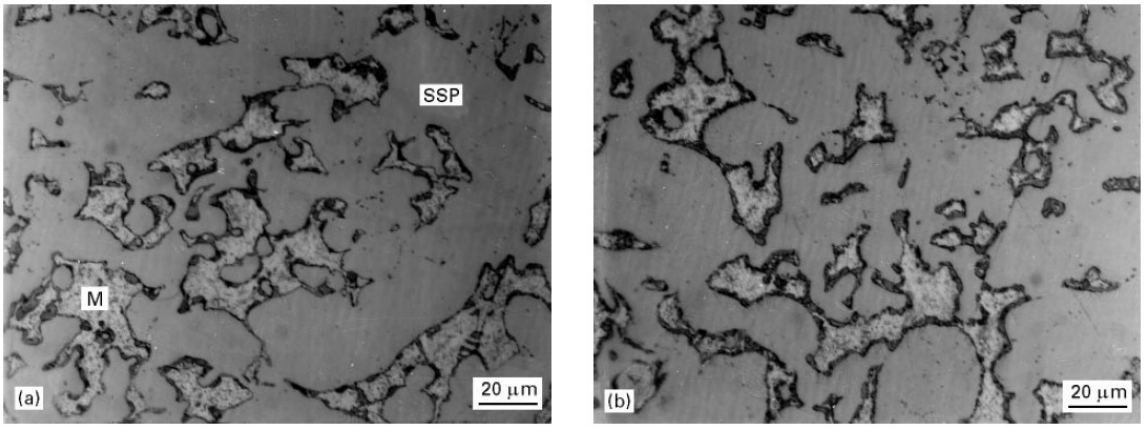


*Figure 17: PM stainless steel insert infiltrated with aluminum. M-Al-matrix, SSP-Stainless steel insert. (a) The midde of insert. (b) The edge of the insert[57].*

In Baron et al [58] study they compared four ferrous PM samples produced with different compositions, especially the chromium compositions. As in their study previous study [57] the steels containing chromium produced less volume fraction of reaction phase.

Patent EP1886747A1 describes a technique in which sintered PM-compact is impregnated in a pressurized die casting procedure. The method involves first heating of the die and insert and then a 2-step pressurized casting procedure. The invention is aimed to reducing the porosity of the resulting component to improve properties like thermal conductivity.[59]

*5.4 Insert preheating*

Preheating the insert will decrease initial temperature difference between the melt and the insert. A higher insert preheating temperature will prevent it from acting as an internal chill in the mold.

Durrant et al. [53] could not see improvement in bonding between the uncoated mild steel insert and the aluminum matrix between preheating temperature of 300 °C and 900 °C. They believe that there is not enough time for reaction to take place due to the quenching effect when the hot melt meets the colder insert. The insert that was preheated to 900 °C demonstrated there is no improvement for the metallurgical bonding. When they analyzed the sample, they found an iron oxide layer between the insert and aluminum matrix. For their titanium coated inserts they got the same results. Figure 18 shows an oxide layer between the steel and the aluminum.

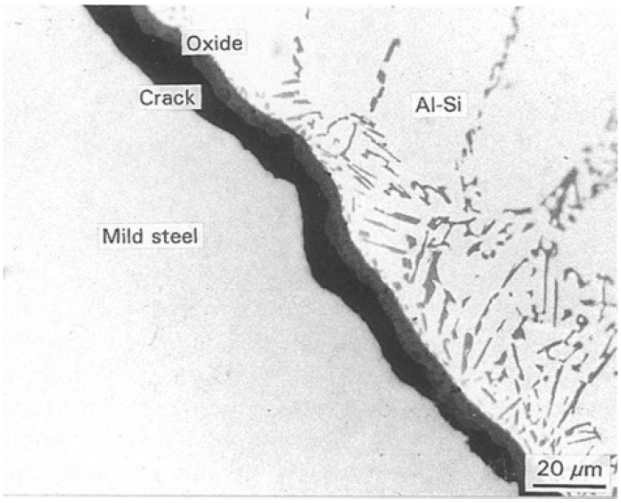


*Figure 18: Oxide inbetween the two metals[53].*

In Bouayad et al [55] studies on sand casting aluminum around a cast iron insert they came to the conclusion that preheating delays aluminum solidification and promotes the development of the bond. However, at the same time iron oxides can also form on the insert which can act as diffusion barriers.

Aguado et al. [51] compared samples that were pickled in HCl and then two out of the three samples preheated to 100 °C respectively 300 °C. There was no metallurgical bond formed and they could not identify and difference in bond strength between the samples. Upon investigation they concluded that metallurgical bonding was prevented by an oxide layer formed on the insert.

*5.5 Alloying element content*

The alloying elements in the insert can also play an important role during the formation of the intermetallic compounds. Hwang et al. [39] and Sasaki et al [28] studied the effect of carbon on the formation of the intermetallic boundary layer. Both of the studies concluded that an increased carbon content in the insert decreases the reaction layer thickness.

Niinomi et al [60] investigated the effect of different alloying elements in the iron base insert. He compared commercially pure Fe with Fe-C, Fe-Si, Fe-Mn, Fe-Cr, Fe-Ni, and Fe-Cu alloys. He concluded that all of the alloying elements reduced the reaction layer thickness and Si, Ni, and Cu had the greatest effect.

Kwon et al. [12] were able to determine that using a high carbon steel or a silicon containing steel will suppress the tongue like structure produced by pure iron and aluminum, instead a more planar interface forms. They were also able to show that the morphology of the interface is not dependent on the structure (ferrite or austenite) of the iron. Komatsu et al [38] saw an absence of carbon in the intermetallic layer which could be due to the low solubility of carbon in the intermetallic layer [61].

## 6. Coatings

Metal coating can be utilized to improve the bonding between the two metals. A coating will completely alter how the interface will interact with the melt. If a coating of aluminum is used properties like the wetting angle and oxidation resistance is altered. If a third metal is added to the system as a coating the interface chemistry and the reaction layer can be completely different. If for example a metal that is known to react exothermically with aluminum is used as a coating for the insert the heat generated can aid the diffusion and create a thicker bond.

*6.1 Aluminum coating*

A common technique to ensure a metallurgical bond between the insert and the melt is to first hot dip the insert in an aluminum melt. During the hot dipping process the reaction between iron and aluminum takes place. After dipping the insert for some time it is quickly transferred to a mold and aluminum is cast around it. This technique has been successfully applied in many studies that were able to show a formed metallurgical bond between the insert and the aluminum matrix. [51-56]

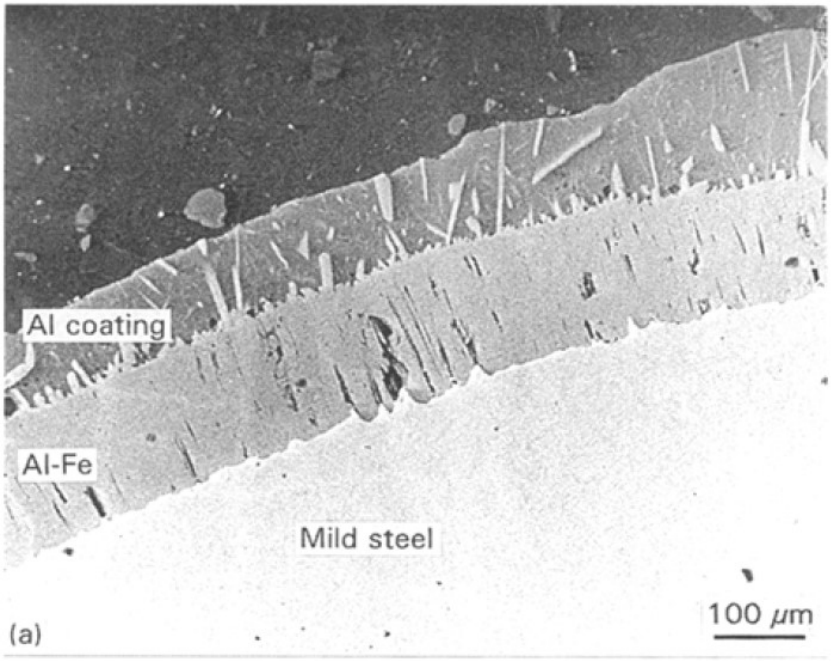


*Figure 19: SEM backscatter micrograph of a hot-dipped insert[53].*

*6.2 Zinc coating*

Instead of using an aluminum coating a metal with a lower melting point, like zinc, can be used. By hot dip galvanizing the insert in zinc a metallurgical bond between iron and aluminum was achieved. At the interface between the ferrous insert and the aluminum melt binary Al-Fe and ternary Al-Fe-Si intermetallic compounds are found. [49, 51, 62]

Choe et al [49] and Zhe et al [33]reports that no zinc is present at the interface and believes this is due to it dissolving into the aluminum matrix due to its high diffusivity in aluminum.

*6.3 Ni/Cu coating*

Coatings utilizing metals like Cu, Ni, Ag and Cr different from the aluminum and zinc coatings due to that their melting point is above the aluminums. The coefficient of thermal expansion is also in between iron and aluminum.

Han et al [63] developed a method in which two layers of coating were electroplated on a steel insert and successfully bonded this with the aluminum matrix. They focused on a Ni/Cu coating with the nickel close to the insert and the copper in contact with the aluminum. With this setup the coefficients of thermal expansion goes from low (iron) to high (aluminum). The outer coating can also be a sacrificial coating that is used only to improve the bonding between the melt and the inner coating. After the plating of the insert, the coatings are diffusion bonded by being heated to 900 °C and held there for four hours and then cooled to room temperature in the furnace. The aluminum is then cast around the coated insert, see Figure 20. Also Aguado et al [51] successfully bonded a Cu/Ni plated insert to the aluminum matrix.

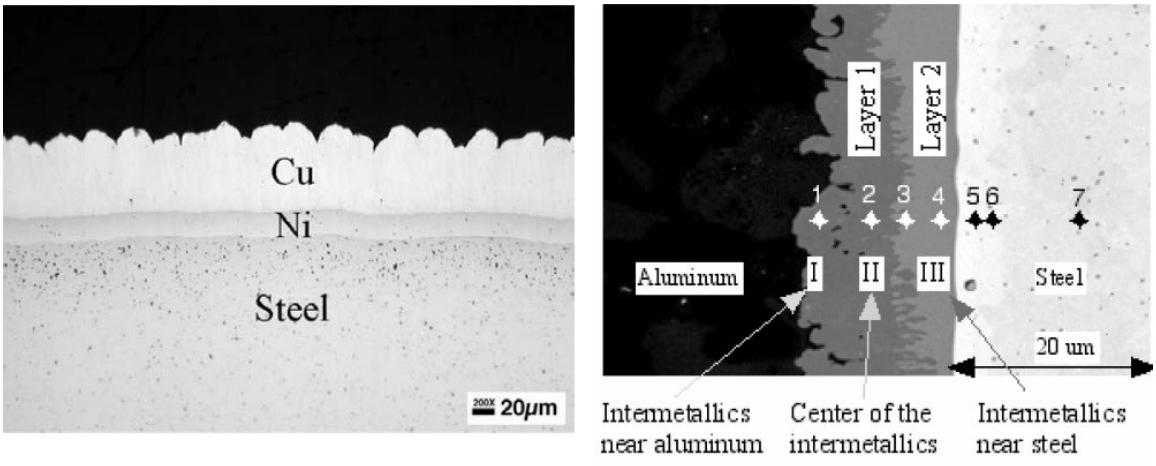


*Figure 20: Right: Deposited layer of copper and nickel on the steel insert. Left: The two layers after casting and T6 heat treatment[63].*

*6.4 Titanium coating*

Durrant et al. [53] tried to bond a mild steel insert to the aluminum by vacuum plasma spraying titanium powder on the insert. They demonstrated a good connection between the titanium and the steel but there was very little to no reaction between the titanium and the aluminum. The reason for the lack of reaction between the aluminum and the titanium were explained by an oxide layer between the two metals and there is very limited reaction between the titanium oxide and the liquid aluminum.

**7. Patent Search for Bonding Techniques**

A patent search revealed these bonding techniques:

One of the techniques developed to promote the bonding is the so-called Al-Fin process. The ferrous insert is immersed into a bath of a metal, normally aluminum, and held there to allow for the formation of a metallurgical bond. The modified insert in then placed in a mold and aluminum is cast around it.[64-66]

Similar methods but with preparation steps involving molten salt baths used to clean add a salt coating for oxidation protection and then casting the aluminum around the insert[67]. A combination of the salt pre-coat plus an additional aluminum pre-coat of the insert has also been patented[68]. Adding a coating of a more oxidation resistant material to reduce the amount of oxidation has also be developed[69].

Zinc has also proven to aid the formation of the bond. The insert is dipped in molten zinc and a reaction layer is allowed to form. The insert is later cast into aluminum and give the high diffusivity in aluminum it will diffuse away and allow for reaction between the iron and the aluminum [70-74].

To increase the reactivity with the melt and promote the bonding, the insert can be coated with materials that are known to exothermically react with aluminum. Once the liquid aluminum comes in contact with the reactive coating the exothermic reaction will release energy that will further promote the bonding [75].

Due to the brittle characteristics of the intermetallics formed at the interface between aluminum and iron, it can be favorable to add other metals to change the characteristics of the bond. Techniques to electroplate the insert with one or multiple layers of other metals than aluminum and zinc have been

developed. The advantages of these techniques are that the metal choice for plating can be picked so it has a thermal expansion coefficient in between aluminum and iron. Metals that can be used are nickel, copper, silver and many other, and combinations of these [76, 77].

**8. Interface strength**

In the literature concerning a ferrous insert cast into an aluminum matrix, the shear strength of the bond has been measured by push-out testing [50-53, 63], a pull-to-fail test [78] and a semi-shear test [49]. Zhe et al [79] also studied the strength of the interface using a modified 4-point bending test.

A typical push-out setup can be seen in Figure 21. Aluminum is cast around a ferrous insert and the sample is sliced into discs. A steel punch pushes the sliced insert out from the bimetallic sample and the force necessary to push until failure is measured.

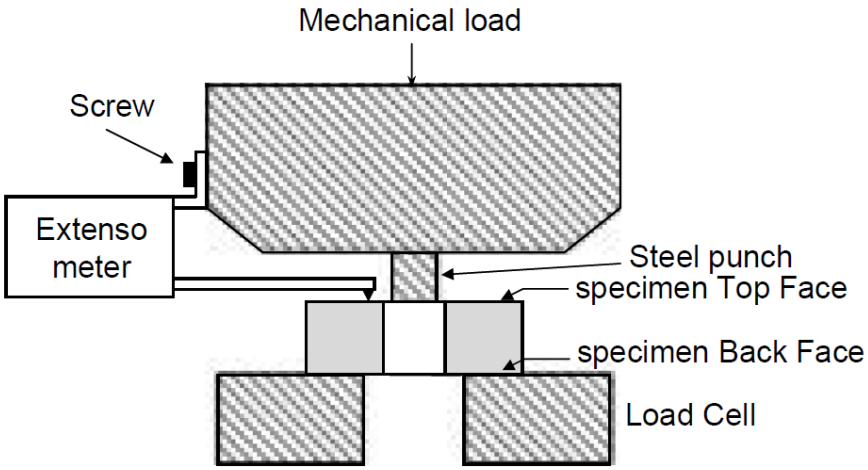


*Figure 21: Schematic drawing of the push-out test setup[52].*

Luo et al [78] and Choe et al [49] pull the sample apart and measures the load necessary for the sample to fail. Table 2 shows the measured interface shear strength from the different studies.

*Table 2: Summary of strength of the metallurgical bond from different authors*

| Authors | Test type | Alloys | Insert | Manufac. Conditions | Layer thickness (µm) | Bond strength (MPa) |
|---|---|---|---|---|---|---|
| Durrant et al 1996[53] | Push-out | Al-7Si | Steel | Preheat 300 °C | - | 30.5 |
| | | | | Preheat 900 °C | - | 44.5 |
| | | | | Al-coat, preheat 300 °C | ~50-80 * | 114 |
| | | | | Al-coat, preheat 900 °C | ~50-80 * | 112 |
| | | | | Ti-coat, smooth, preheat 300 °C | - | 5 |
| | | | | Ti-coat, rough, preheat 300 °C | - | 150 |
| | | | | Ti-coat, smooth, preheat 900 °C | - | 34 |
| | | | | Ti-coat, rough, preheat 900 °C | - | 126 |
| Pan et al 2000[80] | Push-out | A356 | Steel | Ultrasound vibration | 5~8 | 60 |
| Han et al 2003[63] | Push-out | A354 | Steel | Ni/Cu coating, preheat 120 °C | ~10 * | 65 |
| Dezellus et al 2007[52] | Push-out | A413 | Steel | Al-coat, preheat 735 °C | 12~14 | 92 |
| Choe et al 2008[81] | Semi-shear | A356 | Steel | Zn-coat | 15~20* | |
| Li et al 2012[44] | Push-out | Al-2Si | Aust-Cast-iron | Al-coat, preaheat 700 °C | | 3.6 |
| | | Al-6Si | Aust-Cast-iron | Al-coat, preaheat 700 °C | | 8.8 |
| | | Al-11Si | Aust-Cast-iron | Al-coat, preaheat 700 °C | ~20 * | 13.6 |
| | | Al-16Si | Aust-Cast-iron | Al-coat, preaheat 700 °C | | 4.8 |
| Aguado et al 2013[51] | Push-out | AlSi7Mg | Steel | Degrease | - | 13 |
| | | AlSi7Mg | Steel | Pickling | - | 12 |
| | | AlSi7Mg | Steel | Pickling, preheat 100 °C | - | 14 |
| | | AlSi7Mg | Steel | Pickling, preheat 300 °C | - | 12 |
| | | AlSi7Mg | Steel | Shot blast | - | 31 |
| | | AlSi7Mg | Steel | Pickling, Al-coat | | 2 |
| | | AlSi7Mg | Steel | Zinc coat (hot dipped) | | 14 |
| | | AlSi7Mg | Steel | Zinc coat (plated) | | 14 |
| | | AlSi7Mg | Steel | Cu/Ni coating | | 19 |
| | | AlSi7Mg | Steel | Shot blast, Al-coat | | 22 |
| | | AlSi7Mg | Steel | Shot blast, Cu/Ni coating | | 27 |

Dezellus et al [52] were able to determine that crack initiation occurs at the bottom surface in the intermetallic reaction layer by interrupting the tests at certain loading levels of the maximum measured. However, Durrant et al. [53] report that failure occurs in the aluminum matrix for the aluminized samples. Aguado et al [51] report that for samples with no evidence of metallurgical bonding the samples fail at the interface due to an oxide layer. For the samples showing a reaction layer, the failure occurs close to the coating/Al interface. By using a modified 4-point bending test, Zhe et al [79] were able to determine that the crack propagates through the η-($Al_5Fe_2$(Si)) phase layer.

It is known that intermetallic compounds are very brittle and hard which can be attributed to their more valence like bonding. The high hardness and lack of ductility can degrade properties of the composite.

Therefore it can be necessary to limit the thickness of the formed intermetallic layer. Especially if the surface to volume ratio of the component increases when using a PM-insert or coating[57].

References

[1] Gebhardt, E., and Obrowski, W., 1953, "Reaktionen von festem eisen mit schmelzen aus aluminium und aluminiumlegierungen," Zeitschrift fur Metallkunde, 44(4), pp. 154-160.
[2] Eggeler, G., Vogel, H., Friedrich, J., and Kaesche, H., 1985, "Target Preparation for the Transmission Electron Microscopic Identification of the Al sub 3 Fe ( theta -Phase) in Hot-Dip Aluminised Low Alloyed Steel," Praktische Metallographie, 22(4), pp. 163-170.
[3] Bouayad, A., 2003, "Kinetic interactions between solid iron and molten aluminium," Materials science & engineering. A, Structural materials : properties, microstructure and processing, 363(1-2), pp. 53-61.
[4] Takata, N., 2015, "Crystallography of Fe2Al5 phase at the interface between solid Fe and liquid Al," Intermetallics, 67, pp. 1-11.
[5] Heumann, T., and Dittrich, S., 1959, "Uber die Kinetik der Reaktion von festem und flûssigem Aluminium mit Eisen," Zeitschrift fur Metallkunde, 50(10), pp. 617-625.
[6] Heumann, T., and Dittrich, N., 1959, "Structure character of the Fe2Al5 intermetallics compound in hot dip aluminizing process," Z Metallk, 50, pp. 617-623.
[7] Cheng, W.-J., and Wang, C.-J., 2009, "Growth of intermetallic layer in the aluminide mild steel during hot-dipping," Surface & Coatings Technology, 204(6), pp. 824-828.
[8] Sakidja, R., 2014, "Synthesis, Thermodynamic Stability and Diffusion Mechanism of Al5Fe2-Based Coatings," Oxidation of metals, 81(1-2), pp. 167-177.
[9] Eggeler, G., Auer, W., and Kaesche, H., 1986, "Reactions Between Low Alloyed Steel and Initially Pure as Well as Iron-Saturated Aluminium Melts Between 670 and 800 deg C," Zeitschrift für Metallkunde, 77(4), pp. 239-244.
[10] Bouché, K., Barbier, F., and Coulet, A., 1998, "Intermetallic compound layer growth between solid iron and molten aluminium," Materials science & engineering. A, Structural materials : properties, microstructure and processing, 249(1), pp. 167-175.
[11] Shahverdi, H. R., Ghomashchi, M. R., Shabestari, S., and Hejazi, J., 2002, "Microstructural analysis of interfacial reaction between molten aluminium and solid iron," Journal of materials processing technology, 124(3), pp. 345-352.
[12] Kwon, S. C., and Lee, J. Y., 1981, "Interface Morphology Between the Aluminide Layer and Iron Substrate in the Hot Dip Aluminizing Process," Canadian metallurgical quarterly, 20(3), pp. 351-357.
[13] Springer, H., Kostka, A., Payton, E. J., Raabe, D., Kaysser-Pyzalla, A., and Eggeler, G., 2011, "On the formation and growth of intermetallic phases during interdiffusion between low-carbon steel and aluminum alloys," Acta Materialia, 59(4), pp. 1586-1600.
[14] Pasche, G., Scheel, M., Schäublin, R., Hébert, C., Rappaz, M., and Hessler-Wyser, A., 2013, "Time-Resolved X-Ray Microtomography Observation of Intermetallic Formation Between Solid Fe and Liquid Al," Metallurgical and Materials Transactions A, 44(9), pp. 4119-4123.
[15] Denner, S. G., and Jones, R. D., 1976, "Use of Transmission 57-Fe Mossbauer Spectroscopy to Study the Kinetics of Hot-Dip Aluminizing of Fe," Journal of materials science, 11(9), pp. 1777-1778.
[16] Denner, s. G., and Jones, R. D., 1977, "Kinetic interactions between aluminiumliquid and iron/steelsolid for conditions applicable to hot-dip aluminizing," Metals technology, 4(1), pp. 167-174.
[17] Eremenko, V., Natanzon, Y. V., and Dybkov, V., 1973, "Investigation of the Reactions Between Iron and Liquid Aluminium," Russian Metallurgy(5), pp. 66-67.
[18] Eremenko, V., Natanzon, Y. V., and Dybkov, V., 1973, "Study of the Interaction of Fe with Molten Al," Izv. Akad. Nauk SSR Met., Sept.-Oct. 1973,(5), 96-99(Russian).

[19] Eremenko, V., and Natanzon, Y., 1974, "Reaction Between Fe and Molten Al During Simulation of the Welding Process by Melting," Avtomat. Svarka(2), pp. 5-8.
[20] Yeremenko, V. N., Natanzon, Y. V., and Dubkov, V. I., 1981, "The Effect of Dissolution on the Growth of the Fe2Al5 Interlayer in the Solid Iron -- Liquid Aluminum System," Journal of Materials Science, 16(7), pp. 1748-1756.
[21] Dybkov, V. I., 1986, "Reaction diffusion in heterogeneous binary systems Part 1 Growth of the chemical compound layers at the interface between two elementary substances: one compound layer," Journal of materials science, 21(9), pp. 3078-3084.
[22] Dybkov, V. I., 1986, "Reaction diffusion in heterogeneous binary systems Part 2 Growth of the chemical compound layers at the interface between two elementary substances: Two compound layers," Journal of materials science, 21(9), pp. 3085-3090.
[23] Dybkov, V. I., 1987, "Reaction diffusion in heterogeneous binary systems Part 3 Multiphase growth of the chemical compound layers at the interface between two mutually insoluble substances," Journal of materials science, 22(12), pp. 4233-4239.
[24] Dybkov, V. I., 1990, "INTERACTION OF 18CR-10NI STAINLESS-STEEL WITH LIQUID ALUMINUM," JOURNAL OF MATERIALS SCIENCE, 25(8), pp. 3615-3633.
[25] Shahverdi, H. R., Ghomashchi, M. R., Shabestari, S., and Hejazi, J., 2002, "Kinetics of interfacial reaction between solid iron and molten aluminium," Journal of Materials Science, 37(5), pp. 1061-1066.
[26] Ueda, Y., and Niinomi, M., 1978, "On the Alloy Layers Formed by the Reaction Between Ferrous Alloys and Molten Aluminum," Journal of the Japan Institute of Metals and Materials, 42(6), pp. 543-549.
[27] El-Mahallawy, N. A., Taha, M. A., and Shoeib, M. A., 2002, "Analysis of reaction layer formed on steel strips during hot dip aluminising," Materials Science and Technology, 18(10), pp. 1201-1208.
[28] Sasaki, T., 2005, "Effects of carbon contents in steels on alloy layer growth during hot-dip aluminum coating," ISIJ international, 45(12), p. 1887.
[29] Eggeler, G., Auer, W., and Kaesche, H., 1986, "On the Influence of Silicon on the Growth of the Alloy Layer During Hot Dip Aluminizing," J. Mater. Sci, 21(9), pp. 3348-3350.
[30] El-Mahallawy, N. A., Taha, M. A., Shady, M. A., and ElSissi, A. R., 1997, "Analysis of coating layer formed on steel strips during aluminising by hot dipping in Al-Si baths," Materials science and technology, 13(10), pp. 832-840.
[31] Awan, G. H., and ul Hasan, F., 2008, "The morphology of coating/substrate interface in hot-dip-aluminized steels," Materials Science & Engineering A, 472(1), pp. 157-165.
[32] Cheng, W. J., and Wang, C. J., 2010, "Observation of high-temperature phase transformation in the Si-modified aluminide coating on mild steel using EBSD," Materials Characterization, 61(4), pp. 467-473.
[33] Zhe, M., 2011, "Chemical Changes at the Interface Between Low Carbon Steel and an Al-Si Alloy During Solution Heat Treatment," Journal of phase equilibria and diffusion, 32(6), pp. 486-497.
[34] Springer, H., 2011, "Influence of intermetallic phases and Kirkendall-porosity on the mechanical properties of joints between steel and aluminium alloys," Materials science & engineering. A, Structural materials : properties, microstructure and processing, 528(13-14), pp. 4630-4642.
[35] Gittings, D., Rowland, D., and Mack, J., 1951, "Effect of Bath Composition on Aluminum Coatings on Steel," Trans. ASM, 43, p. 587.
[36] Nicholls, J. E., 1964, "HOT-DIPPED ALUMINIUM COATINGS," Anti-corrosion methods and materials, 11(10), pp. 16-21.
[37] Lainer, D., and Kurakin, A., 1964, "Mechanism of the effect of silicon in aluminum on the process of reactive diffusion of iron into aluminum," Fiz. Metal. Metalloved, 18.
[38] Komatsu, N., Nakamura, M., and Fujita, H., 1968, "Effects of silicon on reaction between iron and liquid aluminum " Journal of Japan Institute of Light Metals, 18(9), pp. 467-473.

[39] Hwang, S.-H., Song, J.-H., and Kim, Y.-S., 2005, "Effects of carbon content of carbon steel on its dissolution into a molten aluminum alloy," Materials science & engineering. A, Structural materials : properties, microstructure and processing, 390(1), pp. 437-443.
[40] Fragner, W., Zberg, B., Sonnleitner, R., Uggowitzer, P. J., and Loftier, J. F., 2006, "Interface reactions of al and binary Al-alloys on mild steel substrates in controlled atmosphere," Materials Science Forum, 519-521, pp. 1157-1162.
[41] Shih, T.-S., and Tu, S.-H., 2007, "Interaction of steel with pure Al, Al–7Si and A356 alloys," Materials Science & Engineering A, 454, pp. 349-356.
[42] Schoukensa, I., De Graeve, I., De Strycker, J., and Terryn, H., 2012, "Effect of Local Surface Microstructure and Composition on the Electrochemical Behavior of Hot Dip Aluminum-Silicon Coatings on Steel," Corrosion (Houston, Tex.), 68(11), pp. 982-993.
[43] Kang, S., 2012, "Formation Behavior of an Intermetallic Compound Layer during the Hot Dip Aluminizing of Cast Iron," ISIJ international, 52(7), pp. 1342-1347.
[44] Li, C. A., 2012, "Effect of Si content in hot dipping aluminium bath on Al–Fe bonding layer of aluminium piston with reinforced cast iron ring," Materials science and technology, 28(8), pp. 953-958.
[45] Yin, F.-c., 2013, "Effect of Si on growth kinetics of intermetallic compounds during reaction between solid iron and molten aluminum," Transactions of Nonferrous Metals Society of China, 23(2), pp. 556-561.
[46] Zhang, K., Bian, X., Li, Y., Liu, Y., and Yang, C., 2013, "New evidence for the formation and growth mechanism of the intermetallic phase formed at the Al/Fe interface," Journal of materials research, 28(23), pp. 3279-3287.
[47] Springer, H., 2011, "On the formation and growth of intermetallic phases during interdiffusion between low-carbon steel and aluminum alloys," Acta materialia, 59(4), pp. 1586-1600.
[48] Yousaf, M., Iqbal, J., and Ajmal, M., 2011, "Variables affecting growth and morphology of the intermetallic layer (Fe 2Al 5)," Materials characterization, 62(5), pp. 517-525.
[49] Choe, K., Park, K., Kang, B., Cho, G., Kim, K., Lee, K., Kim, M., Ikenaga, A., and Koroyasu, S., 2008, "Study of the interface between steel insert and aluminum casting in EPC," JOURNAL OF MATERIALS SCIENCE & TECHNOLOGY, 24(1), pp. 60-64.
[50] Pan, J., Yoshida, M., Sasaki, G., Fukunaga, H., Fujimura, H., and Matsuura, M., 2000, "Ultrasonic insert casting of aluminum alloy," Scripta Materialia, 43(2), pp. 155-159.
[51] Aguado, E., 2013, "Comparative Study of Different Interfaces of Steel Inserts in Aluminium Castings," Materials Science Forum, 765, pp. 711-715.
[52] Dezellus, O., Digonnet, B., Sacerdote-Peronnet, M., and Bosselet, F., 2007, "Mechanical testing of steel/aluminium–silicon interfaces by pushout," International journal of adhesion and adhesives, 27(5), pp. 417-421.
[53] Durrant, G., 1996, "Squeeze cast aluminium reinforced with mild steel inserts," Journal of materials science, 31(3), pp. 589-602.
[54] Viala, J. C., Peronnet, M., Barbeau, F., and Bosselet, F., "Interface chemistry in aluminium alloy castings reinforced with iron base inserts," pp. 1417-1420.
[55] Bouayad, A., Gerometta, C., Radouani, M., and Saka, A., 2010, "Interface Characterization in Aluminum Alloy Casting Reinforced with SG Iron Inserts.," 1(4), pp. 226-231.
[56] Liu, Y., and Bian, 2013, "An investigation of metallurgical bonding in Al-7Si/gray iron bimetal composites," Journal of materials research, 28(22), p. 3190.
[57] Baron, R. P., Wert, J. A., Gerard, D. A., and Wawner, F. E., 1997, "The processing and characterization of sintered metal-reinforced aluminium matrix composites," Journal of Materials Science, 32(24), pp. 6435-6445.

[58] Baron, R. P., Jones, C., Wawner, F. E., and Wert, J. A., "Mechanical properties of aluminum matrix composites reinforced with sintered ferrous compacts," ELSEVIER SCIENCE SA, pp. 308-313.
[59] Yamana, K., Kinoshita, K., Tanizawa, M., Sugiura, M., and Enokijima, F., 2008, "Process for producing aluminum composite material," Kabushiki Kaisha Nikkyo Seisakusho.
[60] Niinomi, M., Ueda, Y., and Sano, M., 1982, "Dissolution of ferrous alloys into molten aluminum," Japan. Trans. Japan Inst. of Metals, 23(12), pp. 780-787.
[61] Vaillant, P., and Petitet, J. P., 1995, "Interactions under hydrostatic pressure of a mild steel with liquid aluminium alloys," Journal of Materials Science, 30(18), pp. 4659-4668.
[62] Moosavi-Khoonsari, E., Jalilian, F., Paray, F., and Emadi, D., 2011, "Cast joining of cast iron to aluminium casting matrix," Materials science and technology, 27(11), pp. 1707-1717.
[63] Han, Q., More, K. L., Myers, M. R., Warwick, M. J., and Chen, Y. C., 2003, "Reinforcement of Aluminum Castings with Dissimilar Metals," U.S. Department of Energy (DOE).
[64] Whitfield, M. G., and Victor, S., 1946, "Coating metal," Al Fin Corp.
[65] Hannig, C., 1976, "Method for the manufacture of a compound casting," Mahle Gmbh.
[66] Ohta, M., 1991, "Cylinder liner unit for use in an internal combustion engine," Isuzu Jidosha Kabushiki Kaisha.
[67] Boswell, R. B., Jominy, W. E., and Olson, J. H., 1959, "Method of casting aluminum on ferrous base to form duplex structure," Chrysler Corp.
[68] Grange, H. L., and Hanink, D. K., 1951, "Method of forming composite products consisting of ferrous metal and aluminum or aluminum-base alloy," Gen Motors Corp.
[69] Cole, A. T., and Munro, R., 1991, "Method of making a piston," T&N Technology Limited, Wellworthy Limited.
[70] Grange, H. L., and Hanink, D. K., 1951, "Method of forming composite aluminum-steel parts by casting aluminum onto steel andbonding thereto," Gen Motors Corp.
[71] Pershing, W. H., Mcclain, J. J., and Fulwider, J. A., 1953, "Bonding aluminum or aluminum base alloy to ferrous metal by means of an alloy bond," Gen Motors Corp.
[72] Ulrich, Z., 1958, "Joints between iron and light metals," Fairchild Engine & Airplane.
[73] Voss, K. D., Prucha, T. E., and Kuhn, J. W., 1994, "Coating liner with low melting metal which is melted and alloyed with block and liner," Cmi International.
[74] Jorstad, J. L., Morley, R. A., Overbagh, W. H., and Steele, G. W., 1994, "Process for creation of metallurgically bonded inserts cast-in-place in a cast aluminum article," Reynolds Metals Company.
[75] Wang, Y., Meyers, D. M., and Mikkola, P. H., 1995, "Metallurgical bonding of metals and/or ceramics," General Motors Corporation.
[76] Myers, M. R., Warwick, M. J., Chen, Y., Subramanian, R., Viswanathan, S., More, K., and Han, Q., 2002, "Mettallurgical bonding of inserts having multi-layered coatings within metal castings," Cummins Inc., Ut-Battelle, Llc.
[77] Myers, M. R., Warwick, M. J., Chen, Y., Subramanian, R., Viswanathan, S., More, K., and Han, Q., 2002, "Metallurgical bonding of coated inserts within metal castings," Cummins Inc., Ut-Battelle, Llc.
[78] Luo, A. A., and Sachdev, A. K., 2011, "Process Development and Characterization of Overcasting Systems," Transactions of the American Foundry Society., 119(11-081), pp. 481-486.
[79] Zhe, M., Dezellus, O., Parry, G., Braccini, M., and Viala, J. C., 2012, "Modified 4-Point Bending Test for Adhesion Measurement at the Interface of Iron Coated with Aluminum Casting Alloy," JOURNAL OF ADHESION SCIENCE AND TECHNOLOGY, 26(1-3), pp. 1-17.
[80] Pan, J., Yoshida, M., Sasaki, G., and Fukunaga, H., 2000, "Metal pipe joining with aluminum alloy by ultrasonic insert casting," MATERIALS AND MANUFACTURING PROCESSES, 15(6), pp. 867-881.

[81] Choe, K., Park, K., Kang, B., Cho, G., Kim, K., Lee, K., Kim, M., Ikenaga, A., and Koroyasu, S., 2008, "Study of the interface between steel insert and aluminum casting in EPC," JOURNAL OF MATERIALS SCIENCE & TECHNOLOGY, 24(1), pp. 60-64.

# Appendix B

# Liquid-solid interaction between mild steel and A356 and 390

## Introduction

In dissimilar metal components, there is a necessity to efficiently join the two materials and in similarity to composite materials the bond between the two materials are crucial in determining the properties of the component. Controlling the bond formation can allow to optimize mechanical and physical properties. Due to very limited solubility in the aluminum-iron system there is an intermetallic compound (IMC) formation during the interaction[1]. The type of IMC that forms is dependent on which elements are present. It has also been shown that the presence of alloying element will significantly change the type of intermetallic as well as their morphology[2].The growth of IMC layer has been shown to follow parabolic relationship indicating a diffusion controlled process[3]. Other authors has shown paralinear behavior of the growth due to a combination of reaction and diffusion controlled growth[4]. The addition of alloying elements in the aluminum and/or the ferrous alloy will have an impact on both the morphology and the growth rate of the IMC layer. Specifically, silicon has been shown to have a significant effect on the type and morphology of the IMC layer, and the growth kinetics[2]. It has been shown that the thickness of the intermetallic compound layer will affect the mechanical properties of the bimetallic component[5]. Intermetallic compounds are known to have a lower thermal conductivity compared to the metallic materials from which they form. Therefore, it is of importance to understand the kinetic behavior of the formation of the IMC layer and it is of crucial importance to predict the type of IMCs that can form.

## Experimental

To simulate the casting procedure steel rods were dipped into an aluminum melt. A mild steel (1015) and two commonly used casting alloys (A356 and 390) with different silicon content were chosen for the experiment. 8 cm long steel rods (6.35 mm diameter) were ground using silicon carbide (SiC) grinding paper and ultrasonically cleaned in ethanol. Three types of surface roughness were achieved using three different paper grits. The topography of the surface was measured and the surface roughness were 0.9, 0.6, and 0.3 μm for the different grit papers used. To characterize to dissolution of iron the thickness of dissolved steel was measured for the liquid A356 and mild steel system. Steel rods prepared with 600 grit grinding paper were masked and half covered in a boron nitride coating to prevent any contact between the liquid aluminum and steel. 1 kg was melted and held at temperatures of 625, 660, 700 and 750°C in an electrical resistance furnace in a silicon carbide crucible. Once the desired temperature was reached the steel rods were lowered into the aluminum melt. Care was taken to remove the oxides from the melt surface before immersion of the steel. Three samples were immersed for 10, 30, 120 and 300 seconds and then gently removed from the melt and allowed to air cool. To understand the equilibrium growth in the liquid solid interaction three additional samples were then dipped for 300 seconds, removed and then water quenched. Cross sections of the steel rods were cut and prepared with standard metallurgical preparation methods. To determine the thickness of the IMC layer nine locations in each cross section were examined and six thickness measurements were made and an average was calculated. For phase identification, the samples were analyzed using a JEOL JSM-7000F equipped with Oxford Instruments EDS detector X-Max$^N$ and EBSD detector NordlysMax$^2$.

**Results**

*Kinetics*

Shorter dipping times, 10 and 30 seconds show relatively poor IMC layer bonding. The thickness of the layers had to be measured in the spots where bonding had occurred. A longer dipping time shows much better bonding as well as overall coverage. Especially lack of interaction between the aluminum and steel is for samples prepared using a 120 grit SiC paper were results were only obtained for a dipping time of 300 seconds. An example of a plot of the thickness of the IMC layer and how it changes with time for liquid can be seen in Figure1. The shape of the curve indicates a parabolic growth rate and the rate constant k can be calculated plotting the thickness versus the square root of time, see Equation 1 and Figure 1.

$$x^2 = k_1 t \rightarrow x = k\sqrt{t} \tag{1}$$

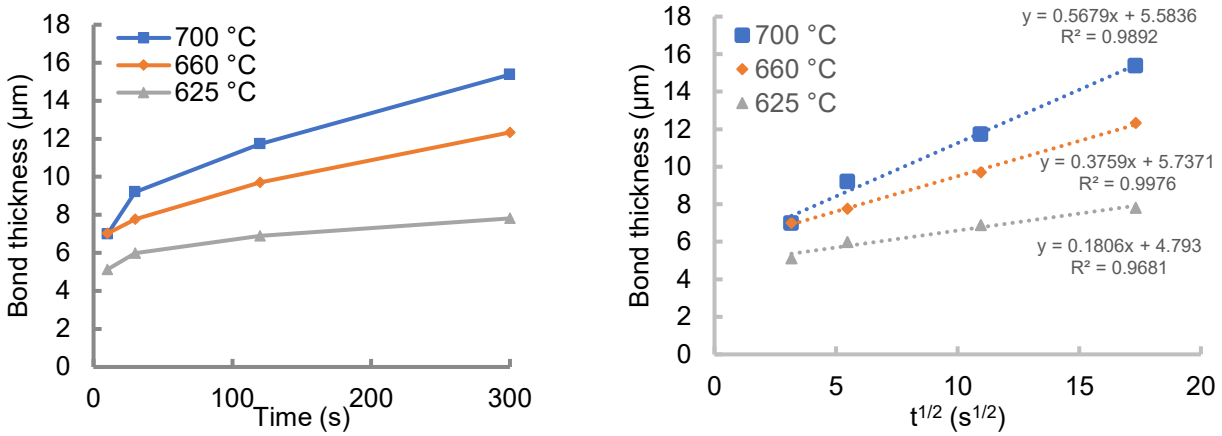


*Figure 1: Left: Growth curve for A356 prepared with 320 grit grinding paper. Right: Rate constants for the growth curve.*

There is a good fit for most of the samples using the parabolic rate law which indicates that the growth process is diffusion controlled which is in agreement with what other authors have reported[2]. The curve does not intersect 0 which could indicate that there is an initial step that is reaction controlled and therefore very fast as suggested by Dybkov[4]. The influence of temperature can be analyzed by assuming that the growth is diffusion controlled and treat the rate constants as diffusion coefficient, see Eq. 2.

$$D = D_0 exp\left(\frac{-Q}{RT}\right) \rightarrow k = k_0 exp\left(\frac{-Q}{RT}\right) \rightarrow k \sim exp\left(\frac{-Q}{RT}\right) \tag{2}$$

The value of the activation energy will give a quantitative measurement of how the temperature affects the growth of the IMC layer. The activation energy for the different parameters can be seen in Table 1. Due to the lack of interaction for the A356 120 grit samples no value could be calculated. The fit for calculating for 390-600 grit is very bad and therefore the results unreliable but the trend is the same.

*Table 1: Table of activation energies for the different experiments.*

| | 120 grit | 320 grit | 600 grit |
|---|---|---|---|
| ***A356*** | --- | 90 kJ/mol | 111 kJ/mol |
| ***390*** | -32 kJ/mol | -30 kJ/mol | (-7 kJ/mol) |

A high value for the activation energy indicates that growth is slower for equal temperatures. The difference between the different surfaces for the A356 samples would indicate that there are other factors than diffusion that influences the measured data. The materials and methods are the same for these samples but the very initial conditions, like the surface roughness, differ and can greatly influence the final results. The samples produced with a 120 grit grinding paper yields very little to none interaction between the liquid aluminum and the steel compared to both the 320 and 600 grit finish.

The activation energies calculated for when 390 is reacting with steel are negative. In a solid-solid diffusion couple this would indicate that diffusion slows down at with higher temperature. However, due to the solubility of iron in the liquid aluminum these values would indicate that the iron dissolution increases more with temperature relative to the IMC layer growth. The kinetics for the dissolution of iron was measured for liquid A356 and mild steel and were found to follow a linear relationship which corresponds well with literature[6].

*Phase characterization - A356*

Figure 2 shows an SEM analysis images of the IMC layer that forms between A356(bottom) and the steel(top) that is allowed to air cool. The layer close to the aluminum side consists of $\tau_5$ ($Al_{7.4}Fe_2Si$) and the layer closer to the steel consist of a $\eta$ ($Fe_2Al_5$) with precipitates of what can be assumed to be ternary Al-Fe-Si IMCs. In between these two layers there is an intermediary layer of $\theta$ ($Fe_3Al_{13}$).

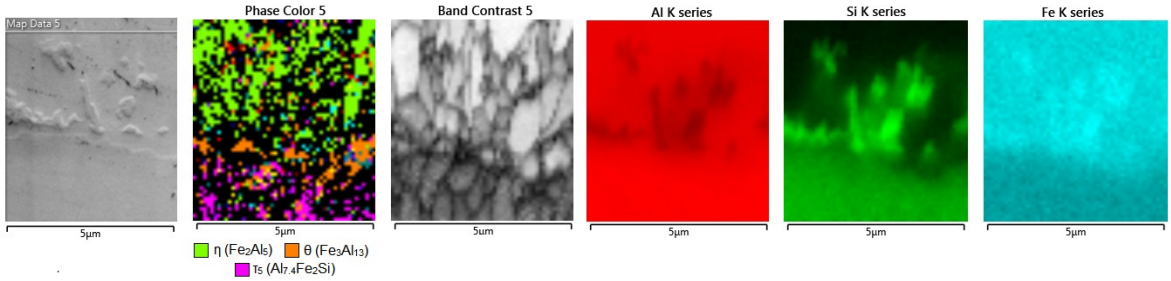


*Figure 2: EBSD and EDS analysis of the IMC layer produced by A356 at 700°C.*

Fig. 3 shows an SEM analysis images of the IMC layer that forms between A356(top) and the steel(bottom) after a water quench. Only one IMC layer is visible and was found to be $\tau_5$ ($Al_{7.4}Fe_2Si$). This indicates that it is the $\tau_5$ phase that grows during the liquid solid interaction. This phase breaks down during the air cooling to form two Al-Fe binary IMCs with precipitates of ternary Al-Fe-Si IMCs with higher silicon and iron content.

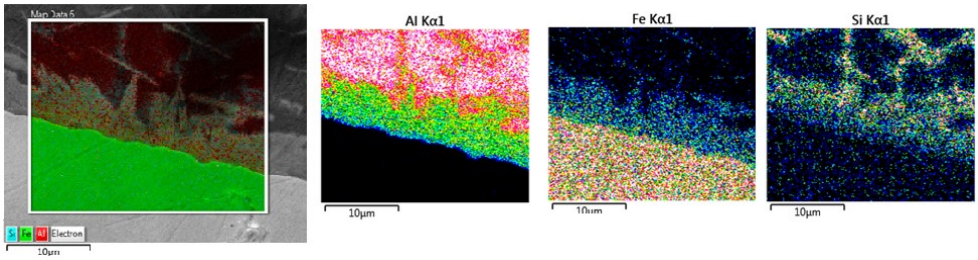


*Figure 3: EDS analysis of water quenched IMC layer formed by A356 at 700°C.*

Phase characterization – *390*
Figure 4 shows an SEM image of the IMC layer that forms between 390(bottom) and the steel(top). The layer close to the aluminum side consists of $\tau_4$ ($Al_3FeSi_2$) and the layer closer to the steel consist of a $\eta$ ($Fe_2Al_5$) with precipitates of what can be assumed to be ternary Al-Fe-Si IMCs. In between these two layers there are two layers, one thick binary consisting of $\theta$ ($Fe_3Al_{13}$) which also has precipitates of ternary Al-Fe-Si IMCs with higher silicon and iron content and a thin layer of $\tau_2$ ($Al_3FeSi$).

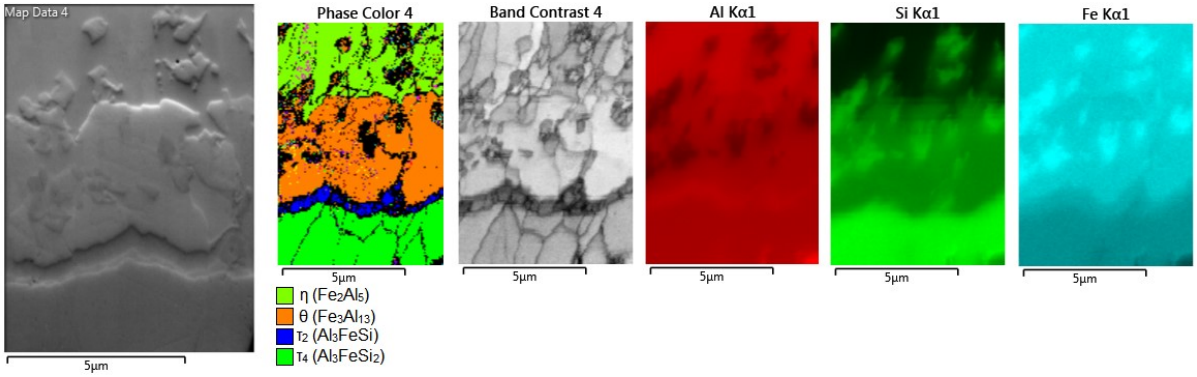


*Figure 4: EBSD and EDS analysis of the IMC layer produced by 390 at 700°C.*

**Conclusion**
Overall the growth of the IMC layer is diffusion controlled. However, there are indications that the very initial growth is governed by a reaction controlled step when diffusion distances are relatively small. For A356 samples the growth in the liquid-solid reaction starts with growth of the ternary $\tau_5$ ($Al_{7.4}Fe_2Si$) phase that is in equilibrium with the melt and the solid steel. Once removed from the melt this phase breaks down into two binary phases with ternary precipitates. The $\eta$ ($Fe_2Al_5$) is the most stable phase in contact with the steel grows into the steel. The growth of these binary layers occurs after the steel rod has been extracted from the melt and adds to its final thickness. The aluminum coated steel cools from the outside in resulting in growth due to the residual heat from the steel.The IMC layer in the 390 samples shows a more complex layered structure. The ternary IMC $\tau_4$ ($Al_3FeSi_2$) first converts to $\tau_2$ ($Al_3FeSi$) which in turns converts to the binary $\theta$ ($Fe_3Al_{13}$) and ternary Al-Fe-Si precipitates with higher Si and Fe content. As the inner $\eta$ ($Fe_2Al_5$) layer grows into the steel consuming the aluminum more $\eta$ ($Fe_2Al_5$) is formed from the $\theta$ ($Fe_3Al_{13}$).

The IMC layers are initially formed during the liquid solid interaction. However, once formed they will continue to develop and grow after solidification of the aluminum has occurred. This growth is accompanied by phase changes and is not negligible and can contribute to significant portions of the resulting metallurgical bond. It was also evident that short interaction times only allowed for very partial bonding and to achieve a continuous bond between the two metals the initial steps of the process needs to be accelerated.

**References**
[1] Eggeler, G., Vogel, H., Friedrich, J., and Kaesche, H., 1985, "Target Preparation for the Transmission Electron Microscopic Identification of the Al sub 3 Fe ( theta -Phase) in Hot-Dip Aluminised Low Alloyed Steel," Praktische Metallographie, 22(4), pp. 163-170.
[2] Springer, H., Kostka, A., Payton, E. J., Raabe, D., Kaysser-Pyzalla, A., and Eggeler, G., 2011, "On the formation and growth of intermetallic phases during interdiffusion between low-carbon steel and aluminum alloys," Acta Materialia, 59(4), pp. 1586-1600.

[3] Bouché, K., Barbier, F., and Coulet, A., 1998, "Intermetallic compound layer growth between solid iron and molten aluminium," Materials science & engineering. A, Structural materials : properties, microstructure and processing, 249(1), pp. 167-175.
[4] Dybkov, V. I., 1986, "Reaction diffusion in heterogeneous binary systems Part 1 Growth of the chemical compound layers at the interface between two elementary substances: one compound layer," Journal of materials science, 21(9), pp. 3078-3084.
[5] Zhe, M., 2011, "Chemical Changes at the Interface Between Low Carbon Steel and an Al-Si Alloy During Solution Heat Treatment," Journal of phase equilibria and diffusion, 32(6), pp. 486-497.
[6] Dybkov, V. I., 1990, "Interaction of 18Cr-10Ni Stainless-Steel with Liquid Aluminum," Journal of Materials Science, 25(8), pp. 3615-3633.

# Appendix C

# The influence of silicon during liquid-solid diffusion of aluminum and iron

## Introduction

The requirements for fuel efficiency in the transportation industry is driving the need for lightweight components. Aluminum castings combine good specific strength with a competitive price. However, for certain applications, it lacks in stiffness, strength, and wear resistance. There are opportunities to further lightweight traditionally ferrous components by replacing them with bimetallic composites of aluminum with cast-in ferrous inserts. The performance of composites depends on the interaction between the matrix and the reinforcing component. A chemical reaction between the aluminum alloy forming a metallurgical bond between the aluminum and the steel has proven to be advantageous for mechanical properties of the bond between the two metals [1, 2].

The chemical interaction forms a reaction layer between the aluminum and the iron which is influenced by both the composition of the ferrous alloy and aluminum alloy. Liquid pure aluminum will in contact with iron form an intermetallic compound (IMC) layer consisting of two phases. At the iron/IMC interface the binary η-phase ($Fe_2Al_5$) will grow with a tongue like an appearance and was first identified by Gebhardt and Obrowski[3]. It was later shown by [4] that there was a thin layer of θ-phase ($Fe_4Al_{13}$) at the IMC/liquid Al interface. The η-phase is easily distinguishable by microscope due to its characteristic tongue like appearance while the θ-phase is a thin layer fairly uniform layer[5-7].

Huemann and Dittrich[5] studied the crystal structure of the η-phase that there is a high vacancy concentration along the c-axis [001] inducing anisotropic diffusion and can thus explain the tongue like structure which has been confirmed by multiple authors[6, 8-11]. Takata et al.[7] studied density of high/low angle grain boundaries and dislocation density using electron backscatter diffraction (EBSD) maps and transmission electron microscopy (TEM) and suggested that the preferential diffusion can be due to the anisotropic volume change during the α-iron to η-phase transformation. The anisotropic change in volume induces stress fields which activates Herring-Nabarro creep and allows for vacancy flow to the sides of the η grains from the tip and aluminum flows in the opposite direction. The growth rate of the η-($Fe_2Al_5$) phase has been shown in principle to follow the parabolic rate law [8, 10] with a slight negative deviation. Parabolic growth behavior indicates that the growth is diffusion controlled and the negative deviation has been shown to be due to saturation of the aluminum melt[9, 12].

At the Al/IMC layer interface a θ-($Fe_4Al_{13}$) layer is present in multiple forms. It can be adhered to the interface, in close proximity, and there is the eutectic θ-($Fe_4Al_{13}$). While the eutectic phase forms due to the dissolution of iron into the liquid aluminum, it was suggested by Denner and Jones[13] the detached θ-($Fe_4Al_{13}$) could be due spallation of the θ-($Fe_4Al_{13}$)due to stress build up during growth of the IMC layer and a similar mechanism was suggested in[14]. The formation and growth of the attached θ-($Fe_4Al_{13}$) layer has been studied by multiple authors, and its formation has been described as either formation and growth by reactive diffusion [8, 10] or for elevated temperatures as precipitation on the η-($Fe_2Al_5$) layer during solidification[15]. Experiments by Bouayad et al. [8] showed that the θ-($Fe_4Al_{13}$) layer followed a linear growth rate indicating dissolution while experiments by Bouche et al. [10] indicated a parabolic growth.

The oxidation resistance of steels can be greatly improved by hot-dip aluminized coatings but a thick, brittle IMC layer is undesirable, and the possible advantages with metallurgical bonding within bimetallic castings of aluminum and steel have led to multiple studies on the effect of the addition of Si to the melt. Additions of Si to the liquid aluminum is known to reduce the thickness of reaction layer, specifically the growth rate of η-($Fe_2Al_5$) is reduced[6, 16-20]. Komatsu et al. [19] reported that there was a change in microstructure (a ternary Al-Fe-Si phase layer at the IMC/Al interface) for more than 3wt.% Si in the liquid aluminum and work done by Eggeler et al. [20] showed that for Si

concentrations below 2 wt.% there is no change in the major constituents ($Fe_2Al_5$ and $Fe_4Al_{13}$) layer. Springer et al.[6] showed that for melts containing 5 wt.% Si formed a third layer consisting of the ternary Al-Fe-Si phase $Al_{7.4}Fe_2Si$ ($\tau_5$). A similar investigation by Zhe et al. [21] using a commercial alloy, A356 (~7.5 wt% Si and 0.35 wt.% Mg), showed that for fast cooling rates the outer $\tau_5$ phase forms and with slower cooling rates an additional ternary phase $Al_{4.5}FeSi$ ($\tau_6$).

Several mechanisms behind the reduced growth rate of η-($Fe_2Al_5$) due to the presence of Si has been suggested. Nicholls [17] suggested that the Si occupies the structural vacancies of the η-($Fe_2Al_5$) phase and slows down diffusion. Komatsu et al.[19] suggested that the addition of Si to the liquid aluminum increases the dissolution of Fe while experiments performed by Eggeler et al. [20] showed that there is no significant increase in dissolution Fe and concluded that the decrease is due to a solid-state phenomenon. In a more recent study, Lemmens et al. [22] were able to detect elevated Si concentrations at the η-($Fe_2Al_5$)/θ-($Fe_4Al_{13}$) interface which could be a contributing factor to the reduced growth.

The maximum concentration of Si in the η-($Fe_2Al_5$) phase is approximately 2 wt.%[20]. In systemic study Springer et al.[6] noticed discrepancies relating to the Si concentration in the η-($Fe_2Al_5$) layer when comparing the growth rate between a solid/solid pure Al/steel and an semi-solid/solid Al(5 wt.% Si)/steel diffusion couples. The Si containing η-($Fe_2Al_5$) layer was growing at a higher rate compared to the pure diffusion couple. A study on the growth rate by [23] indicated an almost constant Si concentration (2 wt.%) in the η-($Fe_2Al_5$) phase for Al-Si/iron with Si concentrations up to 3 wt.%. The work by [6] indicates that the Si concentration in the η-($Fe_2Al_5$) layer cannot by itself explain the differences in growth rate and the data provided in [23] shows a significant reduction in growth rate with an almost constant Si concentration within the η-($Fe_2Al_5$) phase. The microstructure of the growing reaction layer seems to affect the kinetics of the system, and the Si concentration in the aluminum can completely change the microstructure by the formation of ternary Al-Fe-Si compounds. From the above discussion, it is also evident that the analyzed microstructure is dependent on cooling rate and therefore it also needs to be considered. The work by [24] shows a strong relationship between formed IMC layers and the ternary phase diagrams.

**Objective**

The objective of this study is to investigate the effect of Si on microstructure and growth rate for liquid binary Al-Si alloys and solid steel diffusion couples. Low (0.5 - 5wt.% Si) and high (5 - 15 wt.% Si) binary alloys will be investigated to try further to shed light on the relationship between microstructure and growth rate in Al-Fe liquid-solid diffusion couples.

**Experimental**

Mild steel coupons with the dimensions 38 mm x 19 mm x 1.5 mm were cut from the stock cold-rolled 1008 steel, the composition can be seen in Table 1. The specimens were ground to a 600-grit finish, producing a surface roughness value, $R_a$, of 0.3 μm, degreased in ethanol and acetone in an ultrasonic bath for 5 minutes, pickled in a 10%HCl solution for 1 minute, rinsed in deionized water, ultrasonically cleaned in acetone for 30 seconds and allowed to dry. To accurately determine the thickness of the steel after surface preparation and account for any material removal the top section of the coupon was covered in a boron nitride coating to prevent interaction with the aluminum alloy. The maximum time in contact with air before submersion in liquid Al was 10 minutes.

The aluminum alloy was prepared in an induction furnace by melting approximately 4.5 kg of pure Al (99.99%) ingots and adding pure Si (99.95%) chips at a temperature of 750°C±15°C and holding for 30 minutes. Aluminum alloy ingots were cast and cut into smaller pieces. The exact composition of the Al alloys used in the experiments can be seen in Table 1. A resistance furnace was preheated to

50°C above desired reaction temperature, and 0.6 kg of aluminum alloy was placed in a silicon carbide crucible and placed in the furnace.

*Table 1: Composition of the steel and aluminum alloys.*

| | Chemical Composition (wt.%) | | | | |
|---|---|---|---|---|---|
| | C | Mn | P | S | Fe |
| Steel (1008) | 0.09 | 0.36 | 0.033 | 0.025 | Bal. |

| | Si | Fe | Al |
|---|---|---|---|
| 0.5% Si | 0.55 | 0.015 | Bal. |
| 1% Si | 1.02 | 0.012 | Bal. |
| 1.5% Si | 1.63 | 0.034 | Bal. |
| 2% Si | 1.96 | 0.029 | Bal. |
| 2.5% Si | 2.58 | 0.026 | Bal. |
| 5% Si | 4.93 | 0.036 | Bal. |
| 7.5% Si | 7.25 | 0.052 | Bal. |
| 10% Si | 10.51 | 0.04 | Bal. |
| 15% Si | 14.91 | 0.055 | Bal. |

Once the melt had reached the desired reaction temperature the furnace temperature was lowered to a previously determined temperature to keep the reaction temperature constant with minimal variation, ±5°C. The temperature drop due to insertion of the cold steel was measured to be less than ~3°C in the melt. Right before immersion, the aluminum surface was skimmed of oxides and the time between immersion and skimming was less than 1 second. After the desired reaction time the aluminum was carefully extracted and immediately quenched in water at room temperature. The experimental matrix with temperature, time and alloy for all experiments can be seen in Table 2, and two sample for each condition was prepared.

*Table 2: Experimental matrix where X= 625°C, Y=675°C, and Z = 750°C.*

| | | Time (min) | | | |
|---|---|---|---|---|---|
| | | 5 | 20 | 60 | 180 |
| Pure Al | (A) | Y | Y | Y | Y |
| 0.5% Si | (A0.5) | Y | Y | Y | Y |
| 1% Si | (A1) | Y | Y | Y | Y |
| 1.5% Si | (A1.5) | Y | Y | Y | Y |
| 2% Si | (A2) | Y | Y | Y | Y |
| 2.5% Si | (A2.5) | Y | Y | Y | Y |
| 5% Si | (A5) | Y | Y | Y | Y |
| 7.5% Si | (A7.5) | Y | Y | Y | Y |
| 10% Si | (A10) | X Y | X Y | X Y | X Y |
| 15% Si | (A15) | Y Z | Y Z | Y Z | Y Z |
| X = 625°C Y = 675°C Z = 750°C | | | | | |
| One 10 wt.% Si diffusion couple at 875°C for 2 minutes due to excessive dissolution. | | | | | |

Surface roughness measurements of the steel were measured using an Olympus LEXT 3D Measuring Laser Microscope, and the composition of the steel and aluminum alloys was measured using a Spectro Maxx LMM14. A cross section of the diffusion couple was cut perpendicular to the diffusion direction. All samples were cut at the same location. The samples were prepared using standard metallurgical preparation methods and analyzed by optical microscopy and by scanning electron microscopy(SEM) techniques. All of the SEM analysis were performed in a JEOL JSM-7000F equipped with Oxford Instruments EDS detector X-Max$^N$ and EBSD detector NordlysMax$^2$.

The crystal structure data used for phase identification with EBSD analysis and the designations used for the binary and ternary IMC in this paper can be seen in Table 3.

*Table 3: Crystal structure data used for EBSD analysis.*

| Symbol | Composition | Space group | References |
|---|---|---|---|
| $\eta$ | $Fe_2Al_5$ | Cmcm (63); orthorhombic | [25] |
| $\theta$ | $Fe_4Al_{13}$ | C2/m (12); monoclinic | [26] |
| $\tau_1$ | $Al_2Fe_3Si_3$ | P1 (2), triclinic | [27] |
| $\tau_2$ | $Al_3FeSi$ | R-3 (148); hexagonal | [28] |
| $\tau_3$ | $Al_2FeSi$ | Cmma (67); orthorhombic | [29] |
| $\tau_4$ | $Al_3FeSi_2$ | I4/mcm (140); tetragonal | [30] |
| $\tau_5$ | $Al_{7.4}Fe_2Si$ | P6_3/mmc (194); hexagonal | [31] |
| $\tau_6$ | $Al_{4.5}FeSi$ | A2/a (15); monoclinic | [32] |

**Results**

*Microstructural Characterization*

Optical micrographs of the progression of the reaction layer with respect to time (row) and Si concentration (column), for the temperature was 675°C, can be seen in Figure 1(please note the different scales between low and high Si concentrations). The top light gray side of the image is the Al alloy, and the bottom darker gray part is the steel. The well-known characteristic tongue like morphology [6, 8-10] is visible for Si concentrations up to 1.5 wt.%Si at shorter diffusion times (up to 20 minutes) and then transforms to a smoother interface. However, after 60 minutes of reaction time, the $\eta$-($Fe_2Al_5$)/steel interface starts to become serrated for diffusion couple with between 2 and 15 wt.% Si. The thickness of the IMC layer increases with increasing reaction time and decreases with increasing Si content in the liquid aluminum. A crack and pore free reaction layer between the steel and the liquid Al was able to form and withstand the water quench. The porosity visible in the A, A0.5 and A2 180 minutes' samples are due to the relatively rough grit used during sample preparation. For samples with an Si concentration of 7.5 and above only one distinct IMC layer is visible after 5 minutes of diffusion, see top left corner of Figure 1. After 20 minutes, there are two distinct layers visible, and the high Si-containing samples also show significantly thinner reaction layer.

To study the phases growing during the liquid-solid diffusion of Al-Si alloys several samples were selected for further analysis. The Al-steel reaction layer has been extensively studied[6, 7] and it has been reported that ternary Al-Fe-Si compounds start forming at a Si concentration of 2.5 wt% [33], so samples were selected for phase characterization A1, A2, A2.5, A5, A7.5, A10, and A15. As previously mentioned there seems to be a delay in the formation of the inner IMC layer and therefore samples that were hot-dipped at 675°C for 60 minutes were selected. To further study the effect of Si and

temperature an A10 sample prepared at 625°C (60 minutes) and A15 samples dipped at 750°C (60 minutes) and 875°C (2 minutes) were prepared for phase analysis.

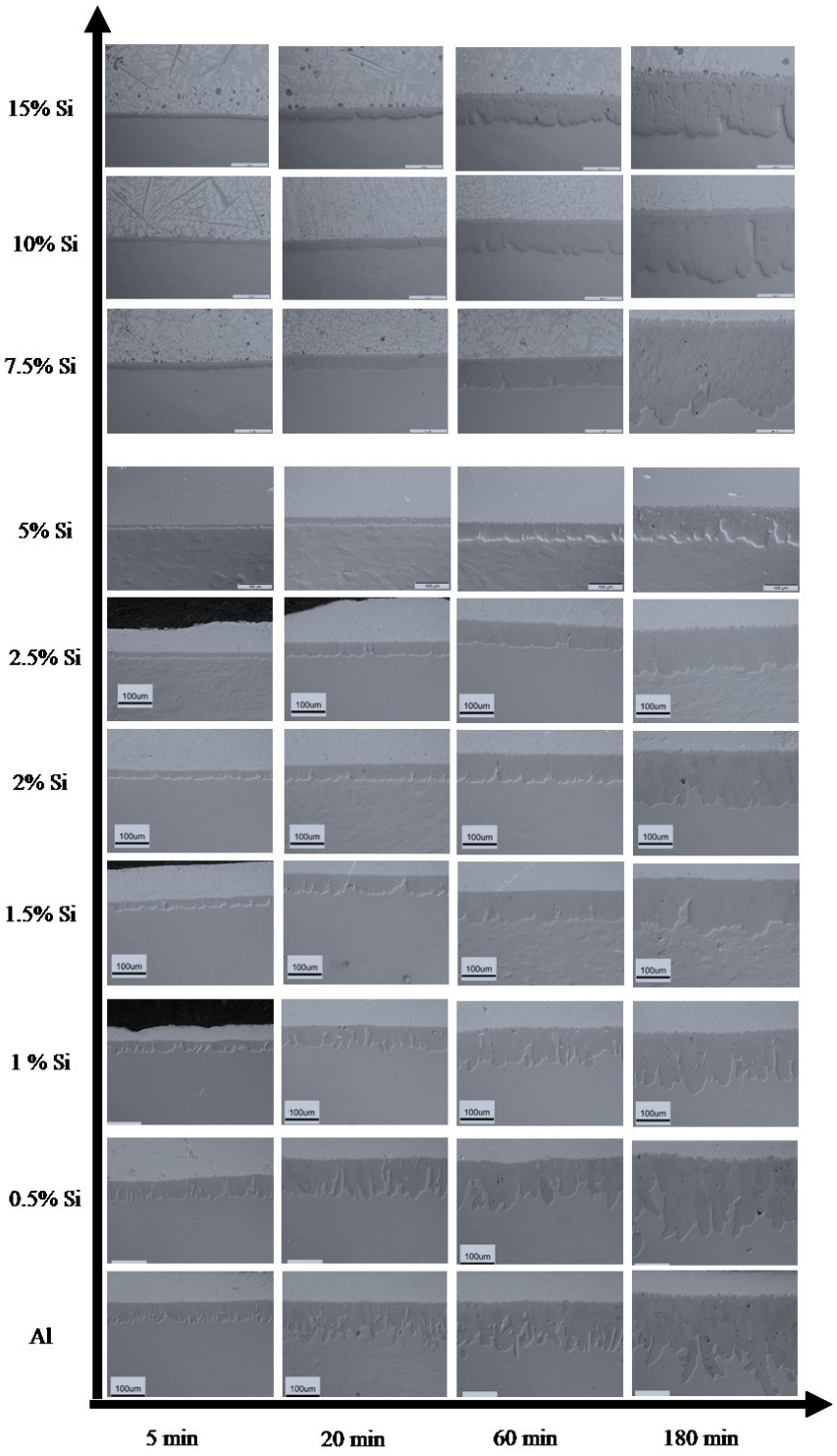


*Figure 1: Microstructural development of the reaction layer with time and Silicon content. Please not the difference in scale for the upper three rows.*

Figure 2 shows representative EBSD phase maps for A1, A2, A2.5, and A5 samples with the band contrast superimposed to indicate the grain structure of four samples. The red color represents BCC Fe, the blue colored phase in contact with the Fe the η-($Fe_2Al_5$) phase, the magenta colored area is the θ-($Fe_4Al_{13}$) phase, and the cyan is FCC Al. The yellow phase represents the ternary Al-Fe-Si phase $\tau_1$-($Al_2Fe_3Si_3$). Overall the reaction layer mostly consists of a thick η-($Fe_2Al_5$) layer in contact with the steel and a thinner θ-($Fe_4Al_{13}$) layer in contact with the aluminum. There are what could be described as $\tau_1$-($Al_2Fe_3Si_3$) precipitates within the η-($Fe_2Al_5$) layer consistent with previous studies [6, 21]. Comparing Figure 2a (A1) with Figure 2b (A2), it can be seen that the difference in thickness that is thickness is largely due to a thinner η-($Fe_2Al_5$) layer. The difference in thickness of the η-($Fe_2Al_5$) layer is even more pronounced in both Figure 2c and 2d and increasing the Si content in the aluminum alloy will increase the amount of $\tau_1$-($Al_2Fe_3Si_3$) precipitates within the η-($Fe_2Al_5$) layer. There is also a rather thick black line of poor band contrast and no phase recognition which is most likely due to uneven polishing due to the difference of chemical attack on the dissimilar metals used during sample preparation. Figure 2d shows the phase map for the 5% sample which shows the θ-($Fe_4Al_{13}$) layer in contact with aluminum while it was previously reported to consist of $\tau_5$-($Al_{7.4}Fe_2Si$) [6, 33, 34] which could be due to the high cooling rate the sample is exposed to during the water quench. Figure 2e shows the inverse pole figure(IPF) of Figure 2d and confirms the directional growth of the η-($Fe_2Al_5$) layer is along the c-axis [001] similarly to [5-7, 9].

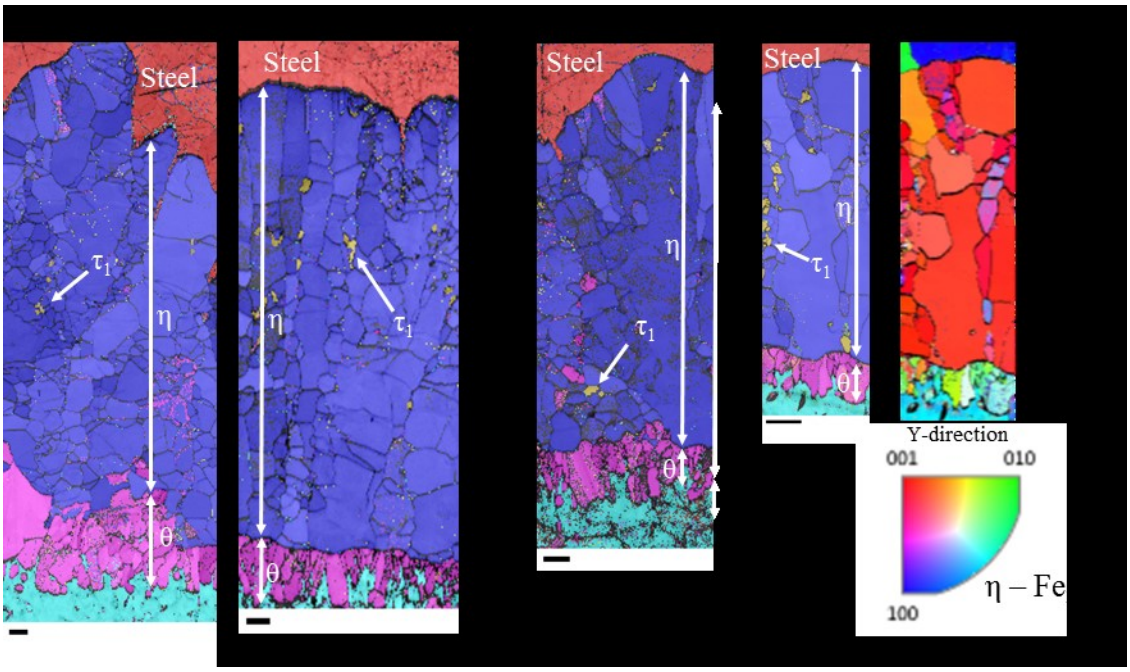


Figure 2: EBSD phase maps with superimposed band contrast for a) A1, b) A2, c) A2.5, and d) A5 samples dipped for 60 minutes at 675°C. e) is the IPF map in the Y direction for the A5 sample with the corresponding orientation triangle for the η-($Fe_2Al_5$) phase.

The Si concentration within the microstructure of the samples consisting of the two binary η-($Fe_2Al_5$) and θ-($Fe_4Al_{13}$) phase layers was measured by EDS analysis. The average Si concentration within the η-($Fe_2Al_5$) layer, can be seen in Figure 3 and is very close to the composition of the liquid Al up to the saturation limit of the η-($Fe_2Al_5$) (2wt%) which corresponds well with [20].

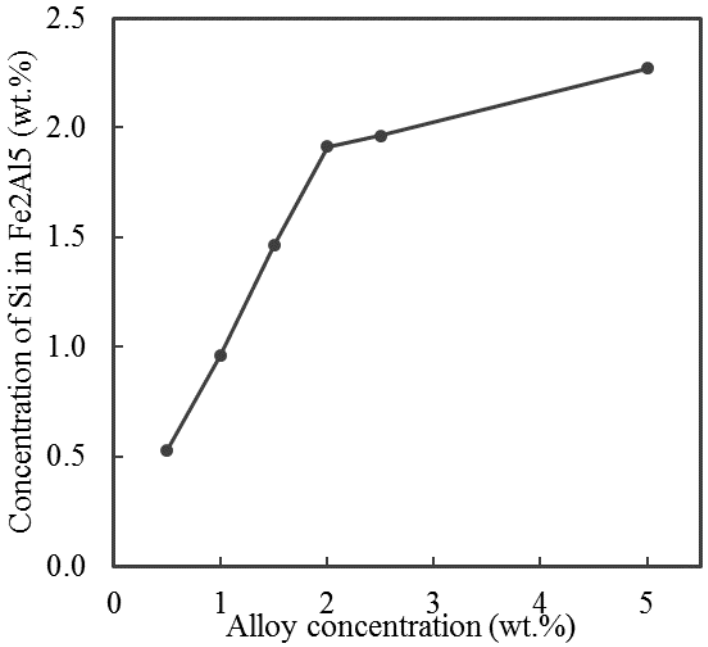


*Figure 3: Si concentration within the η-($Fe_2Al_5$) layer for Si concentrations up to 5 wt.% Si.*

Additions of 7.5 wt.% of Si to the liquid aluminum resulted in a change of the phases present within the reaction layer. Figure 4a shows an EBSD phase map of the phases formed after one hour for the A7.5 sample, and there are four phases present in the formed reaction layer. Similarly, to the lower Si-containing samples, the η-($Fe_2Al_5$)(blue) is in contact with the steel and is the major phase contributing to the thickness. There is an outer $\tau_5$-($Al_{7.4}Fe_2Si$)(green) layer in contact with aluminum and precipitates of $\tau_1$-($Al_2Fe_3Si_3$)(yellow) within the η-($Fe_2Al_5$) layer. At the interface of η-($Fe_2Al_5$) and $\tau_5$-($Al_{7.4}Fe_2Si$), there are in certain locations a thin discontinuous layer of θ-($Fe_4Al_{13}$)(magenta) phase. The inverse IPFs for the EBSD map can be seen in Figure 4b while the previously mentioned directional growth of the η-($Fe_2Al_5$) layer can be seen. However, the IPFs does not reveal a preferential growth direction for the columnar grains of the $\tau_5$-($Al_{7.4}Fe_2Si$) phase.

The phases present in the reaction layer for the A10 sample at 675°C is almost identical to the A7.5 sample, compare Figure 4a with 4c, with one difference in lacking any formation of θ-($Fe_4Al_{13}$) phase at the η-($Fe_2Al_5$)(blue)/$\tau_5$-($Al_{7.4}Fe_2Si$)(green) interface. Columnar $\tau_5$-($Al_{7.4}Fe_2Si$) crystals seem to stack on top of each other forming a slightly thicker layer. There also seems to be a larger quantity of $\tau_1$-($Al_2Fe_3Si_3$)(yellow) precipitates within the η-($Fe_2Al_5$) layer. Figure 4d shows an EBSD phase map of the A15 sample after one hour of reaction time at 675°C and additionally to the η-($Fe_2Al_5$) layer there is two ternary Al-Fe-Si layers, $\tau_2$-($Al_3FeSi$) (dark red) and $\tau_4$-($Al_3FeSi_2$)(dark blue). There is also a very small amount of θ-($Fe_4Al_{13}$) phase present at the η-($Fe_2Al_5$)/$\tau_2$-($Al_3FeSi$) interface as well as a significant amount of $\tau_1$-($Al_2Fe_3Si_3$) precipitates.

The absence or a very small amount of θ-($Fe_4Al_{13}$) between the outer ternary phase layer is interesting since a relatively thick layer is commonly reported for longer diffusion times[6, 33, 34]. A very thin θ-($Fe_4Al_{13}$) layer could be present is and not detected by the analytical tools used. Or due to the very high cooling rate during quenching, the θ-($Fe_4Al_{13}$) layer does not have time to form during this step.

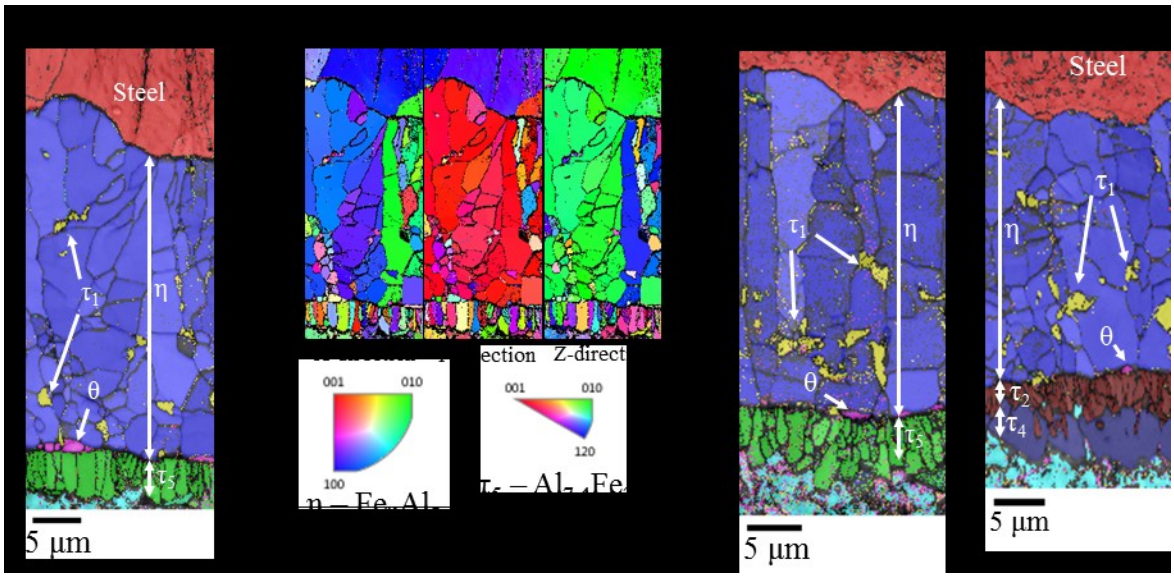


Figure 4: EBSD phase maps with superimposed band contrast for a) A7.5, c) A10, d) A15 samples dipped for 60 minutes at 675°C. b) is the IPF map in the X, Y, and Z direction for the A7.5 sample with the corresponding orientation triangle for the $\tau_5$-($Al_{7.4}Fe_2Si$) and η-($Fe_2Al_5$) phase.

The effect of temperature on microstructure for the A10 and A15 samples can be seen in Figure 5. Reducing the temperature to 625°C for the A10 sample forms a reaction layer composition of η-($Fe_2Al_5$)(blue) and $\tau_5$-($Al_{7.4}Fe_2Si$)(green) there are an outer $\tau_6$-($Al_{4.5}FeSi$)(orange) in contact with the aluminum, see Figure 5a. There is also a significant amount of θ-($Fe_4Al_{13}$) phase that seems to have grown into the η-($Fe_2Al_5$) phase, and there appear to be less and smaller $\tau_1$-($Al_2Fe_3Si_3$) precipitates compared to the A10 sample at 675°C (Figure 4c). Figure 5b and c show the reaction layer of 15 wt.% Si at 750 and 875°C respectively. Increasing the temperature significantly reduces the overall thickness of the IMC layer which is due in large part to the absence of a thick η-($Fe_2Al_5$) layer. The outer layer consists of $\tau_2$-($Al_3FeSi$) phase, and there is a visible θ-($Fe_4Al_{13}$) layer within the structure. At 875°C there is an absence of the η-($Fe_2Al_5$) layer in Figure 5c only one layer of $\tau_2$-($Al_3FeSi$) grains compared to multiple layers at 750°C.

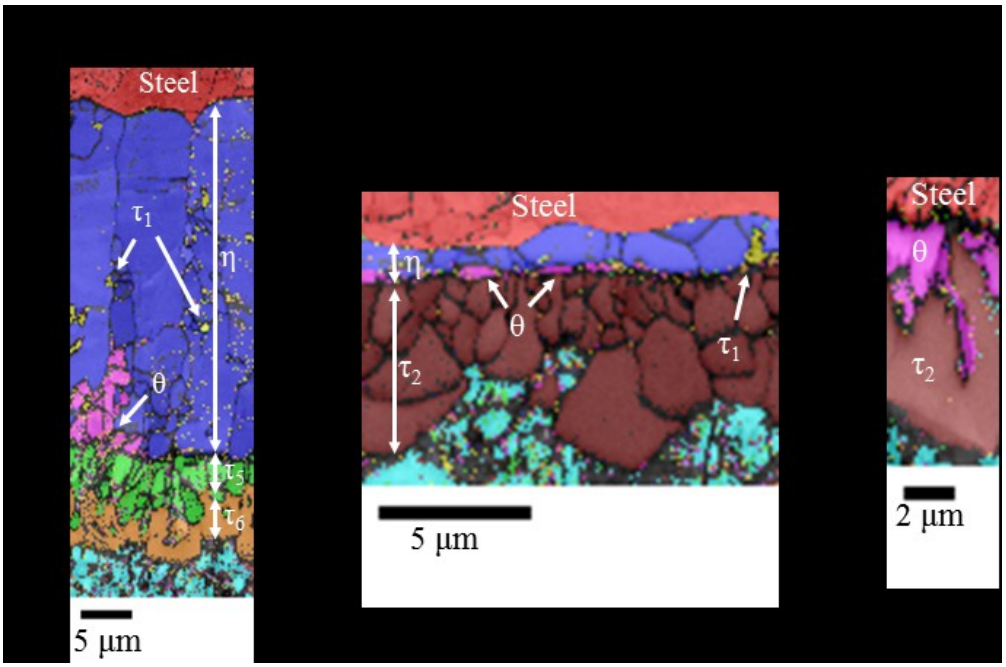

Figure 5: EBSD phase maps with superimposed band contrast for a) A10 sample dipped for 60 minutes at 625°C. b) A15 sample dipped for 60 minutes at 750°C and c) the A15 samples dipped for 2 minutes at 875°C.

*Growth Kinetics of the Reaction layer*

The growth kinetics of the IMC layer is known to be parabolic in nature [6, 8-10, 12]. A plot of the growth rate of the η-($Fe_2Al_5$) layer for samples with 5 wt.% and less Si content can be seen in Figure 6a. A linear fit with the square root of time shows a parabolic growth rate relationship with time the rate constant can be calculated using Equation 1.

$$x = k\sqrt{t} \qquad \text{(Equation 1)}$$

Rate constants for the diffusion couples are summarized in Table 4, and the thickness data shows some scatter but overall a good fit. The standard deviation was larger for samples containing less Si due to the tongue like morphology difference. Increasing the Si content in the liquid aluminum decreases the growth rate constant without a change of in the major constitutes of the reaction layer. Comparing the thickness of the θ-($Fe_4Al_{13}$) layer in Figure 2 there is noticeable thickness difference between the A1 sample and the A2 sample while the difference between the other (A2, A2.5, and A5) is less noticeable. In Figure 4b the measured thickness of the θ-($Fe_4Al_{13}$) layer is plotted vs. the square root of time. While it shows a good fit to the parabolic equation, it is more difficult to distinguish a clear relationship between the thickness and the Si content. There is a tendency as mentioned above that the layer gets thinner with increasing silicon content.

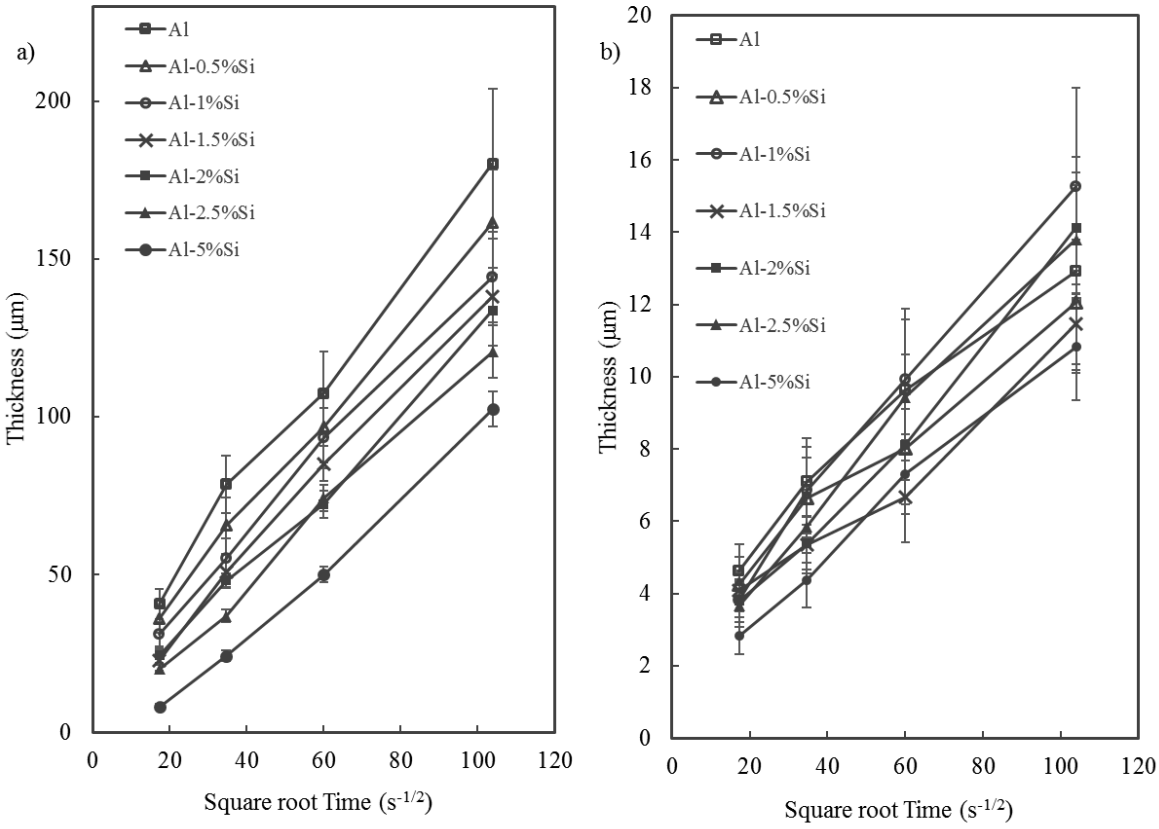


*Figure 6: Thickness vs. square root of time curves for a) the η-($Fe_2Al_5$) layer and b) the θ-($Fe_4Al_{13}$) layer.*

The growth rate of the η-($Fe_2Al_5$) layer for the high Si-containing (7.5 wt.% and above) can be seen in Figure 7a and shows a good fit. Increasing Si content tends to decrease the growth rate of the of the η-($Fe_2Al_5$) layer. The thickness vs. time plot for the outer ternary Al-Fe-Si layer is shown in Figure 7b. Interestingly highest growth rate of the ternary Al-Fe-Si layers is the low-temperature A10, and the growth rate of the η-($Fe_2Al_5$) phase in the A10 samples at 625°C and 675°C are very similar despite the temperature difference, see Table 4. The A7.5 and A10 sample have the same microstructure, but the growth rate of $\tau_5$-($Al_{7.4}Fe_2Si$) is slightly higher. The growth of $\tau_2$-($Al_3FeSi$) phase in the A15 sample at 750°C shows a negative growth rate which is likely due to the excessive dissolution of the steel substrate and the entire sample was dissolved before 180 minutes of reaction time.

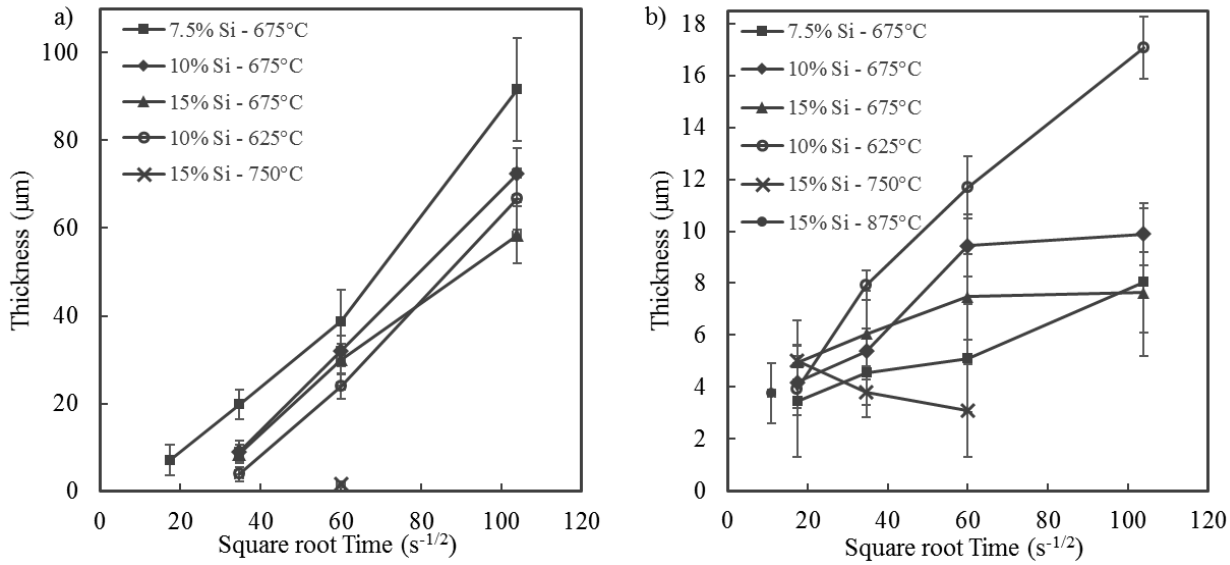


*Figure 7: Thickness vs. square root of time curves for a) the η-($Fe_2Al_5$) layer and b) the ternary layer/layers.*

*Table 4: Calculated rate constants for the different the IMC layers of the different samples.*

| | Temperature | 675°C | | | | | | | | | | 625°C | 750°C |
|---|---|---|---|---|---|---|---|---|---|---|---|---|---|
| | Sample | Al | A0.5 | A1 | A1.5 | A2 | A2.5 | A5 | A7.5i | A10 | A15 | A10 | A15 |
| Rate constant (µm/s$^{1/2}$) | η | 1.56 | 1.42 | 1.31 | 1.32 | 1.24 | 1.18 | 1.09 | 0.98 | 0.91 | 0.65 | 0.91 | |
| | θ | 0.09 | 0.08 | 0.13 | 0.08 | 0.12 | 0.12 | 0.09 | | | | | |
| | $\tau_5$ | | | | | | | | 0.05 | 0.07 | | | |
| | $\tau_4 + \tau_2$ | | | | | | | | | | 0.03 | | |
| | $\tau_6 + \tau_5$ | | | | | | | | | | | 1.48 | |
| | $\tau_2$ | | | | | | | | | | | | -0.04 |

*Dissolution of Fe*

The dissolution of Fe into the liquid Al was investigated by measuring the remaining cross-sectional area of steel and reaction layer. The remaining area of the steel in the diffusion couples was measured and is summarized in Figure 8a. The steel area reduction (left y-axis) is plotted with respect to Si concentration(x-axis) for different diffusion times and the saturation limit of Fe in the liquid Al alloy is plotted as a dotted line with the corresponding values on the right y-axis. The area reduction initially decreases with increasing Si content and increasing until it reaches a minimum between 1 and 2.5 wt% of Si. Then the steel area of steel seems to slightly decrease up 10 wt.%Si. Interestingly, initially, the amount of steel transformed to IMC decreases with increasing solubility of Fe in Al alloy which is inversely proportional to the solubility limit of Fe in the liquid.

The area of dissolved solid of the diffusion couple is plotted in Figure 8b (if the area measured in Figure 5a is subtracted from the area measured in Figure 5b it equals the total area of the reaction layer). The results show that the dissolution of Fe into the melt increases with increasing Si content of the melt and which is to be expected since the solubility limit of the liquid aluminum increases with Si concentration in the liquid aluminum.

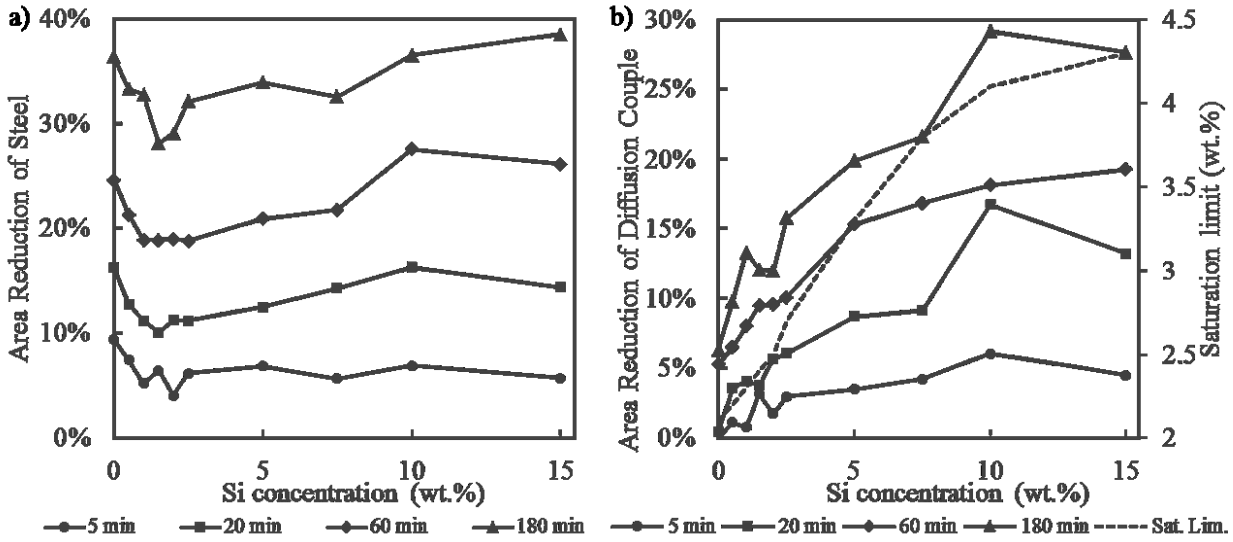


*Figure 8: a) Area reduction in percent of the steel b) Total area reduction of the diffusion couple. The dotted line represents the saturation limit of Fe in the liquid aluminum and reads of the right y-axis.*

**Discussion**

*Effect of Si on Microstructure of Liquid-Solid Al-Fe Diffusion Couples*

The microstructure formed between liquid Al-Si alloys of various composition is shown in Figure 2, 4 and 5. Composition, temperature and time change phase composition of the formed reaction layer. The outer layer of the reaction layer in contact with the melt is the phase that is in equilibrium with the melt at elevated Fe concentrations and is thus both dependent on Si concentration and temperature. Shorter diffusion time (5 minutes) combined with higher Si concentrations (10 wt.% and above) did not show the presence of the binary Al-Fe compounds η-($Fe_2Al_5$) and θ-($Fe_4Al_{13}$). Since the outer layer generally consists of the phase that is in equilibrium with the liquid composition and there seems to be a delay time for the binary phases to break through and start growing. Similar results have been shown for other aluminum alloys in studies by [21, 34]. There is an interesting difference between the A7.5 sample and A10 sample since at 675°C they should consist of the same microstructure but the elevated Si concentration seems to delay the formation of a binary layer further.

The A5 sample showed an anomaly by the presence of an outer θ-($Fe_4Al_{13}$) layer when compared to literature where $\tau_5$-($Al_{7.4}Fe_2Si$) has been reported[6, 34]. This is likely due to the difference in cooling rate since $\tau_5$-($Al_{7.4}Fe_2Si$) becomes more stable for lower Fe concentrations as temperature decreases, see the isopleth of ternary Al-Fe-Si phase diagram generated in Thermocalc in Figure 9.

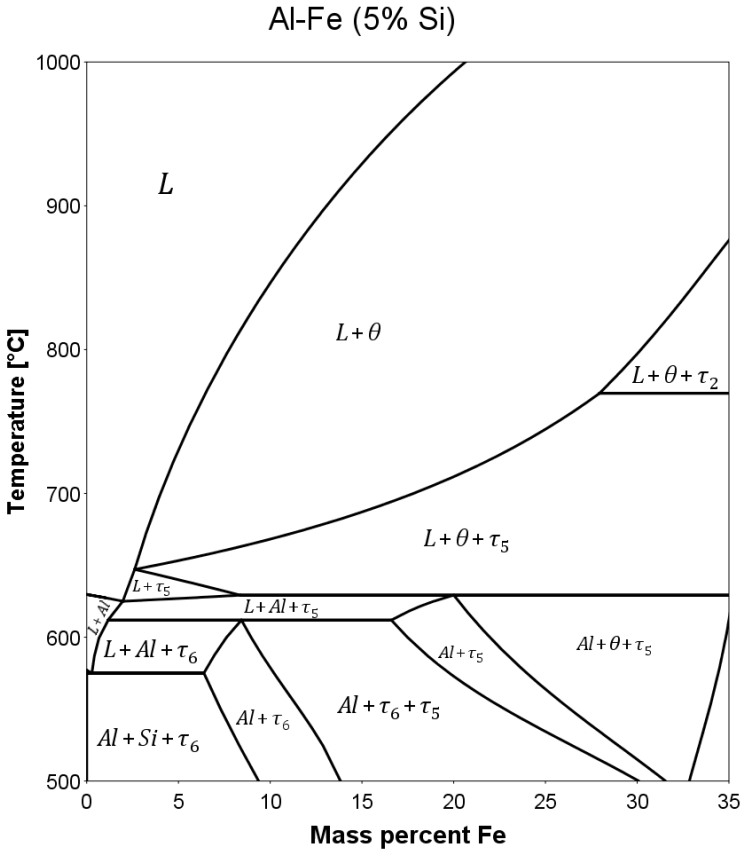


*Figure 9: Al-Fe phase diagram isopleth at 5 wt.% Si.*

The absence of a continuous θ-($Fe_4Al_{13}$) layer phase in Figure 2, 4 and 5 could be an artifact due to insufficient resolution of the characterization methods or excessive removal during the sample preparation. A thin θ-($Fe_4Al_{13}$) layer could be indicating two things. Either that diffusion rate of Al through the η-($Fe_2Al_5$) layer is higher compared to the Al diffusion through the ternary compound layer or diffusion of Fe out through the ternary layer is slow causing a higher iron concentration stabilizing the η-($Fe_2Al_5$) layer. Assuming that θ-($Fe_4Al_{13}$) has a slow formation time and/or low growth rate. Similarly, the $FeAl_2$ or FeAl were not present during the analysis which was explained by Bouche et al.[10] and is due to slow nucleation rates and low growth rate.

From microstructural observations, it was observed that after 20 minutes of reaction time what seems to be a stationary reaction layer sequence is formed, and diffusion paths in the ternary phase diagram can describe the microstructure[21, 24]. Based on the identified phases shown in Figure 2, 4, and 5 suggested diffusion paths for the formed microstructures can be seen in Figure 10 in isothermal ternary Al-Fe-Si phase diagrams generated Thermocalc. The red lines indicate a phase of interest which are $\tau_1$-($Al_2Fe_3Si_3$), $\tau_2$-($Al_3FeSi$), $\tau_4$-($Al_3FeSi_2$), $\tau_5$-($Al_{7.4}Fe_2Si$), $\tau_6$-($Al_{4.5}FeSi$), η-($Fe_2Al_5$), and θ-($Fe_4Al_{13}$). The diffusion path starts in the liquid (see color coded arrow for alloy) and follows the path indicated by the colored line. In Figure, 10a suggested diffusion paths for the experiments performed at 675°C with the different Si concentrations are color-coded. The red triangle shows where a magnification of the ternary phase diagram was taken and is shown in Figure 10b and the purple line shows the diffusion path from the binary θ-($Fe_4Al_{13}$) phase to the Fe with a dotted purple line indicates the missing $FeAl_2$ and FeAl phase. A magnified phase diagram is taken at 675°C but represents this section fairly well

for the temperature range 625-875°C. The diffusion paths at for the A10 sample at 625°C can be seen in Figure 10c and for the A15 sample in Figure 10d.

The solid and dotted blue lines in Figure 10e shows two possible diffusion paths. The corresponding microstructure can be seen in Figure 5c and consists of a θ-($Fe_4Al_{13}$) layer in contact with the steel and a $\tau_2$-($Al_3FeSi$) layer in contact with the aluminum. If the diffusion path follows the same pattern as the others, it should follow the solid blue line while the microstructure indicates that it follows the dotted blue line. A SEM micrograph of the reaction layer can be seen in Figure 11 the θ-($Fe_4Al_{13}$), and $\tau_2$-($Al_3FeSi$) layers and the boundary are indicated. The white arrows show spots of Al in between the two reaction layers and the $\tau_2$-($Al_3FeSi$) layer shows a blocky morphology compared to the $\tau_2$-($Al_3FeSi$) layer formed at 750°C. This indicates that the phase formed during cooling and precipitated onto the interface making the solid blue line the more likely diffusion path.

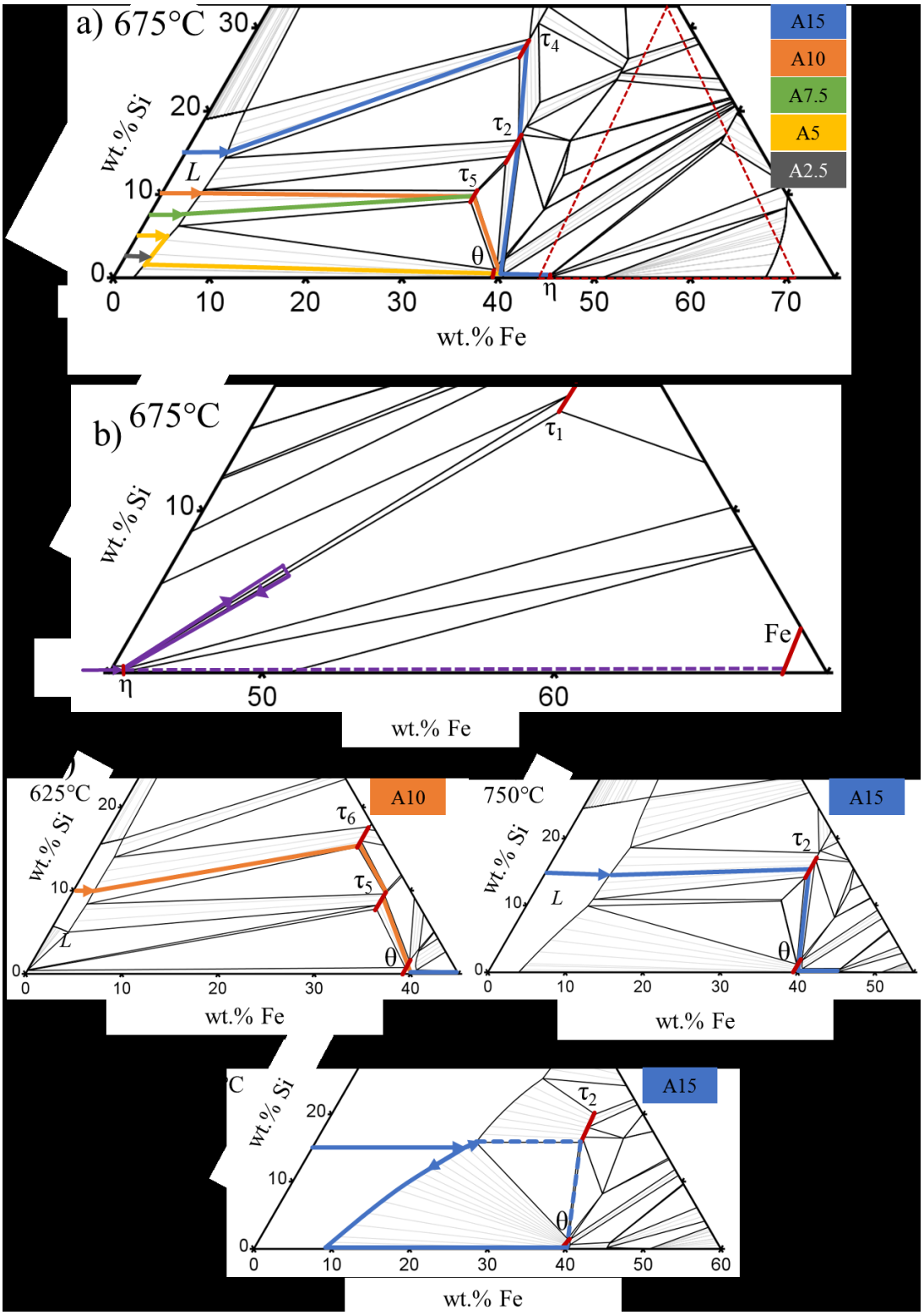


*Figure 10: Isothermal sections of the Al-rich side of the ternary Al-Fe-Si phase diagram. The red lines indicate a phase and the diffusion path starts in the liquid (see color coded arrow for alloy) and follows the path indicated by the colored line. a) 675°C and b) is the magnification of the red triangle, c) at 625°C, d) at 750°C and e) at 875°C.*

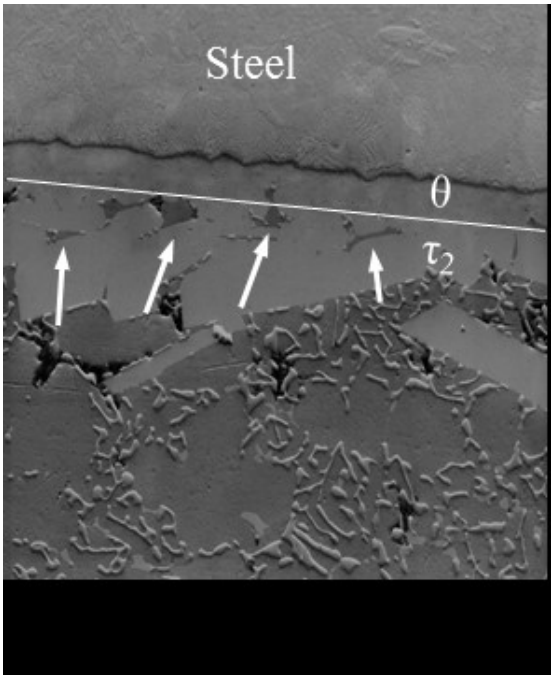


*Figure 11: SEM micrograph of the A15 sample dipped at 875°C for 2 minutes.*

*Effect of Si on Growth Rate*

The above results show that Si reduces the growth rate of the reaction layer which confirms previous results [6, 17-20, 23, 33] and the following discussion will concern the samples made at 675°C. There are several suggested mechanisms to account for this behavior. As previously mentioned Nicholls [17] suggested that Si atoms occupy interstitial spaces of the η-($Fe_2Al_5$) crystal and efficiently reduces the Al diffusion. Lainer et al.[18] suggested that the reduction in growth rate could be due to slow forming ternary Al-Fe-Si compounds which take more time to form. Komatsu et al.[19] suggested that the Si improved the rate of dissolution of Si to the liquid aluminum resulting in a thinner reaction layer and more recently a study of the η-($Fe_2Al_5$)/θ-($Fe_4Al_{13}$) grain boundaries by Lemmens et al.[22] using an atomic probe equipped microscope noticed elevated concentrations of Si within the boundary which could hinder Al diffusion.

According to the results shown in Figure 4 there is very little ternary phase present within the reaction layer up to 5 wt.% Si and it is not a continuous layer as reported by Layner et al.[18] suggesting that this theory is not likely the cause for the reduction in growth rate for these low concentrations of Si. The reduction of steel area in Figure 8a shows the advancement of the η-($Fe_2Al_5$)/steel interface which decreases with increasing Si content up to between 2 and 2.5 wt.%. A thinner reaction layer which should increase the Fe concentration gradient across the reaction zone speeding up the advancement of the η-($Fe_2Al_5$)/steel interface. These results confirm the conclusion by Eggeler et al.[20] that the reduction in growth rate is at least partly due to a solid-state phenomenon. The advancement of the η-($Fe_2Al_5$)/steel interface is dependent on the Si concentration as is shown in Figure 8a.

Figure 9 shows a summary of available growth rate constants in literature plotted vs the inverse in temperature. Dotted lines represent represents the trendline used to extrapolate the activation energy for η-($Fe_2Al_5$) growth according to the Arrhenius expression that can be seen in Equation 2. The solid black vertical line indicates the melting temperature of aluminum. There are two things that are particularly interesting in the plot. There seems to be a disconnect between the activation energies for solid-solid (open markers) and liquid-solid (solid markers) reaction layer growth. Secondly, the liquid-

solid diffusion couples carried out with an Fe-saturated aluminum melt similar growth rates (crossed markers) as non-saturated melts do.

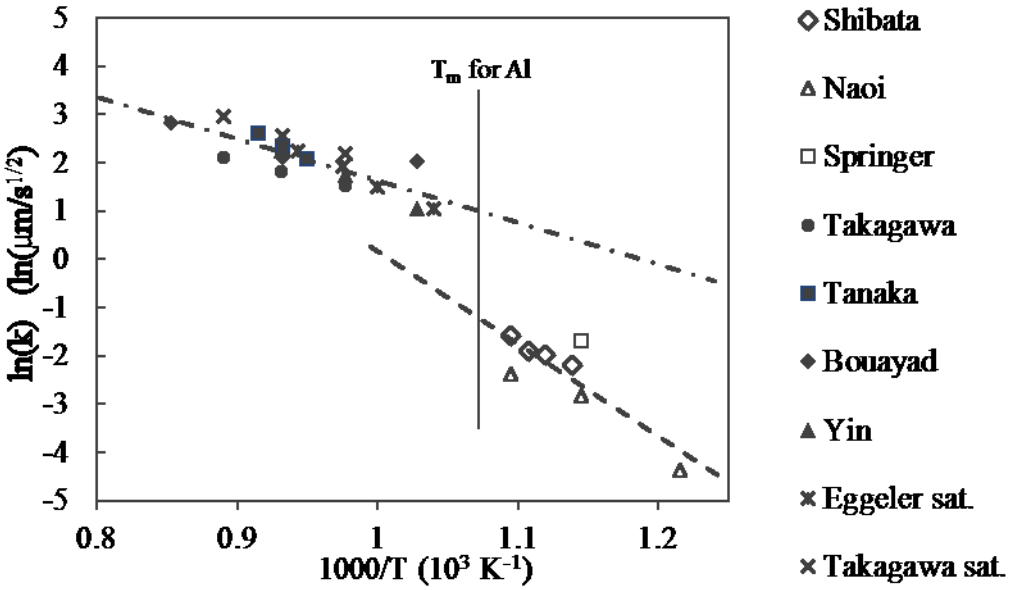


*Figure 9: The logarithmic value of available rate constants in literature for solid-solid, open markers, and liquid-solid, solid markers, plotted vs the inverse of time. The dotted from the dotted lines the activation energy can be extracted using Equation 2. The solid line represents the melting point of aluminum.*

$$k = k_0 e^{(-\frac{Q}{RT})} \qquad \text{Equation 2}$$

For comparison three established diffusion couples are sketched in Figure 10a with the reported microstructures[6, 35]. The red arrows represent the direction of growth for the interfaces present in the diffusion couples. Comparing case 1 with 2 the layer grows in both directions and have different microstructures. The presence of β-(FeAl) in case 1 instead of η-($Fe_2Al_5$) would suggest that the diffusion rate of Al is not high enough sustain the η-($Fe_2Al_5$) growth that is present in case 2 and 3. For case 3, the non-saturated aluminum melt, there is dissolution of iron and θ-($Fe_4Al_{13}$) phase into the liquid and thus for the interface the total growth velocity will be $v_\eta - v_D$. For the microstructure to be stable and for the η-($Fe_2Al_5$) layer to increase in thickness $v_\eta$ must be larger or equal to $v_\theta$ and a similar argument can be made for the θ-($Fe_4Al_{13}$) layer. An argument can then be made that the η-($Fe_2Al_5$)/steel interface must have the highest velocity and is thus rate controlling. The advancement of the η-($Fe_2Al_5$)/steel interface will depend on the transformation of Fe to η-($Fe_2Al_5$), the atomic transfer of Fe across the interface, and diffusion through the η-($Fe_2Al_5$) layer. The crystal cell volume of BCC Fe is 23.55Å$^3$ [36] and contains 2 Fe atoms while the crystal cell volume of η-($Fe_2Al_5$) phase is 206.55Å$^3$ [25] and contains 4 Fe atoms. This means that for every unit cell of η-($Fe_2Al_5$) that forms more than 12 Fe atoms needs to diffuse away from the interface. The parabolic nature of the movement of the η-($Fe_2Al_5$)/steel, see Figure 8a, growth would indicate that the velocity is not controlled by a reaction rate but by a diffusion rate. If movement of Fe atoms across the η-($Fe_2Al_5$)/steel interface would be rate controlling it would be independent of the reaction layer thickness. But the difference in growth rate for the A2, A2.5, and A5 samples, see Table 4, and the increase in η-($Fe_2Al_5$)/steel movement would suggest that the flux of Fe atoms is proportional to the concentration gradient within the η-($Fe_2Al_5$) layer, see Equation 3 and Figure 10b.

$$v_\eta \sim J_{Fe} \sim \frac{\partial c_{Fe}}{dx}$$ Equation 3

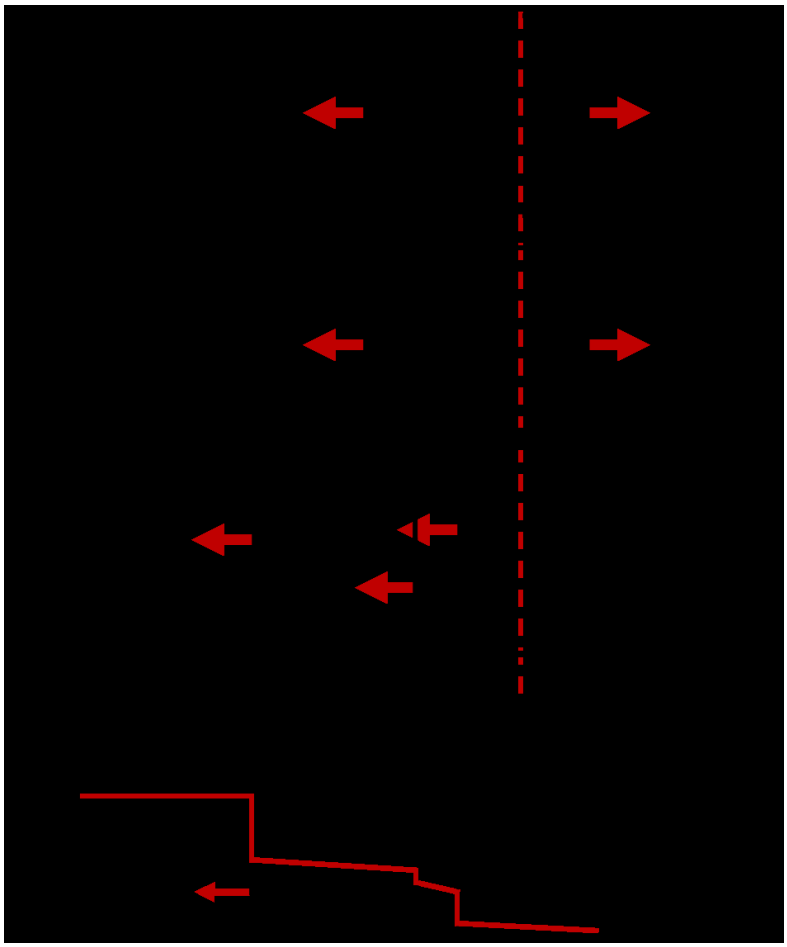

*Figure 10: a) Sketch of different Al-Fe diffusion couples. 1) solid-solid diffusion couple, 2) liquid-solid diffusion couple with a Fe-saturated aluminum alloy, and 3) a liquid-diffusion couple. The red arrows represent the interface velocity direction and the black the diffusion of atomic species. The dotted red line is the original interface. b) Concentration gradients within diffusion couple 3.*

In a study by Springer et al.[6], it was shown that when comparing the thickness of the semi-solid Al-5wt%Si/steel diffusion couple to a solid-solid Al/steel diffusion couple at 600°C the Si-containing η-($Fe_2Al_5$) layer grew at a faster rate than one without. During interdiffusion between the solid steel and semi-solid aluminum, it is more likely that the liquid content of the semi-solid is in contact with the steel. A possible explanation for this if the atomic transfer of Al across the Al/ η-($Fe_2Al_5$) interface is the rate limiting step for solid-solid diffusion couples. This would explain the disconnect of the activation energies calculated from the rate constants as seen in Figure 9 and the difference in microstructure despite the fast growing η-($Fe_2Al_5$) phase. The liquid-solid diffusion couple as previously mentioned two binary layers θ-($Fe_4Al_{13}$) and η-($Fe_2Al_5$) while for solid-solid diffusion, [37] only reported an η-($Fe_2Al_5$) layer for and [6] reported an η-($Fe_2Al_5$) layer with two additional IMC (FeAl and $AlFe_3C$) layers present at the η-($Fe_2Al_5$)/steel interface. The phase change of Al from solid to liquid impacts the chemical diffusivity in Al in the solid state is approximately is in the order of $10^{-12}$ $m^2s^{-1}$ [38] at 650°C and in liquid state the self-diffusivity of Al is $7.2x10^{-9}$ $m^2s^{-1}$ [39] which could

change the interaction Al with the IMC interface. The liquid also acts as a vacancy sink which if Al is the fast diffuser through the structure prevents any gap to form at the interface.

Marker et al.[40] characterized the lattice cell parameters for multiple compounds within the Al-Fe-Si system at a temperature of 800°C and 900°C and measured the η-($Fe_2Al_5$) cell parameters for different Si compositions. The lattice parameters for the η-($Fe_2Al_5$) cell for different Si concentration can be seen in the top part of Figure 11, please note the difference in scales on the y-axis, and the size of the a and b axis are decreasing with increasing Si concentration. η-($Fe_2Al_5$) crystals containing Si also seems to have an increased amount of Fe, see the bottom of Figure 11. The slightly elevated Fe concentration corresponds better with the results from the EDS measurements, the measured average concentration of Fe for the low Si-containing samples is 45.5 wt.%. Diffusion in intermetallic compounds is rather complex due to their ordered nature and depends on their defect structure[41]. Measurements of diffusion coefficients with in intermetallics will often strongly depend on composition [41, 42] and it is, therefore, likely that this changes the diffusion coefficients of both Al and Fe within the η-($Fe_2Al_5$) layer. Lemmens et al.[22] suggested that the reduction of growth rate of the η-($Fe_2Al_5$) layer could be due to elevated Si concentration at the θ-($Fe_4Al_{13}$)/η-($Fe_2Al_5$) interface. However, the columnar grains within the η-($Fe_2Al_5$) layer could also provide high diffusivity pathways for Si in the form of grain boundary diffusion which was not considered. Their study showed elevated Si concentrations within the η-($Fe_2Al_5$)/η-($Fe_2Al_5$) grain boundaries which could significantly impact and reduce the grain boundary diffusion. Clearly, a more controlled diffusion study would be needed to characterize further the effect of Si on the defect structure of η-($Fe_2Al_5$) and how it affects diffusion.

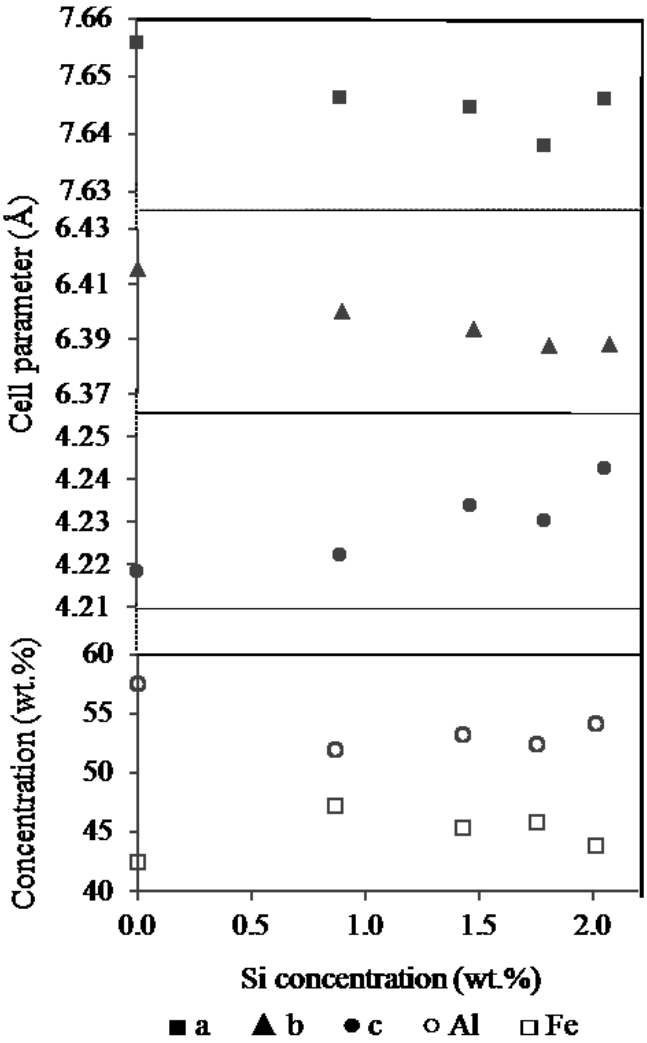


*Figure 11: The change of cell parameters of the η-($Fe_2Al_5$) crystal on Si concentration.*

Interestingly increasing the Si content to 5 wt.%, more than twice the saturation limit of η-($Fe_2Al_5$), further decreased the growth rate of the η-($Fe_2Al_5$) layer, see Figure 6, with the same phases present within the IMC layer. The reduction of steel area also increased slightly indicating a faster movement of the η-($Fe_2Al_5$)/steel interface. A thin reaction layer would increase the concentration gradient for Fe which could speed up the flux of Fe atoms and thus the η-($Fe_2Al_5$)/steel interface see previous discussion. A thinner IMC layers is also an indication of increased dissolution which was also shown by Dybkov[43].

Increasing the Si concentration from 5 to 7.5 wt.% changes the microstructure, and a $\tau_5$-($Al_{7.4}Fe_2Si$) phase is formed at the interface. The growth rate constant for the η-($Fe_2Al_5$) layer decreases from 1.09 to 0.98 μm/$s^{1/2}$ which is similar to the difference between the growth rate constants of the A2.5 and A5 samples. Figure 12 shows the growth rate constant of the η-($Fe_2Al_5$) layer plotted vs. the Fe saturation limit of the liquid alloy. Once the η-($Fe_2Al_5$) layer starts to be saturated in Si (between 1.5 to 2 wt.% Si) there is a linear relationship between the growth rate constant and the Fe saturation limit up to 10 wt.% Si. The more complex ternary multilayer structure of the A15 sample, see Figure 4d, seems to reduce the growth rate of the η-($Fe_2Al_5$) layer. A decrease in both the advancement of η-($Fe_2Al_5$)/steel

interface and the dissolution could indicate that the multilayer structure changes the diffusion across the layers, but a more focused study on the kinetics of for this type of phase layers would be needed to confirm.

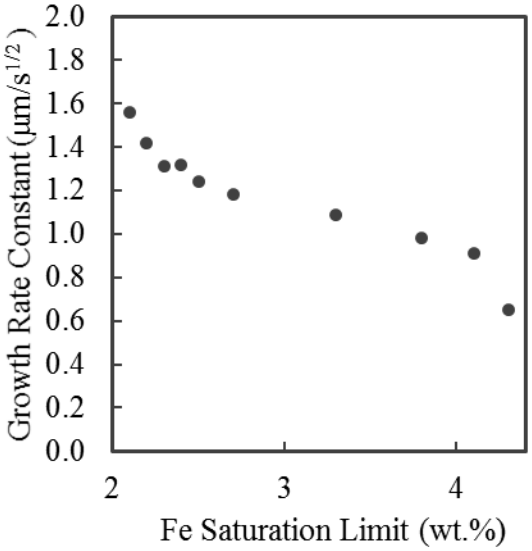


*Figure 12: Growth rate constant of η-($Fe_2Al_5$) plotted vs. Fe saturation limit in the liquid aluminum alloy.*

The growth rate of the ternary layers in contact with aluminum does not exhibit the same relationship with the Fe saturation limit, see Figure 7b. There is also a tendency for a negative deviation which is typically explained by the enrichment of Fe to the Al melt[9] which is also evident for the θ-($Fe_4Al_{13}$) layers in Figure 6b. Interestingly, the growth of $\tau_5$-($Al_{7.4}Fe_2Si$) is faster and η-($Fe_2Al_5$) slower for the A10 sample compared to the A7.5 sample. This could be due to a faster dissolution, but the elevated Si concentration for the A10 sample is closer to the composition of the $\tau_5$-($Al_{7.4}Fe_2Si$) phase which is 9.5 wt.% which improves its growth rate. The A15 sample dipped at 750°C shows a reduction in IMC layer thickness with increasing dipping time and dissolution progresses relatively fast, and the entire steel was dissolved before 3 hours of dipping time which has been reported before but for higher temperatures[15, 44].

**Conclusion**

The undertaken study mapped the growing microstructure of the reaction layer between binary liquid Al-Si alloy with varying Si concentration (0.5 – 15 wt.%) and a mild steel (US grade 1008, 0.10 wt.% C, 0.4 wt.% Mn) for a time span of 5 to 180 minutes. The focus was characterizing the growing microstructure and how it relates to the growth kinetics of the formed reaction layer. From the results presented above the following conclusions can be made.

1) Phase layers formed in the diffusion couples have been characterized by EBSD and them reasonable match the theoretical diffusion paths in ternary phase diagrams generated in Thermocalc with exceptions for phases that are not present due to very low growth rates.
2) The microstructure of the reaction layer depends on the composition, temperature, time and cooling rate. While the effect of composition and temperature can be predicted by diffusion paths, the cooling rate and diffusion time can change the microstructure and therefore influence the characterization of the kinetics of the system.

3) For a reaction temperature of 625°C and 675°C, the majority of the reaction layer consisted of the η-($Fe_2Al_5$) phase, and the growth follows a parabolic rate curve. At Si concentrations of 5 wt.% and below a θ-($Fe_4Al_{13}$) layer was present and its growth rate was also parabolic.
4) Si additions to the liquid aluminum seem two growth rate controlling mechanisms. (1) Si changes the crystal size of the η-($Fe_2Al_5$) layer which could reduce the diffusion coefficient of both Al and Fe within the η-($Fe_2Al_5$) layer. Elevated Si concentration within the η-($Fe_2Al_5$)/η-($Fe_2Al_5$) grain boundaries could prove to be effective at slowing down grain boundary diffusion. (2) For Al melts that are not iron-saturated, dissolution of Fe reduces the thickness of the IMC layer. The dissolution is dependent on the saturation limit of Fe in the liquid aluminum which increases with increasing Si content.
5) The movement of the η-($Fe_2Al_5$)/steel interface depends on the rate at which diffusion of iron atoms can move from the steel and through the η-($Fe_2Al_5$) phase. For a reaction layer to be stable in a non-saturated melt and increase in thickness, its advancement has to be faster than the dissolution making the diffusion of Fe the rate determining step.

[1] Viala, J. C., Peronnet, M., Barbeau, F., and Bosselet, F., "Interface chemistry in aluminium alloy castings reinforced with iron base inserts," pp. 1417-1420.
[2] Durrant, G., 1996, "Squeeze cast aluminium reinforced with mild steel inserts," Journal of materials science, 31(3), pp. 589-602.
[3] Gebhardt, E., and Obrowski, W., 1953, "Reaktionen von festem eisen mit schmelzen aus aluminium und aluminiumlegierungen," Zeitschrift fur Metallkunde, 44(4), pp. 154-160.
[4] Eggeler, G., Vogel, H., Friedrich, J., and Kaesche, H., 1985, "Target Preparation for the Transmission Electron Microscopic Identification of the Al sub 3 Fe ( theta -Phase) in Hot-Dip Aluminised Low Alloyed Steel," Praktische Metallographie, 22(4), pp. 163-170.
[5] Heumann, T., and Dittrich, N., 1959, "Structure character of the Fe2Al5 intermetallics compound in hot dip aluminizing process," Z Metallk, 50, pp. 617-623.
[6] Springer, H., Kostka, A., Payton, E. J., Raabe, D., Kaysser-Pyzalla, A., and Eggeler, G., 2011, "On the formation and growth of intermetallic phases during interdiffusion between low-carbon steel and aluminum alloys," Acta Materialia, 59(4), pp. 1586-1600.
[7] Takata, N., 2015, "Crystallography of Fe2Al5 phase at the interface between solid Fe and liquid Al," Intermetallics, 67, pp. 1-11.
[8] Bouayad, A., 2003, "Kinetic interactions between solid iron and molten aluminium," Materials science & engineering. A, Structural materials : properties, microstructure and processing, 363(1-2), pp. 53-61.
[9] Eggeler, G., Auer, W., and Kaesche, H., 1986, "Reactions Between Low Alloyed Steel and Initially Pure as Well as Iron-Saturated Aluminium Melts Between 670 and 800 deg C," Zeitschrift für Metallkunde, 77(4), pp. 239-244.
[10] Bouché, K., Barbier, F., and Coulet, A., 1998, "Intermetallic compound layer growth between solid iron and molten aluminium," Materials science & engineering. A, Structural materials : properties, microstructure and processing, 249(1), pp. 167-175.
[11] Shahverdi, H. R., Ghomashchi, M. R., Shabestari, S., and Hejazi, J., 2002, "Microstructural analysis of interfacial reaction between molten aluminium and solid iron," Journal of materials processing technology, 124(3), pp. 345-352.
[12] Denner, s. G., and Jones, R. D., 1977, "Kinetic interactions between aluminiumliquid and iron/steelsolid for conditions applicable to hot-dip aluminizing," Metals technology, 4(1), pp. 167-174.

[13] Denner, S. G., and Jones, R. D., 1976, "Use of Transmission 57-Fe Mossbauer Spectroscopy to Study the Kinetics of Hot-Dip Aluminizing of Fe," Journal of materials science, 11(9), pp. 1777-1778.
[14] Rezaei, H., Akbarpour, M. R., and Shahverdi, H. R., 2015, "Effects of Interfacial Layers Fracture on the Dissolution Mechanism of Solid Fe in Liquid Al," JOM, 67(7), pp. 1443-1450.
[15] Chen, S., Yang, D., Zhang, M., Huang, J., and Zhao, X., 2016, "Interaction Between the Growth and Dissolution of Intermetallic Compounds in the Interfacial Reaction Between Solid Iron and Liquid Aluminum," Metallurgical and Materials Transactions A, 47(10), pp. 5088-5100.
[16] Gittings, D., Rowland, D., and Mack, J., 1951, "Effect of Bath Composition on Aluminum Coatings on Steel," Trans. ASM, 43, p. 587.
[17] Nicholls, J. E., 1964, "Hot-dipped aluminum coatings," Anti-corrosion methods and materials, 11(10), pp. 16-21.
[18] Lainer, D., and Kurakin, A., 1964, "Mechanism of the effect of silicon in aluminum on the process of reactive diffusion of iron into aluminum," Fiz. Metal. Metalloved, 18.
[19] Komatsu, N., Nakamura, M., and Fujita, H., 1968, "Effects of silicon on reaction between iron and liquid aluminum " Journal of Japan Institute of Light Metals, 18(9), pp. 467-473.
[20] Eggeler, G., Auer, W., and Kaesche, H., 1986, "On the Influence of Silicon on the Growth of the Alloy Layer During Hot Dip Aluminizing," J. Mater. Sci, 21(9), pp. 3348-3350.
[21] Zhe, M., 2011, "Chemical Changes at the Interface Between Low Carbon Steel and an Al-Si Alloy During Solution Heat Treatment," Journal of phase equilibria and diffusion, 32(6), pp. 486-497.
[22] Lemmens, B., Springer, H., Duarte, M. J., De Graeve, I., De Strycker, J., Raabe, D., and Verbeken, K., 2016, "Atom probe tomography of intermetallic phases and interfaces formed in dissimilar joining between Al alloys and steel," Materials Characterization, 120, pp. 268-272.
[23] Yin, F.-c., 2013, "Effect of Si on growth kinetics of intermetallic compounds during reaction between solid iron and molten aluminum," Transactions of Nonferrous Metals Society of China, 23(2), pp. 556-561.
[24] Pierre, D., Barbeau, F., Peronnet, M., and Bosselet, F., "Reaction layer sequences at the interface between iron and Al-Si alloys," pp. 1593-1598.
[25] Burkhardt, U., Grin, Y., Ellner, M., and Peters, K., 1994, "Structure refinement of the iron–aluminium phase with the approximate composition Fe2Al5," Acta Crystallographica Section B: Structural Science, 50(3), pp. 313-316.
[26] Grin, J., Burkhardt, U., Ellner, M., and Peters, K., 1994, "Refinement of the Fe4Al13 structure and its relationship to the quasihomological homeotypical structures," Zeitschrift fuer Kristallographie, 209(6), pp. 479-487.
[27] Yanson, T. I., Manyako, M. B., Bodak, O. I., German, N. V., Zarechnyuk, O. S., Cerný, R., Pacheco, J. V., Yvon, K., and IUCr, 1996, "Triclinic Fe3Al2Si3 and Orthorhombic Fe3Al2Si4 with New Structure Types," Acta Crystallographica Section C: Crystal Structure Communications, 52(12), pp. 2964-2967.
[28] Roger, J., Jeanneau, E., and Viala, J. C., 2011, "Crystal structure of the ternary compound γ-Al3FeSi," Zeitschrift für Kristallographie Crystalline Materials, 226(11), pp. 805-813.
[29] German, N. V., Zavodnik, V. E., Yanson, T. I., and Zarechnyuk, O. S., 1989, "Crystal Structure of FeAl sub 2 Si," Kristallografiya, 34(3), pp. 738-739.
[30] Gueneau, C., Servant, C., d'Yvoire, F., and Rodier, N., 1995, "FeAl3Si2," Acta Crystallographica Section C: Crystal Structure Communications, 51(2), pp. 177-179.
[31] Corby, R. N., and Black, P. J., 1977, "The structure of α-(AlFeSi) by anomalous-dispersion methods," Acta Crystallographica Section B: Structural Crystallography and Crystal Chemistry, 33(11), pp. 3468-3475.
[32] Rømming, C., Hansen, V., and Gjønnes, J., 1994, "Crystal structure of β-Al4.5FeSi," Acta Crystallographica Section B: Structural Science, 50(3), pp. 307-312.

[33] Cheng, W.-J., and Wang, C.-J., 2011, "Effect of silicon on the formation of intermetallic phases in aluminide coating on mild steel," Intermetallics, 19(10), pp. 1455-1460.
[34] Cheng, W.-J., and Wang, C.-J., 2011, "Microstructural evolution of intermetallic layer in hot-dipped aluminide mild steel with silicon addition," Surface and Coatings Technology, 205(19), pp. 4726-4731.
[35] Takata, N., Nishimoto, M., Kobayashi, S., and Takeyama, M., 2015, "Growth of Fe2Al5 Phase on Pure Iron Hot-Dipped in Al–Mg–Si Alloy Melt with Fe in Solution," ISIJ International, 55(7), pp. 1454-1459.
[36] Wyckoff, R. W. G., 1963, "Crystal Structures 1, 7-83," American Mineralogist Crystal Structure Database.
[37] Naoi, D., and Kajihara, M., 2007, "Growth behavior of Fe2Al5 during reactive diffusion between Fe and Al at solid-state temperatures," MATERIALS SCIENCE AND ENGINEERING A-STRUCTURAL MATERIALS PROPERTIES MICROSTRUCTURE AND PROCESSING, 459(1-2), pp. 375-382.
[38] Brandes, E. A., and Brook, G. B., 1992, Smithells Metals Reference Book, Butterworth-Heinemann.
[39] Kargl, F., Weis, H., Unruh, T., and Meyer, A., "Self diffusion in liquid aluminium," IOP Publishing, p. 012077.
[40] Marker, M. C. J., Skolyszewska-Kühberger, B., Effenberger, H. S., Schmetterer, C., and Richter, K. W., 2011, "Phase equilibria and structural investigations in the system Al–Fe–Si," Intermetallics, 19(12), pp. 1919-1929.
[41] Mehrer, H., 1996, "Diffusion in intermetallics," Materials Transactions, JIM, 37(6), pp. 1259-1280.
[42] Frank, S., Divinski, S. V., Södervall, U., and Herzig, C., 2001, "Ni tracer diffusion in the B2-compound NiAl: Influence of temperature and composition," Acta materialia, 49(8), pp. 1399-1411.
[43] Dybkov, V. I., 2000, "Interaction of iron-nickel alloys with liquid aluminium Part II Formation of intermetallics," Journal of materials science, 35(7), pp. 1729-1736.
[44] Shahverdi, H. R., Ghomashchi, M. R., Shabestari, S., and Hejazi, J., 2002, "Kinetics of interfacial reaction between solid iron and molten aluminium," Journal of Materials Science, 37(5), pp. 1061-1066.

# Appendix D

# Effect of thermal treatments on the metallurgical bond

## Introduction

Stricter requirements on the reduction of $CO_2$ emissions in the transportation sector pushes the further light weighting of vehicles which impose challenges for materials selection. Aluminum castings combine excellent specific strength with a competitive price. However, for certain applications, it lacks in stiffness, strength, and wear resistance. There are opportunities to further lightweight traditionally ferrous components by replacing them with bimetallic composites of aluminum with cast-in ferrous inserts. Allowing aluminum to chemically react with steel to form a metallurgical bond has been shown that the performance of these composites depends on the interaction between the matrix and the reinforcing component and a metallurgical bond can improve the properties[1].

The metallurgical bond has been utilized in the hot-dip aluminizing industry to bond aluminum coatings to steel substrates[2]. Research has shown the composition and phases of the metallurgical bond between pure aluminum and iron to consist of two binary intermetallic compound (IMC) layers, the η-phase (Fe2Al5), with a characteristic saw-tooth morphology close to the steel and a thinner flat outer layer consisting of θ-phase (Fe4Al13) in contact with the aluminum[3-5]. The growth kinetics of the intermetallic compound(IMC) layer tend to follow a parabolic growth curve with a slight negative deviation due to iron saturation of the aluminum melt[6-8].

Silicon has been used to reduce the thickness of the brittle bond due to its natural ability to slow down the growth of the reaction layer. AS a major alloying element for casting alloys its effect on microstructure and growth rate has been extensively studied[9-11]. The A356 aluminum alloy (7.5wt% Si and 0.3wt% Mg) has specifically been studied in detail. It tend to form three distinct layers are present in the metallurgical bond, the layer in contact with the aluminum consists of the ternary phase $\tau_5$-($Al_{7.4}Fe_2Si$), an intermediary layer of the binary θ-($Fe_4Al_{13}$), and in contact with the steel the binary η-($Fe_2Al_5$) phase[11-13].

To achieve optimal properties of aluminum alloys, thermal treatment of the castings is required. The treatment generally consists of three steps; isothermal holding at temperatures close to the solidus line for 2-10 hours, water quenching, and isothermal holding at 180°C for 5-10 hours[14]. Therefore, it is important to know the effects of these treatments on the metallurgical bond between the aluminum and ferrous alloys.

Viala et al.[1] studied the effect of a heat treatments on a metallurgical bond formed between a cast iron insert and A356 and were able to show that the η-($Fe_2Al_5$) layer grows thicker and two ternary phases, $\tau_2$-($Al_5Fe_2Si_2$) and $\tau_{10}$-($Al_{12}Fe_5Si_3$), forms at the expense of the preexisting $\tau_5$-($Al_{7.4}Fe_2Si$) and $\tau_6$-($Al_{4.5}FeSi$) layer. Zhe et al.[12] performed a more extensive study on the effect of solution heat treatments on metallurgically bonded steel to A356 alloy. The study showed that the metallurgical bond broke down into several layers, after 10 hours of isothermal holding an IMC layer consisting of a mixture between $\tau_2$-($Al_5Fe_2Si_2$) and $\tau_{10}$-($Al_{12}Fe_5Si_3$) forms in between the $\tau_6$-($Al_{4.5}FeSi$) and η-($Fe_2Al_5$). The preexisting $\tau_5$-($Al_{7.4}Fe_2Si$) had completely disappeared even after short holding times (less than 3h). For longer holding times (over 40h) a fourth layer appeared consisting of $\tau_1$-($Al_5Fe_2Si$). Both authors also showed that Kirkendall voids forms for longer holding times and crack formation during the quenching step due to the large difference in thermal expansion.

While the composition of the formed IMC layer changes during isothermal holding close to the solidus line, the layer seemed structurally intact for shorter holding times (less than 40 hours) if the quenching step is avoided and can thus still be useful. There is limited information on how a change of the aluminum alloy composition changes the thermal stability of the metallurgical bond and how it changes during exposure to lower temperatures. Formation of porosity in the metallurgical bond can damage

its properties and it has also been shown that the strength of the bond depends on the type and size of the intermetallic compounds present in the bond [15] and thus the growth behavior and microstructural changes needs to be known for selection of a suitable casting alloy.

**Objective**

This study aims to investigate the growth rate, thermal stability and phase transformations in the metallurgical bond formed between two different aluminum alloys, 390 (17wt% Si, 4.5wt% Cu, and 0.6wt% Mg), and an Al-Mg-Zn alloy (10wt%Mg and 2wt%Zn), and a mild steel during both high and low-temperature thermal treatments.

**Experimental Procedure**

Liquid-solid and solid-solid diffusion couple experiments between a low-carbon steel and aluminum alloys were performed. All of the steel samples were 76 mm long and were cut from the same 6.3 mm diameter rod, the composition of the steel and the initial composition of the aluminum alloys used is presented in Table 1. The steel was ground to a 600-grit surface producing a surface roughness value, $R_a$, of 0.3 μm measured using a Olympus LEXT 3D Measuring Laser Microscope. After grinding the samples were pickled in a 10% HCl solution for 30 seconds, rinsed in deionized water, ultrasonically cleaned in ethanol, then acetone and allowed to dry.

The diffusion couples were prepared using standard metallurgical preparation methods, and all of the scanning electron microscope analysis were performed in a JEOL JSM-7000F equipped with Oxford Instruments EDS detector X-Max$^N$ and EBSD detector NordlysMax$^2$.

Table 1: Chemical composition of the steel and aluminum alloys used during the experiments.

| | Chemical Composition (wt%) | | | | | |
|---|---|---|---|---|---|---|
| | C | Mn | P | S | Si | Fe |
| Steel (1015) | 0.14 | 0.53 | 0.023 | 0.032 | 0.06 | Bal. |
| | | | | | | |
| | Mg | Zn | Si | Fe | Cu | Al |
| Al-Mg-Zn alloy | 14.71 | 2.29 | 0.05 | 0.11 | - | Bal. |
| B390 | 0.44 | 1.43 | 16.87 | 0.8 | 4.81 | Bal. |

Table 2 shows the designations for the binary and ternary phases and its compositional limits. The Al-Fe-Si ternary designations are adapted from Krendelsberger et al.[16], the ternary Al-Fe-Cu designations are adapted from Raghavan [17], and the references refer to the crystal structure data used for phase identification using EBSD.

*Table 2: Binary Al-Fe, ternary Al-Fe-Si, and ternary Al-Cu-Fe phases with crystal structure data and their designations. The ternary Al-Fe-Si designations are adapted from Krendelsberger et al.[16] and the references are the crystal structure data used for EBSD identification.*

| Symbol | Composition | Space group | References |
|---|---|---|---|
| η | $Fe_2Al_5$ | Cmcm (63); orthorhombic | [18] |
| θ | $Fe_4Al_{13}$ | C2/m (12); monoclinic | [19] |
| $\tau_1$ | $Al_2Fe_3Si_3$ | P1 (2), triclinic | [20] |
| $\tau_2$ | $Al_3FeSi$ | R-3 (148); hexagonal | [21] |
| $\tau_3$ | $Al_2FeSi$ | Cmma (67); orthorhombic | [22] |
| $\tau_4$ | $Al_3FeSi_2$ | I4/mcm (140); tetragonal | [23] |
| $\tau_5$ | $Al_{7.4}Fe_2Si$ | P6_3/mmc (194); hexagonal | [24] |
| $\tau_6$ | $Al_{4.5}FeSi$ | A2/a (15); monoclinic | [25] |
| $\tau_7$ | $Al_3Fe_2Si_3$ | P2_1/n (14); monoclinic | [26] |
| $\tau_8$ | $Al_2Fe_3Si_4$ | Cmcm (63); orthorhombic | [20] |
| ω | $FeCu_2Al_7$ | - | [17] |
| I | $FeCu_2Al_6$ | - | [17] |
| φ | $FeCu_{10}Al_{10}$ | - | [17] |

*Liquid-Solid diffusion*

To characterize the IMC layer growth kinetics between Al-Mg-Zn alloy and steel liquid-solid diffusion experiments were set up. In a resistance furnace, a silicon carbide crucible with 700 grams of the aluminum alloy heated to 680°C, and the steel inserted into the aluminum melt. Prior experiments showed that the temperature of the aluminum melt decreases 5°C as the steel rod is introduced into the aluminum melt. After submersion, the aluminum melt was then kept at a temperature of 675°C ± 5°C during the experiment. Three samples were produced for each of the following time steps; 10 seconds, 30 seconds, 120 seconds, and 300 seconds.

After the desired diffusion time the steel rod was extracted and allowed to air cool. Once at room temperature three cross-sectional samples were cut at a spacing of 10 mm. The samples were prepared for metallographic examination by light optical microscopy and scanning electron microscopy. The average total thickness of the IMC layer was measured from each sample, and the average thickness was calculated by taking nine images from each sample and ten measurements from each image.

*Solid-Solid Diffusion*

The solid-solid diffusion couples were made by submerging the steel rod in the liquid alloy at 675°C ± 5°C for 120 seconds and quickly transfer it to the brass mold in which the aluminum is cast. Time between removal from the melt to pouring the casting did not exceed 5 seconds. The mold had a diameter of 32 mm and 50 mm long with a slight taper at the bottom to ease centering of the steel rod.

Each sample was cut in two 20 mm tall slices and placed in a preheated furnace at the preselected temperature. The temperatures and holding times for the different alloy combinations can are presented in Table 3. A third slice was used as a reference sample for the as-cast condition.

After the desired diffusion time the compound casting was removed from the furnace and allowed to air cool. Once at room temperature the samples were cut along the steel axis and were prepared for metallographic examination by light optical microscopy and scanning electron microscopy.

*Table 3: Temperature and schedule for the solid-solid diffusion couples.*

| Al Alloy | Temperature | Holding time (hours) | | | |
|---|---|---|---|---|---|
| Al-Mg-Zn | 430°C | 4 | 8 | 16 | 24 |
| | 180°C | 24 | 120 | 336 | 870 |
| B390 | 480°C | 4 | 8 | 16 | 24 |
| | 180°C | 24 | 120 | 336 | 870 |

**Results**

*Liquid-Solid diffusion - Al-Mg-Zn alloy*

The microstructural features and phase composition can be seen in Figure 1. Figure 1a shows a micrograph of the reaction layer formed by the Al-Mg-Zn alloy. The morphology is jagged finger-like in shape (aluminum was removed during sample preparation). Figure 1b shows a phase map (with superimposed band contrast to reveal grain structure) of the phases present in the reaction layer formed between the steel and the alloy after being submerged at 675°C for 300 seconds. The red colored phase at the top of the image indicates BCC iron, the blue upwards protrusion corresponds to η-($Fe_2Al_5$), and the magenta at the bottom of the map matches θ-($Fe_4Al_{13}$) which is in contact with aluminum. The η-($Fe_2Al_5$) layer is relative to the θ-($Fe_4Al_{13}$) layer much thicker and contributes to the majority of the reaction layer thickness.

Figure 1c shows the characteristic Kα x-rays for different elements of interest. There is only a small amount of magnesium and zinc present in the reaction zone and point analysis (location where measured and indicated by white arrow in Figure 1a) and the average concentration of magnesium and zinc is less than 0.2wt% in the θ-($Fe_4Al_{13}$) phase while only zinc could be is detected in the η-($Fe_2Al_5$) layer (0.2 wt%).

No morphological or microstructural difference could be seen between the dipped and as-cast samples. The average thickness of the IMC layer after 120 seconds of dipping time was 29 (standard deviation of 6 μm) and 24 μm (standard deviation of 5 μm). This could be explained by the high cooling rate and fast solidification of the brass mold.

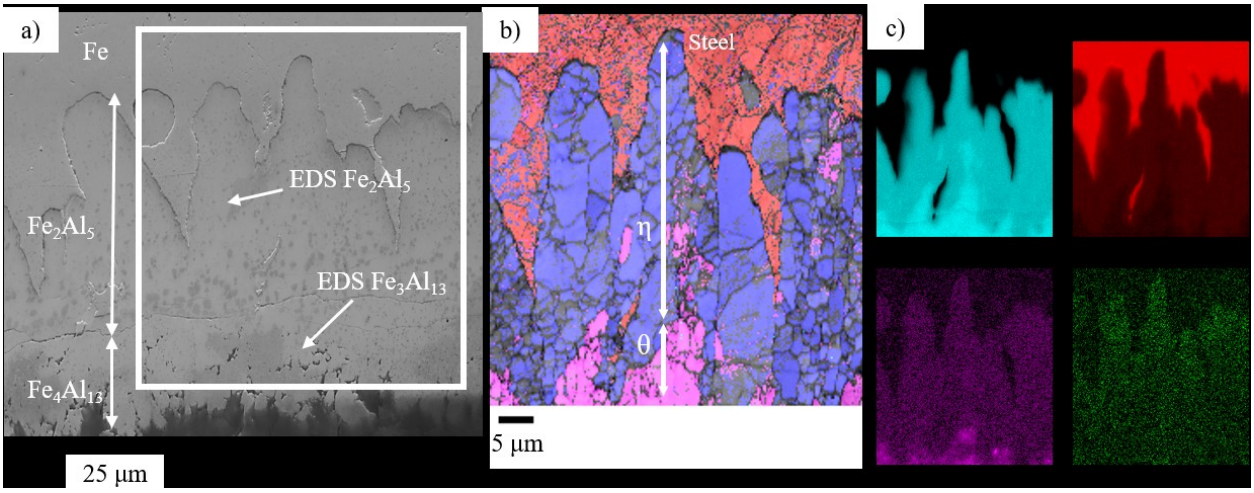


*Figure 1: EBSD analysis of the formed reaction layer after 5 minutes of dipping in the Al-Mg-Zn alloy at 675°C for 5 minutes. a) SEM micrograph with white arrows showing the relative size of the two phase layers and indicating arrows to where the compositional EDS data was captured. The white square show where the EBSD map was collected. b) EBSD phase map with band contrast overlay to indicate grains. c) EDS maps of the corresponding to the same region as the EBSD map.*

*Liquid-Solid diffusion – B390*

The SEM analysis of the IMC layer formed between 390 and the mild steel can be seen in Figure 2. The reaction layer is does not exhibit the ragged morphology protruding into the steel, there are however protrusions reaching out into the aluminum and small eutectic silicon can be seen on the next to the IMC layer on the aluminum side(Figure 2a). The also seems to be a tendency for primary silicon to nucleate on the outer IMC layer, see Figure 6a. The final polishing step reveals four distinct layers and the phases identified are visible in the phase map in Figure 2b. There are two ternary Al-Fe-Si layers, consisting of $\tau_4$-($Al_3FeSi_2$) closest to the aluminum (bottom of phase map) with a dark red thin layer identified as $\tau_2$-($Al_3FeSi$) next to it. Subsequently, there is a layer of θ-($Fe_4Al_{13}$) (magenta) and η-($Fe_2Al_5$) (blue). The EBSD patterns also identified the ternary precipitates within the two binary Al-Fe phases to be $\tau_1$ – ($Al_2Fe_3Si_3$).

The EDS analysis, shown in Figure 2c, shows that there is a copper-rich zone which corresponds to the $\tau_2$-($Al_5Fe_2Si_2$) suggesting that this compound has a higher solubility of copper compared to the other IMCs present in the reaction layer.

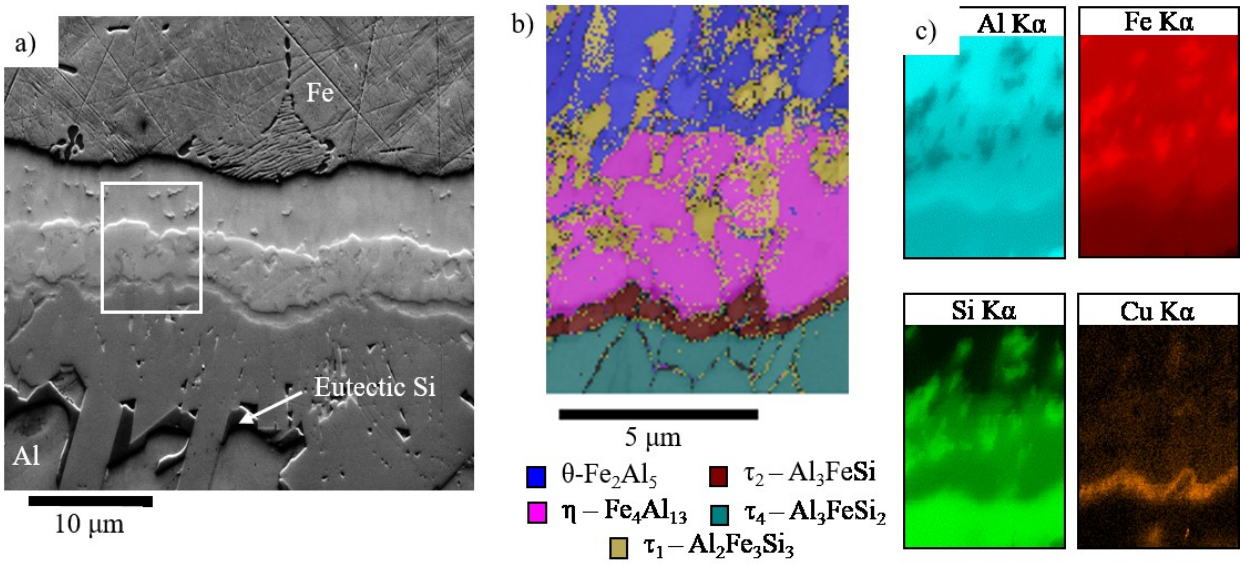


*Figure 2: EBSD analysis of the formed reaction layer after 5 minutes of dipping in the B390 alloy at 675°C for 5 minutes. a) SEM micrograph showing the location of the EBSD phase map (white square). b) EBSD phase map with band contrast overlay to indicate grains. c) EDS maps of the corresponding to the same region as the EBSD map.*

*Liquid Solid Diffusion - Growth rate*

If the total measured thickness of the IMC layer is plotted vs time the shape of the curve is parabolic in nature. A parabolic curve indicates a diffusion controlled growth rate and can be described by Equation 1 and if solved for x (layer thickness) a growth rate constant can be calculated using Equation 2.

$$x^2 = k_1 t \qquad \text{(Equation 1)}$$

$$x = k\sqrt{t} \qquad \text{(Equation 2)}$$

The growth rate constant, k, for the Al-Mg-Zn alloy was calculated to 2.4 µm $s^{-1/2}$ and for 390 to 1.1 µm $s^{-1/2}$. The fit of the approximation can be seen in Figure 3 when a linear curve is fitted to the data and the $R^2$ value is calculated. The coefficient of determination for both alloys is above 98% which indicates a good fit. The protrusions require many (290) measurements for an accurate average.

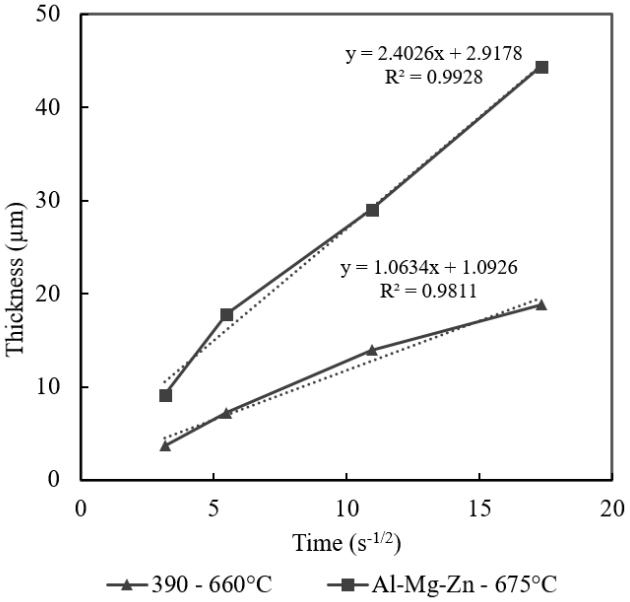


*Figure 3: Total thickness plotted vs. the square root of time for the liquid-solid diffusion couples. The linear fit indicates diffusion controlled growth and the growth rate constant k can be seen as the slope.*

*Solid-Solid diffusion - Al-Mg-Zn alloy*

Figure 4a shows a timeline of micrographs that illustrates the development of IMC layer between the Al-Mg-Zn alloy and a mild steel after exposure to 430°C for different time steps. After 4 hours, voids started to form at the aluminum-IMC layer interface and gradually starts to interconnect as holding time increases. Minor defects in the center of the reaction layer after 4 hours and the extent of this porosity increases with increasing solutionizing time. After 8 hours, there is significant porosity in the middle reaction layer IMC layer, see Figure 4b, which increases with time. Quantitative measurements of the porosity are difficult due to possible loss of material during sample preparation, and a larger porous network will increase the uncertainty of the measurements. Increasing solutionizing time gradually changes the morphology of the microstructure from the jagged edge to progressively smoother interface.

To establish in what phase the porosity starts to form a phase map of the reaction zone heat treated for 8 hours at 430°C can be seen in Figure 4c. The same two phases are present as in the as-cast sample, but their relative amount has changed. There is a thick θ-($Fe_4Al_{13}$) layer (the color magenta in Figure 4c) close to the aluminum and small remains of η-($Fe_2Al_5$) (blue color) in contact with the steel.

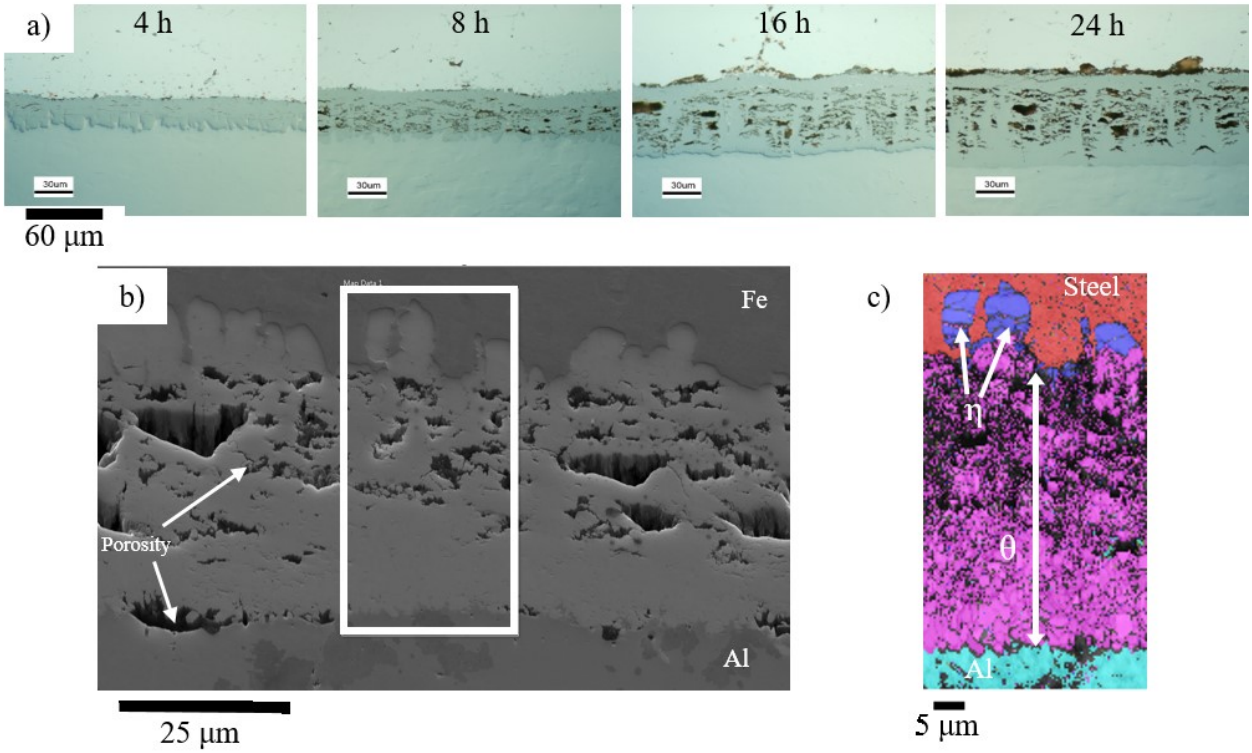


*Figure 4: a) a timeline of micrographs for Al-Mg-Zn alloy being isothermally held at 430°C. b) SEM micrograph of the bonding are after 8 hours of exposure and the white square represents the area in which the EBSD phase map data was collected. c) EBSD phase map with band contrast overlay to indicate grains.*

A timeline of the microstructural development for samples isothermally held at 180°C can be seen in Figure 5a and shows no signs of increase in thickness. In fact, there was no measureble change in IMC layer thickness. Figure 5b shows an electron micrograph of the reaction layer formed between the Al-Mg-Zn alloy after isothermal holding at 180°C for 870 hours. There are signs of porosity forming at the interface between the reaction layer and the aluminum alloy which indicates that diffusion of aluminum into the θ-($Fe_4Al_{13}$) phase activates at this relatively low temperature. Figure 5c is showing a phase map of the layer would suggest that there is an increase in the relative amount of θ-($Fe_4Al_{13}$) to η-($Fe_2Al_5$) compared to the as cast layer.

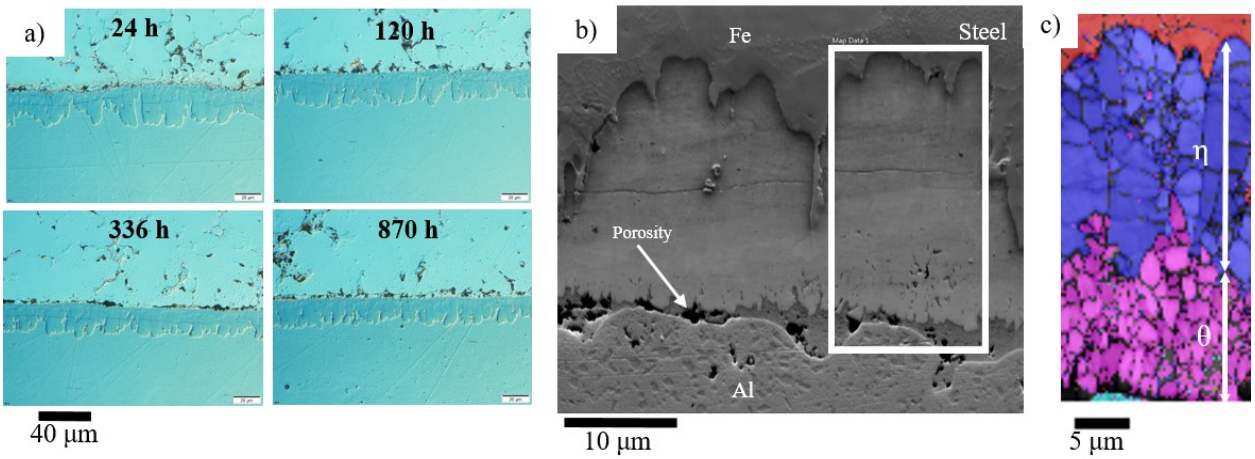


*Figure 5: a) Timeline of micrographs for Al-Mg-Zn alloy being isothermally held at 180°C. b) SEM micrograph of the bonding are after 336 hours of exposure and the white square represents the area in which the EBSD phase map data was collected. c) EBSD phase map with band contrast overlay to indicate grain structure.*

*Alloy 390*

The development of the metallurgical bond for isothermal holding at 480°C is presented in Figure 6a. Minor voids start forming between the bond and the aluminum after 4 hours, and after between 8 and 16 hours of thermal treatment, the voids begin to interconnect. The protrusions of the bond that extend out in the aluminum and the primary silicon that formed on the IMC layer form barriers that prevent the coalescence of the voids. Comparing the micrographs in Figure 2a and Figure 6b it is clear that a new phase has appeared. After 4 hours, the phase is present in both the steel and the aluminum side of the reaction layer, but after 8 hours it is completely it has disappeared from the steel/IMC layer interface and is gradually disappearing from the aluminum/IMC layer interface with increased holding time.

Figure 6b shows a SEM micrograph of the reaction layer with the different visible phases marked. The ternary Al-Fe-Cu phase marked by an arrow in Figure 8a did not yield a clear EBSD pattern and thus had to be identified through EDS. The average composition was 50wt% Al, 34wt% Cu, 15wt% Fe and 1 wt% Si (69at% Al. 20at%Cu, 10at% Fe and 1%Si) which corresponds well with the ternary ω-($Al_7Cu_2Fe$) phase.

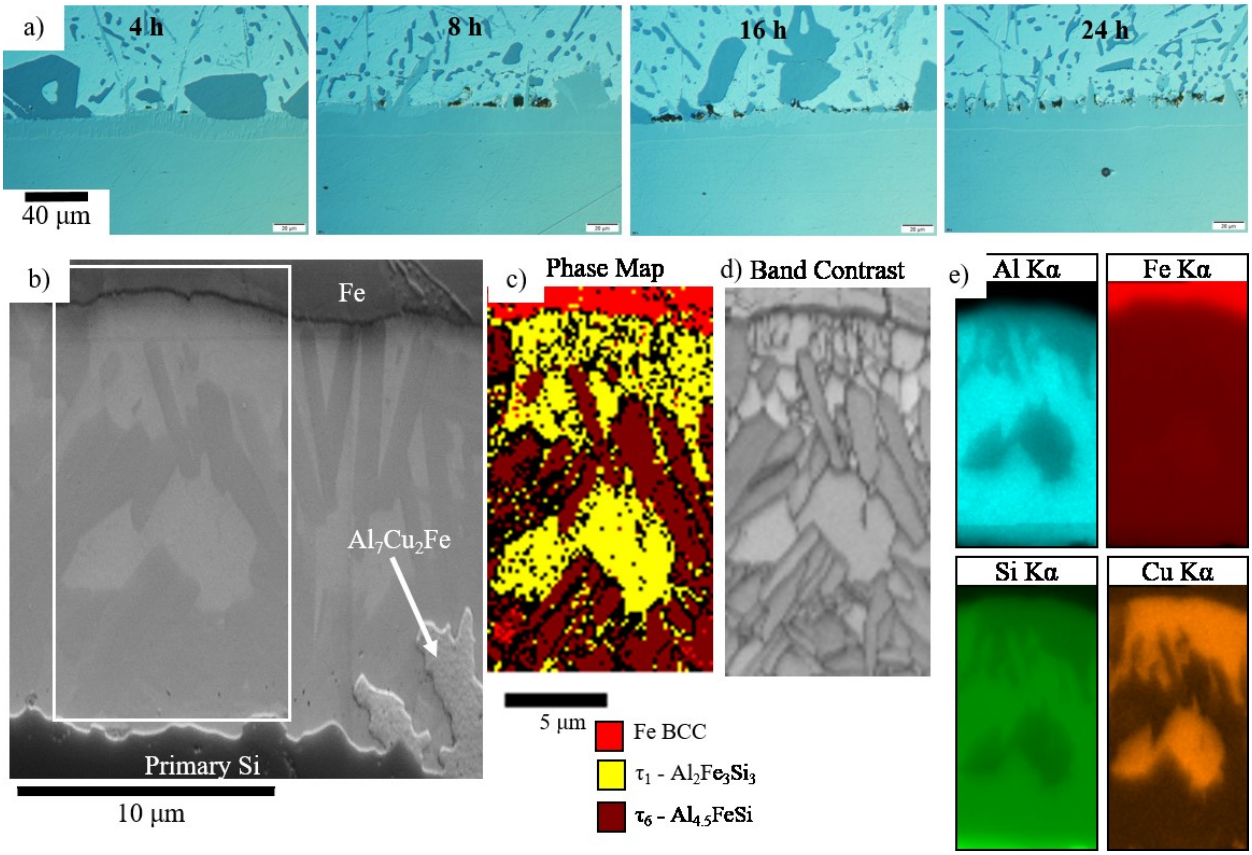


Figure 6*: a) Timeline of micrographs for B390 alloy being isothermally held at 480°C. b) SEM micrograph of the bonding are after 336 hours of exposure and the white square represents the area in which the EBSD phase map data was collected. c) EBSD phase map with band contrast overlay to indicate grain structure.*

The phase constituents of the reaction layer after 8 hours of solutionizing treatment at 480°C are mapped in Figure 6c and seems to mainly consist of two phases, $\tau_1$-($Al_2Fe_3Si_3$) and $\tau_6$-($Al_{4.5}FeSi$). Comparing Figure 2b and 6c the binary Al-Fe phase layers have disappeared and transformed into two a three-layered structure with $\tau_6$-($Al_{4.5}FeSi$) close to the aluminum, $\tau_1$-($Al_2Fe_3Si_3$) in contact with the steel, and a mixture of the two in between. Figure 6d shows how the band contrast of the EBSD patterns changes and indicates that the $\tau_1$-($Al_2Fe_3Si_3$) grains are more equiaxed while the $\tau_6$-($Al_{4.5}FeSi$) grains are elongated. The EDS map of the same area, Figure 6e, shows that copper is segregated to $\tau_1$-($Al_2Fe_3Si_3$) with much less solubility in the $\tau_6$ – ($Al_{4.5}FeSi$).

**Discussion**

*Effects of alloying elements on microstructure during liquid-solid diffusion*

The finger-like shape of the reaction layer formed between the Al-Mg-Zn alloy clearly resembles the morphology of the bond that forms between pure aluminum and iron and forms due to the preferential growth along the c-axis of the η-($Fe_2Al_5$) crystal [4, 11]. Heumann and Dittrich [27] were the first to suggest that this was due to structural vacancies along the c-axis. Takata et al.[4] reported that the directional growth could be explained by induced vacancy generation and diffusion because of stress build-up between the η-($Fe_2Al_5$) and iron due to the size difference in the crystal structure.

Figure 7a shows an isopleth of a Thermocalc generated Al-Fe phase diagram in the presence of 10wt%Mg and 2wt%Zn. The red dotted line marks the reaction temperature (675°C) and at increasing iron concentrations both the θ-($Fe_4Al_{13}$) and the η-($Fe_2Al_5$) phase are predicted to be stable. There is evidently very low concentration of both Mg and Zn present in the binary Al-Fe phases. The low Zn concentration corresponds well to results in previous studies[28], and the thermodynamic simulations do not predict the presence of Mg in θ-($Fe_4Al_{13}$) or η-($Fe_2Al_5$) which confirms similar findings in[29]. Due to the low solubility of the of the major alloying elements(Mg and Zn) and high stability of the binary Al-Fe phases the microstructure formed is determined by the Al-Fe phase diagram.

The microstructure formed between B390 and the mild steel, see Figure 2a, is strongly influenced by the presence of silicon. Similar to previous studies [springer eggeler silicon papers] the finger like morphology is no longer present even though there is the presence η-($Fe_2Al_5$) layer in contact with the steel. Figure 2b shows the presence of two ternary IMC layers, a thicker $\tau_4$-($Al_3FeSi_2$) in contact with the aluminum and a thinner a $\tau_2$-($Al_3FeSi$) layer. A Thermocalc generated Al-Fe phase diagram with 17 wt% Si and 4.5 wt% Cu, plotted in Figure 7b, shows that $\tau_4$-($Al_3FeSi_2$) is in equilibrium with the melt at 675°C and with increasing iron content both $\tau_4$-($Al_3FeSi_2$) and $\tau_2$-($Al_3FeSi$) is in equilibrium. The phase diagram indicates that there should be other ternary compounds ($\tau_3$, $\tau_7$, $\tau_1$, and I) present at iron concentrations where θ-($Fe_4Al_{13}$) is stable. This indicates that the binary layers most likely form due to the rapid diffusion of aluminum through the outer layers keeping the concentration of both copper and silicon below the liquid concentration. Al-Si alloys with Si concentrations between 5-10 wt% have been studied in by previous authors [11, 30] and were also able to identify the presence of $\tau_1$-($Al_2Fe_3Si_3$) precipitates within the binary phase layers.

There is an elevated concentration of copper (approximately 0.9 to 1.7 wt%) within the $\tau_2$-($Al_3FeSi$) layer. However, measurements of an accurate copper concentrations are difficult due to the large interaction volume of the x-rays and the semi-quantitative nature of EDS concentration measurements but it does suggest a higher solubility limit.

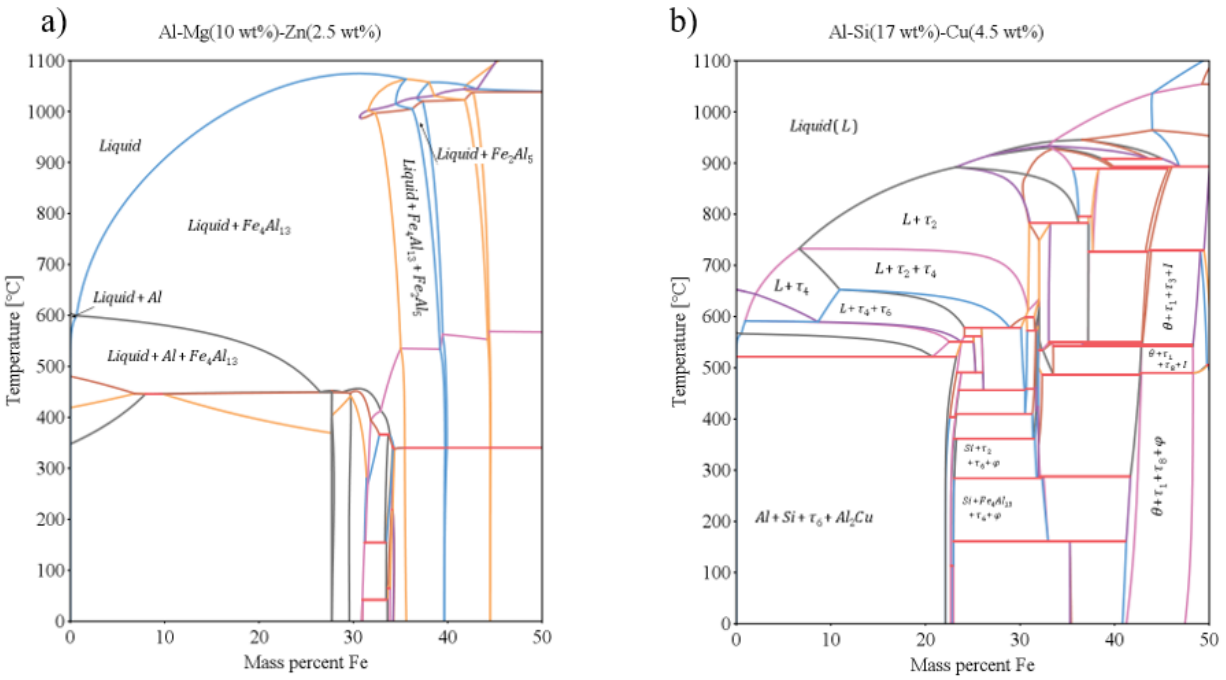


Figure 7: a) *Al-Fe phase diagram isopleth at 10 wt.% Mg and 2.5 wt.% Zn. b) Al-Fe phase diagram isopleth at 17 wt.% Si, and 4.5 wt.% Cu*

Figure 2b shows the presence of two ternary IMC layers, a thicker $\tau_4$-($Al_3FeSi_2$) in contact with the aluminum and a thinner a $\tau_2$-($Al_3FeSi$) layer. A Thermocalc generated Al-Fe phase diagram with 17 wt% Si and 4.5 wt% Cu, plotted in Figure 7b, shows that $\tau_4$-($Al_3FeSi_2$) is in equilibrium with the melt at 675°C and with increasing iron content both $\tau_4$-($Al_3FeSi_2$) and $\tau_2$-($Al_3FeSi$) is in equilibrium. The phase diagram indicates that there should be other ternary compounds ($\tau_3$, $\tau_7$, $\tau_1$, and I) present at iron concentrations where θ-($Fe_4Al_{13}$) is stable. This indicates that the binary layers most likely form due to the rapid diffusion of aluminum through the outer layers keeping the concentration of both copper and silicon below the liquid concentration.
Al-Si alloys with Si concentrations between 5-10 wt% have been studied in by previous authors [11, 30] and were also able to identify the presence of $\tau_1$-($Al_2Fe_3Si_3$) precipitates within the binary phase layers.

There is an elevated concentration of copper (approximately 0.9 to 1.7 wt%) within the $\tau_2$-($Al_3FeSi$) layer. However, measurements of an accurate copper concentrations are difficult due to the large interaction volume of the x-rays and the semi-quantitative nature of EDS concentration measurements but it does suggest a higher solubility limit.

*Growth rate of intermetallic layer during liquid-solid diffusion*
The curves in Figure 3 shows the thickness of the IMC layer for different time steps. To determine how well they fit the criteria for parabolic growth the thickness can be plotted vs. the square root of time. Figure 8, with additional data adapted from [13], shows this plot and the $R^2$ value for a linear fit gives a value close to 1 which indicates that the growth is diffusion controlled which is common for these systems [11, 31, 32].

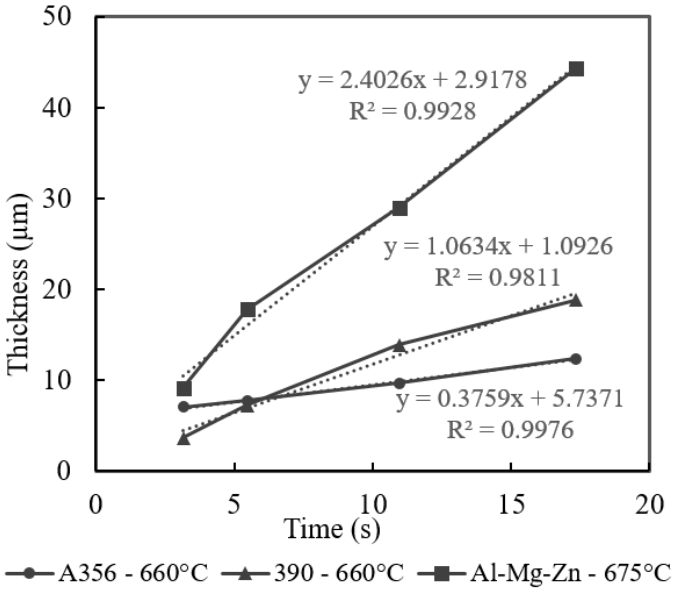


*Figure 8: Thickness plotted vs. the square root of time for three different alloys with the corresponding growth rates as the slopes of the fitted straight lines.*

The total thickness of the IMC layer for the Al-Mg-Zn alloy is significantly higher than both the A356 and B390 alloy which is also represented in a high growth rate constant. It is known that the presence of silicon in the liquid aluminum reduces the growth rate of the reaction layer [27, 31]. However, for these alloys, a larger quantity of silicon present in the alloy does not equal a lower growth rate. The growth rate constant is higher for the B390 compared to A356 while it has more than twice the silicon content. The two silicon-containing alloys also shows significantly different microstructure which changes the diffusional behavior of the atoms due to the difference in the crystal structure. B390 also contains more iron in solution which would reduce the driving force for dissolution of the outer IMC layer.

*Heat treatment of Al-Mg-Zn/Mild steel reaction layer*

The microstructure of the metallurgical bond between the Al-Mg-Zn alloy and the steel during liquid-solid diffusion is in composition identical to the structure formed by pure aluminum and iron. The isothermal holding of this microstructure does change relative amounts of the two binary phases (compare Figure 1b and Figure 4c), and there is also significant void generation in the θ-($Fe_4Al_{13}$) layer which is not seen in pure Al-Fe solid-solid diffusion couples at higher temperatures(600°C)[11].A more similar experiment[28] without the pre-formation of the reaction layer between a hot-dip galvanized steel and pure aluminum exposed to isothermal holding for 4 hours at 400°C with what seems to be a single layer of binary phase with porosity within. The porosity forming at the aluminum-IMC layer interface would indicate that aluminum is a faster diffuser compared to the iron.

During the liquid-solid diffusion, the growth of the θ-($Fe_4Al_{13}$) layer is competing with its dissolution into the liquid aluminum. For the solid-solid diffusion, the θ-($Fe_4Al_{13}$) layer grows in two directions due to no dissolution and the higher diffusion rates of aluminum generates a higher concentration of aluminum which seems to transform η-($Fe_2Al_5$) to θ-($Fe_4Al_{13}$). Difference in thermal expansion could cause growth of θ-($Fe_4Al_{13}$) towards the aluminum to relieve stress and fill space

There appears to be a threshold for the activation of diffusion of iron from the steel to the η-($Fe_2Al_5$) layer that is not met. It could be that a lower temperature will reduce the vacancy concentration in the steel which slows down diffusion and growth of the η-($Fe_2Al_5$) into the steel. It has also been shown that new intermetallic layers start forming at the steel/η-($Fe_2Al_5$) interface during solid-solid diffusion[11] which were not detected during this analysis and could inhibit growth rate.

Isothermal holding at 180°C does, similarly to the high-temperature solid-solid diffusion, change the relative amount of θ-($Fe_4Al_{13}$) and η-($Fe_2Al_5$). There is no visible porosity within the reaction layer, but there is porosity present at the interface between the θ-($Fe_4Al_{13}$)/aluminum interface which would indicate that the diffusion of aluminum atoms into the θ-($Fe_4Al_{13}$) layer activates even at low temperatures. There is, however, no measurable increase in reaction layer thickness since the deviation within the samples is larger than the difference in thickness.

*Heat treatment of B390/Mild steel reaction layer*

Figure 8a shows the formation of the ω-($Al_7Cu_2Fe$) phase at the interface of both the iron and aluminum reaction interface after 4 hours of holding at 480°C. After 8 hours the ω-($Al_7Cu_2Fe$) phase has completely disappeared from the iron/IMC layer interface and is only present at the aluminum/IMC interface. The increased copper concentration (between 4 and 7wt%) present in the $\tau_1$-($Al_2Fe_3Si_3$) phase and its location would indicate that there is a transformation of ω-($Al_7Cu_2Fe$) into $\tau_1$-($Al_2Fe_3Si_3$) with prolonged high-temperature exposure. Figure 9 shows the thickness change of the reaction layer and the majority of the growth occurs before 4 hours of heat treatment and could be due to the formation of the ω-($Al_7Cu_2Fe$) phase.

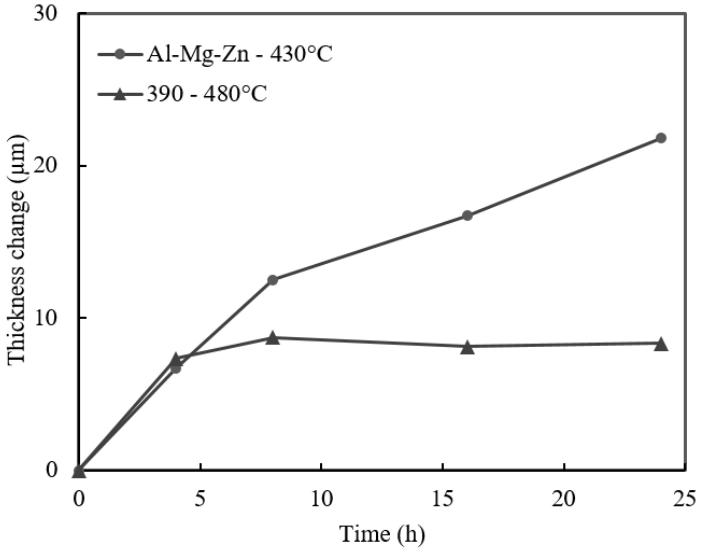


*Figure 9: The thickness change of the IMC layer plotted vs isothermal holding time.*

Comparing Figure 2b and Figure 6c it is clear that there is a significant change in the phases present in the formed IMC layer. The binary Al-Fe phases have disappeared, and the $\tau_4$-($Al_3FeSi_2$) and $\tau_2$-($Al_3FeSi$) layers have been replaced by a mixture of $\tau_1$-($Al_2Fe_3Si_3$) and $\tau_6$-($Al_{4.5}FeSi$). Studying the phase diagram at 480°C in Figure 7b $\tau_1$-($Al_2Fe_3Si_3$) is not stable until iron concentrations of ~40wt% indicating that it grows from the diffusion of iron from the Fe or this is not the stationary phase layers forming within the diffusion couple. $\tau_6$-($Al_{4.5}FeSi$) is more stable at lower temperatures and is in the equilibrium phase for higher aluminum concentrations and can support its growth by being in contact

with aluminum. $\tau_6$-($Al_{4.5}FeSi$) was also identified by Zhe et al.[12] in a solid-solid diffusion couple when studying an aluminum alloy containing 17 wt% Si.

*Porosity formation*

To optimize the properties of bimetallic castings the properties of both metals and the bond between them. The aluminum alloys studied here both require a heat treatment program to achieve their required properties and the metallurgical bond has to be able to withstand the high-temperature exposure. For optimal heat and load transfer between the two materials, it is crucial that the bond be continuous and stays intact during the materials processing. The rapid change in dimensions due to quenching steps has proven to initiate cracks along the brittle IMC layer, and prolonged exposure to elevated temperatures induce porosity in an already brittle layer.

Comparing solid-solid diffusion couple of Al-Fe and Al-Si alloys[11, 28, 33, 34] the location of the formed porosity is slightly different. Zhe et al.[12] showed that there is a difference between diffusion couples that are coated and those that are cast-in. Similar to their cast-in steel samples severe porosity was formed between the aluminum/IMC layer interface before 16 hours of heat treatment. Another influencing parameter could be the difference in thermal expansion between the aluminum and the iron. Aluminum will expand at a faster rate as the temperature increases which would reduce the contact area between the two metals. This would make these types of diffusion couples size and shape dependent. Similar to what Zhe et al. the effects are exaggerated by the presence of oxygen at the joint, see Figure 10.

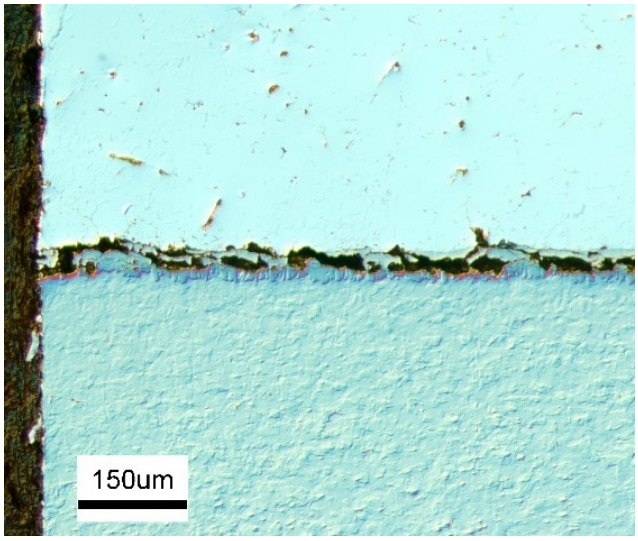


*Figure 10: Formed crack at the interface of the high temperature Al-Mg-Zn sample likely due to the influence of oxidation.*

**Conclusion**

The purpose of this study was to investigate the microstructure and growth kinetics of the formed reaction layer during liquid-solid interaction and its transformation during sub sequential thermal treatments. Two alloys were investigated, a magnesium-based aluminum alloy and a hyper-eutectic silicon-based alloy. The as-cast microstructure was characterized, and then small bimetallic castings were subjected to isothermal holding at their respective solutionizing temperature and an aging temperature. From the above results the following conclusions can be made:

1. The as cast metallurgical bond microstructure of the Al-Mg-Zn alloy formed two distinct binary Al-Fe phase layers, θ-($Fe_4Al_{13}$) and η-($Fe_2Al_5$). The growth rate follows a parabolic curve with a growth rate constant of 2.4 μm $s^{-1/2}$. High-temperature temperature (430°C) isothermal exposure for less than 24 hours did not change the phase composition of the alloy but changed the relative amounts indicating preferential growth of the θ-($Fe_4Al_{13}$) phase and the growth of the reaction layer follows a parabolic curve. Low temperature (180°C) isothermal exposure also changed the relative amounts indicating θ-($Fe_4Al_{13}$) and η-($Fe_2Al_5$) phase due to preferential growth of θ-($Fe_4Al_{13}$) phase although no significant increase in thickness was could be measured.

2. The as cast metallurgical bond microstructure of the B390 formed four distinct phase layers(in order from aluminum alloy side), $\tau_4$-($Al_3FeSi_2$), $\tau_2$-($Al_3FeSi$), θ-($Fe_4Al_{13}$) and η-($Fe_2Al_5$). The binary layers had precipitates of $\tau_1$-($Al_2Fe_3Si_3$) imbedded. The growth rate follows a parabolic curve with a growth rate constant of 1.1 μm $s^{-1/2}$. High-temperature temperature (480°C) isothermal exposure changed the microstructure of the bond to three layers, $\tau_6$ – ($Al_{4.5}FeSi$) with elongated grains, a mixture of $\tau_6$ – ($Al_{4.5}FeSi$) and $\tau_1$-($Al_2Fe_3Si_3$), and a layer $\tau_1$-($Al_2Fe_3Si_3$) with more equiaxed grains. The growth rate showed deviations from the parabolic curve, and most of the change occurred before 4 hours of exposure.

3. High-temperature (430°C) exposure of Al-Mg-Zn alloy showed that there was significant damage to the metallurgical bond due to porosity after less than 8 hours. Even low temperature (180°C) exposure showed signs of porosity formation at the IMC layer/aluminum interface. High-temperature temperature (480°C) exposure of B390 indicates that porosity starts to form at the IMC layer/aluminum interface between 4-8 hours. No internal porosity within the bond could be detected for holding times up to 24 hours.

**References**

[1] Viala, J. C., Peronnet, M., Barbeau, F., and Bosselet, F., "Interface chemistry in aluminium alloy castings reinforced with iron base inserts," pp. 1417-1420.
[2] Nicholls, J. E., 1964, "Hot-dipped aluminum coatings," Anti-corrosion methods and materials, 11(10), pp. 16-21.
[3] Eggeler, G., Vogel, H., Friedrich, J., and Kaesche, H., 1985, "Target Preparation for the Transmission Electron Microscopic Identification of the Al sub 3 Fe ( theta -Phase) in Hot-Dip Aluminised Low Alloyed Steel," Praktische Metallographie, 22(4), pp. 163-170.
[4] Takata, N., 2015, "Crystallography of Fe2Al5 phase at the interface between solid Fe and liquid Al," Intermetallics, 67, pp. 1-11.
[5] Bouayad, A., 2003, "Kinetic interactions between solid iron and molten aluminium," Materials science & engineering. A, Structural materials : properties, microstructure and processing, 363(1-2), pp. 53-61.
[6] Eggeler, G., Auer, W., and Kaesche, H., 1986, "Reactions Between Low Alloyed Steel and Initially Pure as Well as Iron-Saturated Aluminium Melts Between 670 and 800 deg C," Zeitschrift für Metallkunde, 77(4), pp. 239-244.
[7] Denner, s. G., and Jones, R. D., 1977, "Kinetic interactions between aluminiumliquid and iron/steelsolid for conditions applicable to hot-dip aluminizing," Metals technology, 4(1), pp. 167-174.
[8] Shahverdi, H. R., Ghomashchi, M. R., Shabestari, S., and Hejazi, J., 2002, "Kinetics of interfacial reaction between solid iron and molten aluminium," Journal of Materials Science, 37(5), pp. 1061-1066.
[9] Gittings, D., Rowland, D., and Mack, J., 1951, "Effect of Bath Composition on Aluminum Coatings on Steel," Trans. ASM, 43, p. 587.
[10] Lainer, D., and Kurakin, A., 1964, "Mechanism of the effect of silicon in aluminum on the process of reactive diffusion of iron into aluminum," Fiz. Metal. Metalloved, 18.
[11] Springer, H., Kostka, A., Payton, E. J., Raabe, D., Kaysser-Pyzalla, A., and Eggeler, G., 2011, "On the formation and growth of intermetallic phases during interdiffusion between low-carbon steel and aluminum alloys," Acta Materialia, 59(4), pp. 1586-1600.
[12] Zhe, M., 2011, "Chemical Changes at the Interface Between Low Carbon Steel and an Al-Si Alloy During Solution Heat Treatment," Journal of phase equilibria and diffusion, 32(6), pp. 486-497.
[13] Soderhjelm, C., and Apelian, D., 2016, "Metallurgical bonding between cast-in ferrous inserts and aluminum," La Metallurgia Italiana, 6, pp. 93-100.
[14] Kaufman, J. G., Rooy, E. L., Books24x, I., and American Foundry, S., 2004, Aluminum alloy castings: properties, processes, and applications, ASM International, Materials Park, OH.
[15] Zhe, M., Dezellus, O., Parry, G., Braccini, M., and Viala, J. C., 2012, "Modified 4-Point Bending Test for Adhesion Measurement at the Interface of Iron Coated with Aluminum Casting Alloy," JOURNAL OF ADHESION SCIENCE AND TECHNOLOGY, 26(1-3), pp. 1-17.
[16] Krendelsberger, N., Weitzer, F., and Schuster, J. C., 2007, "On the Reaction Scheme and Liquidus Surface in the Ternary System Al-Fe-Si | SpringerLink," Metallurgical and materials transactions A, 38(8), pp. 1681-1691.
[17] Raghavan, V., 2010, "Al-Cu-Fe (Aluminum-Copper-Iron)," Journal of Phase Equilibria and Diffusion, 31(5), pp. 449-452.
[18] Burkhardt, U., Grin, Y., Ellner, M., and Peters, K., 1994, "Structure refinement of the iron–aluminium phase with the approximate composition Fe2Al5," Acta Crystallographica Section B: Structural Science, 50(3), pp. 313-316.
[19] Grin, J., Burkhardt, U., Ellner, M., and Peters, K., 1994, "Refinement of the Fe4Al13 structure and its relationship to the quasihomological homeotypical structures," Zeitschrift fuer Kristallographie, 209(6), pp. 479-487.

[20] Yanson, T. I., Manyako, M. B., Bodak, O. I., German, N. V., Zarechnyuk, O. S., Cerný, R., Pacheco, J. V., Yvon, K., and IUCr, 1996, "Triclinic Fe3Al2Si3 and Orthorhombic Fe3Al2Si4 with New Structure Types," Acta Crystallographica Section C: Crystal Structure Communications, 52(12), pp. 2964-2967.
[21] Roger, J., Jeanneau, E., and Viala, J. C., 2011, "Crystal structure of the ternary compound γ-Al3FeSi," Zeitschrift für Kristallographie Crystalline Materials, 226(11), pp. 805-813.
[22] German, N. V., Zavodnik, V. E., Yanson, T. I., and Zarechnyuk, O. S., 1989, "Crystal Structure of FeAl sub 2 Si," Kristallografiya, 34(3), pp. 738-739.
[23] Gueneau, C., Servant, C., d'Yvoire, F., and Rodier, N., 1995, "FeAl3Si2," Acta Crystallographica Section C: Crystal Structure Communications, 51(2), pp. 177-179.
[24] Corby, R. N., and Black, P. J., 1977, "The structure of α-(AlFeSi) by anomalous-dispersion methods," Acta Crystallographica Section B: Structural Crystallography and Crystal Chemistry, 33(11), pp. 3468-3475.
[25] Rømming, C., Hansen, V., and Gjønnes, J., 1994, "Crystal structure of β-Al4.5FeSi," Acta Crystallographica Section B: Structural Science, 50(3), pp. 307-312.
[26] Gueneau, C., Servant, C., d'Yvoire, F., and Rodier, N., 1995, "Fe2Al3Si3," Acta Crystallographica Section C: Crystal Structure Communications, 51(12), pp. 2461-2464.
[27] Heumann, T., and Dittrich, N., 1959, "Structure character of the Fe2Al5 intermetallics compound in hot dip aluminizing process," Z Metallk, 50, pp. 617-623.
[28] Springer, H., Szczepaniak, A., and Raabe, D., 2015, "On the role of zinc on the formation and growth of intermetallic phases during interdiffusion between steel and aluminium alloys," Acta Materialia, 96, pp. 203-211.
[29] Takata, N., Nishimoto, M., Kobayashi, S., and Takeyama, M., 2014, "Morphology and formation of Fe–Al intermetallic layers on iron hot-dipped in Al–Mg–Si alloy melt," Intermetallics, 54, pp. 136-142.
[30] Cheng, W. J., and Wang, C. J., 2010, "Observation of high-temperature phase transformation in the Si-modified aluminide coating on mild steel using EBSD," Materials Characterization, 61(4), pp. 467-473.
[31] Eggeler, G., Auer, W., and Kaesche, H., 1986, "On the Influence of Silicon on the Growth of the Alloy Layer During Hot Dip Aluminizing," J. Mater. Sci, 21(9), pp. 3348-3350.
[32] Bouché, K., Barbier, F., and Coulet, A., 1998, "Intermetallic compound layer growth between solid iron and molten aluminium," Materials science & engineering. A, Structural materials : properties, microstructure and processing, 249(1), pp. 167-175.
[33] Kobayashi, S., and Yakou, T., 2002, "Control of intermetallic compound layers at interface between steel and aluminum by diffusion-treatment," Materials Science & Engineering A, 338(1), pp. 44-53.
[34] Danzo, I. I., Houbaert, Y., and Verbeken, K., 2014, "Diffusion driven columnar grain growth induced in an Al–Si-coated steel substrate," Surface and Coatings Technology, 251, pp. 15-20.

# Appendix E

# Effect of coatings on the metallurgical bond formation

**Introduction**

The automotive industry is pushing further light-weighting of components to meet future regulations on the carbon footprint of motor vehicles. This push requires further development of lightweight metals such as aluminum and magnesium and their manufacturing methods. While aluminum exhibits good specific strength, certain requirements like high stiffness or wear resistance at elevated temperatures does require the heavier ferrous alloys. However, by selectively reinforcing aluminum castings with ferrous inserts it is possible to utilize the materials superior properties and still reduce the weight. A cost-effective method to manufacture these bimetallic casting is by placing the insert within the mold and casting aluminum around it.

The performance of the aluminum-iron macrocomposite can be improved by ensuring a chemical bond between them[1, 2]. Limited solubility of aluminum in iron produces a metallurgical bond consisting of intermetallic compounds (IMC) at the interface. The IMC formed tend to be dependent on the composition of the aluminum alloy. It has been shown that when silicon is present in the liquid aluminum it drastically changes the growth rate, morphology and composition of the formed metallurgical bond. The most commonly researched alloy is A356 (7.5wt%Si and 0.35wt%Mg) and tends to form a reaction layer consisting of three layers, an η-($Fe_2Al_5$) layer in contact with the steel, a middle layer consisting of θ-($Fe_4Al_{13}$), and $\tau_5$-($Al_{7.4}Fe_2Si$) in contact with the aluminum and the growth of the interaction layer is diffusion controlled[3-5].

The diffusional nature of the bond formation on ferrous insert has proven to be difficult during casting without any interfacial engineering due to the short time in contact with liquid aluminum[2, 6-9]. Nucleation of the IMCs on the insert requires both time for diffusion and unobstructed contact between the two metals. The ferrous substrate needs to be free of contaminations and an oxide layer can prevent the bond formation[2, 6][durrant, aguado]. This makes it challenging to preheat the substrate due to the formation of iron oxides at the insert interface when exposed to elevated temperature in atmospheric conditions. A continuous metallurgical bond can be formed by utilizing the so-called Al-Fin process [10] where the steel is dipped in liquid aluminum alloy then quickly transferred to the mold and cast in[1, 2, 9, 11, 12].

Zinc has proven to be effective for improving the bond formation during casting. Choe et al.[7] were able to form a bond between a 1045 steel and A356 utilizing a zinc plated coating in an expandable pattern casting process which in comparison to a non-coated steel formed a bond and gave superior shear strength properties of the interface area. Liu et al.[13] successfully bonded mild steel samples to aluminum in a permanent mold casting process. They compared an electroplated zinc coating with a hot-dip galvanized samples that were transferred directly from the Zn bath to the mold with the conclusion that the preheated galvanized coating yielded better results. Aguado et al.[6] investigated the metallurgical bond formation of sandcast A356/low alloy steel castings which were both electroplated and hot-dip galvanized, and in both cases ternary Al-Fe-Si phases were present at the interface. However, they noticed the presence of both Zn, Al, and Mg oxides present within the interface for the electroplated samples. A systematic study on the effects of Zn in the aluminum alloy and Zinc coatings (electroplated and hot-dip) on the reaction layer growth by Springer et al. [14] showed that the presence of a zinc coating during liquid-solid interaction enhances the regularity of the reaction layer. While the effect is most pronounced for the hot-dipped coating the electroplated coating was still proven to be effective and it is believed that this is due to the ability of the applied coatings to keep the steel surface insert clean while quickly dissolving into the liquid aluminum.

Another attractive coating for bonding aluminum and steel would be steel due to its exothermic reaction with aluminum. Durrant et al. [2] investigated the formed microstructure of thermally sprayed titanium coatings and their reaction with Al-7wt%Si alloy during a squeeze casting process. The samples were preheated to 300°C and 900°C before casting and the results of the study shows only minimal interfacial reaction (only noticed reduction of the titanium oxide) of the sample preheated to 900°C.

Forming a metallurgical bond between aluminum and steel during casting is as previously mentioned a difficult task. Application of a zinc coating has been reported [14] to improve the wettability of liquid aluminum and solid steel which helps initiate the otherwise slow metallurgical bond formation. Fast formation of the metallurgical bond is a requirement casting processes that does not allow much time for diffusional growth processes. A metallic coating such as Zn or Sn is interesting due to that it is sacrificial nature and that there is a relatively high tolerance for these in the aluminum alloy specifications.

A titanium coating is of interest due to the stability of the titanium aluminides which could prove to be more stable compared to the ternary Al-Fe-Si phases that tend to form Kirkendall porosity during subsequent heat treatment of the bimetallic casting[5]. Cold spray is a technique in which powder particles are accelerated to supersonic velocity and impacted on a substrate and adhere due to deformation of the particles and the substrate[15]. This versatile coating technology could prove ideal for powder metal coating applications.

**Objective**

This study aims to investigate the efficiency of three metallic (Zn, Sn, and Ti) coatings on the metallurgical bond formation between a coated mild steel and liquid aluminum alloy. The efficiency of the coating will be measured by its ability to form a continuous reaction layer between the aluminum and the iron during hot-dipping in aluminum alloy and casting experiments.

**Experimental**

*Zinc and Tin Coating*

Hot-dip coated steel samples were prepared from a 6.3 mm and 12.6 mm diameter mild steel (1018) rod and cut in to 76 mm long sections. The steel samples were ground to a 600-grit surface finish, degreased in ethanol and acetone in an ultrasonic bath for 2 minutes, pickled in a 10%HCl solution for 5 minutes, submerged in a water solution of ZnCl and $NH_4Cl$ at 38°C ± 4°C, and drying in furnace at 100°C±5°C.

The hot-dip galvanized samples were submerged in preheated zinc (99.99%) bath (0.65 kg) at 480°C ± 10°C) for 30 seconds and carefully extracted from the melt and allowed to air cool. The dipping time was experimentally determined to achieve a continuous well adhered coating with a limited reaction layer thickness. The hot-dip tinned samples were submerged in preheated tin (99.97%) bath (0.65 kg) at 300°C ± 10°C) for 60 seconds and carefully extracted from the melt and allowed to air cool. The dipping time was experimentally determined to achieve a continuous well adhered coating with a limited reaction layer thickness.

Hot-dip experiments were carried out with the 6.3 mm diameter coated samples in A356 (7.5 wt%Si, 0.35wt% Mg, and 0.15 wt%Ti) aluminum alloy at 700°C±10°C in a electrical resistance furnace, for several timesteps to determine the progression of the metallurgical bond formation. The coated samples were submerged into the aluminum for 1, 3, 5 seconds and carefully removed and quickly quenched in

water. As mentioned before, the dipping time is measured to be for example 1 second, the real interaction time between the sample and the melt is more like 3 seconds for certain parts of the sample. Although care was taken to extract it slowly it still introduces a melt flow around the surface of the steel.

Bimetallic samples were cast by placing the coated samples (6.3 and 12.6 mm diameter samples) in a sand mold with the dimensions 25 mm diameter and 39 mm tall. Approximately 10 kg of aluminum alloy, A356, was melted in an induction furnace and brought up to 725°C and degassed using Ar in a rotary degasser for 30 minutes and the samples were cast.

The samples were prepared by standard metallurgical preparation methods, and analyzed by optical microscopy (OM; Nikon), scanning electron microscopy (SEM; JEOL JSM-7000F) equipped with an energy dispersive spectrometer (EDS, Oxford Instruments or X-Max$^N$).

*Cold Spray Titanium Coating*

The as-received stock of titanium coated steel was CP-Ti powder cold sprayed on a 1018 mild steel rod with a diameter of 25 mm. Round samples with a thickness of 8 mm were cut from the stock and cut in quarters. The preexisting oxide layer of the titanium coating was removed by grinding the coating with 400 grit SiC paper, etching in a HF(48%):$H_2O_2$(30%):$H_2O$ = 1:1:20 solution at room temperature for 15 minutes, rinsed in deionized water and degreased in ultrasonic bath of acetone for 5 minutes. Three hot-dip experiments of titanium coated steels were performed aimed investigate the effect of oxide layer presence and chemistry of the aluminum alloy.

For all of the experiments 0.67 kg of either pure Al (99.99%) or A356 alloy and placed in a silicon carbide crucible and heated to 700°C ± 10°C in an electrical resistance furnace. The samples were dipped with the coated surface facing away from the melt surface to allow for a fresh melt front to flow over the coating. Special attention was put on inserting the substrate within 2 seconds of skimming the melt surface to remove any excessively thick oxide layer on the melt surface. After removal from the melt the samples were allowed to air-cool.

The first experiment the samples were submerged in liquid A356 aluminum alloy for 5, 7, 10 and 15 minutes. In the second experiment the samples were dipped in pure aluminum for 1, 2, 5 and 10 minutes. For the third experiment the titanium coating was covered in a commercial titanium brazing flux, with the composition; 10-25 wt.% Potasium Bifloride, 10-25 wt.% Lithium Flouride, 25-45 wt.% Potasium Flouride. Then preheated in the furnace for 2 minutes before insertion into the melt and kept for the following timesteps; 30 seconds, 1 minute, 2 minutes and 5 minutes.

The samples were prepared by standard metallurgical preparation methods, and analyzed by optical microscopy(OM; Nikon ), scanning electron microscopy (SEM; JEOL JSM-7000F) equipped with an energy dispersive spectrometer(EDS, Oxford Instruments or X-Max$^N$).

**Results**

*Zinc and Tin Coatings*

The hot-dip galvanization procedure yielded a continuous coating with an average Zn layer thickness 19 μm (standard deviation of 6 μm) and on average 23 μm (standard deviation of 7 μm) IMC layer. The tip of the coated steel rod had a small bulge of a slightly thicker zinc layer. A micrograph of the typical microstructure of a zinc coated steel rod can be seen in Figure 1a, and two phase layers could be detected using EDS analysis, an inner δ-($FeZn_{10}$) with the measured composition(11at%Fe and 89

at%Zn) and the ξ-($FeZn_{13}$) with the average composition (6.5 at%Fe and 93.5 at%Zn) see Figure 1b, which is consistent with literature.

The hot-dip tinning produced a tin coating consisting of an average 8 µm (standard deviation of 2 µm) thick tin layer and a 2 µm ± 0.5 µm thick IMC layer. A representative micrograph of the tin coated steel can be seen in Figure 1c. During SEM analysis of the reaction layer it was difficult to get consistent quantitative measurements of the IMC layer and the average of 9 measurements was calculated to be 69.9 at.%Sn and 30.1 at.%Fe. The values fit best with $FeSn_2$ and the slightly high value of tin is likely due to the large interaction volume of the electrons producing the characteristic x-rays and the relatively thin reaction layer.

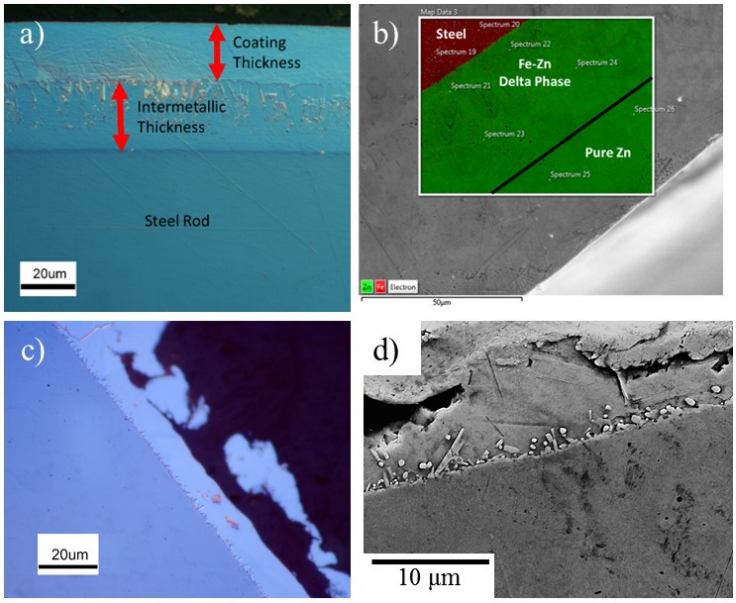


*Figure 1: a) Micrograph of a hot-dip galvanized steel. b) EDS map of hot-dip galvanized steel with the phases present indicated. c) Micrograph of hot-dip tinned sample with the corresponding SEM micrograph in d).*

*Titanium Coating*

A typical micrograph of the cold sprayed titanium coating can be seen in Figure 2a. The average thickness of the coating is 149 µm (standard deviation of 28 µm) the relatively high standard deviation is due some areas of the sprayed coating has a thinner coating. The thinnest thickness measured was 86 µm while the thickest measurement of the coating was 206 µm. No chemical reaction layer was discovered between the titanium coating and the steel substrate. Figure 2b shows the surface topography of the titanium coating which is pointy in nature and is likely due to the etchants used to remove the preexisting oxide layer. There is a visible residue particle from one of the cleaning steps circled in Figure 2c.

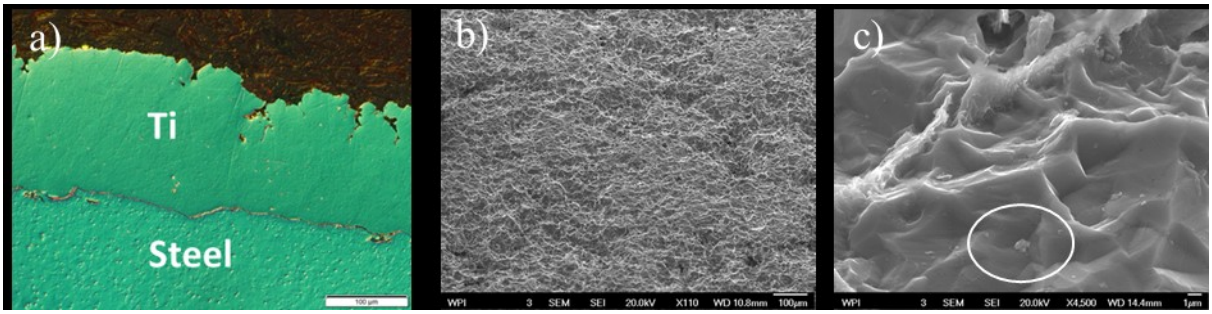

*Figure 2: a) Micrograph of titanium coated steel. b) and c) SEM image of the titanium surface after oxide removal.*

*Hot-dipping of Zn Coated Steel in A356*

The samples dipped for 1 second in the aluminum alloy still contains a thick layer of metal on the outside indicating that some of the aluminum instantly solidifies the cold steel surface and the short dipping time is not enough to reheat it enough for it to melt. Figure 3a shows an SEM micrograph with elemental EDS mapping of the interface between the steel and the remaining metal on the surface. It appears that Zn melts very quickly upon contact with the liquid aluminum and there is mixing of the two metals, see white arrow. There is however, an inner layer that contains on average according to EDS point analysis 27 at%Zn, 63 at%Al, and 6at%Fe and 4Si at%. Figure 3b is a SEM micrograph from the same sample at a different location where the inner layer where no reaction is observed. An outer layer of aluminum can be seen covering the Zn layer without any interaction.

The micrograph in Figure 3c which is after 3 seconds of dipping time there are still areas in which the zinc layer has not completely melted and mixed with the aluminum melt and one area similar to the one shown in Figure 3b with unmelted zinc was found. Figure 3d is from the same sample but a different cross section and the white arrow indicates a phase layer present at the steel interface, quantitative measurements of the composition of the layer proved difficult due to the thin layer in combination with a relatively large interaction volume of the electrons producing the characteristic x-rays. The dendritic nature of the aluminum is also visible and the EDS map indicates relatively large amounts of Zn present, an average of 33 at%Zn was present in the matrix.

After 5 seconds of dipping time no zinc or zinc rich IMCs are present at the interface, see Figure 3e, and the concentration of zinc within the aluminum matrix has decreased to 14 at%Zn. A very uniform metallurgical bond formed between the aluminum and steel and was measured to be 7 μm (standard deviation of 1 μm) thick. Figure 3f shows a magnified micrograph of the metallurgical bond after 5 seconds of dipping and the measured composition of the reaction layer formed is 2 at%Zn, 71 at%Al, and 20 at%Fe and 7 at%Si which corresponds fairly well with $\tau_5$-($Al_{7.4}Fe_2Si$) [16].

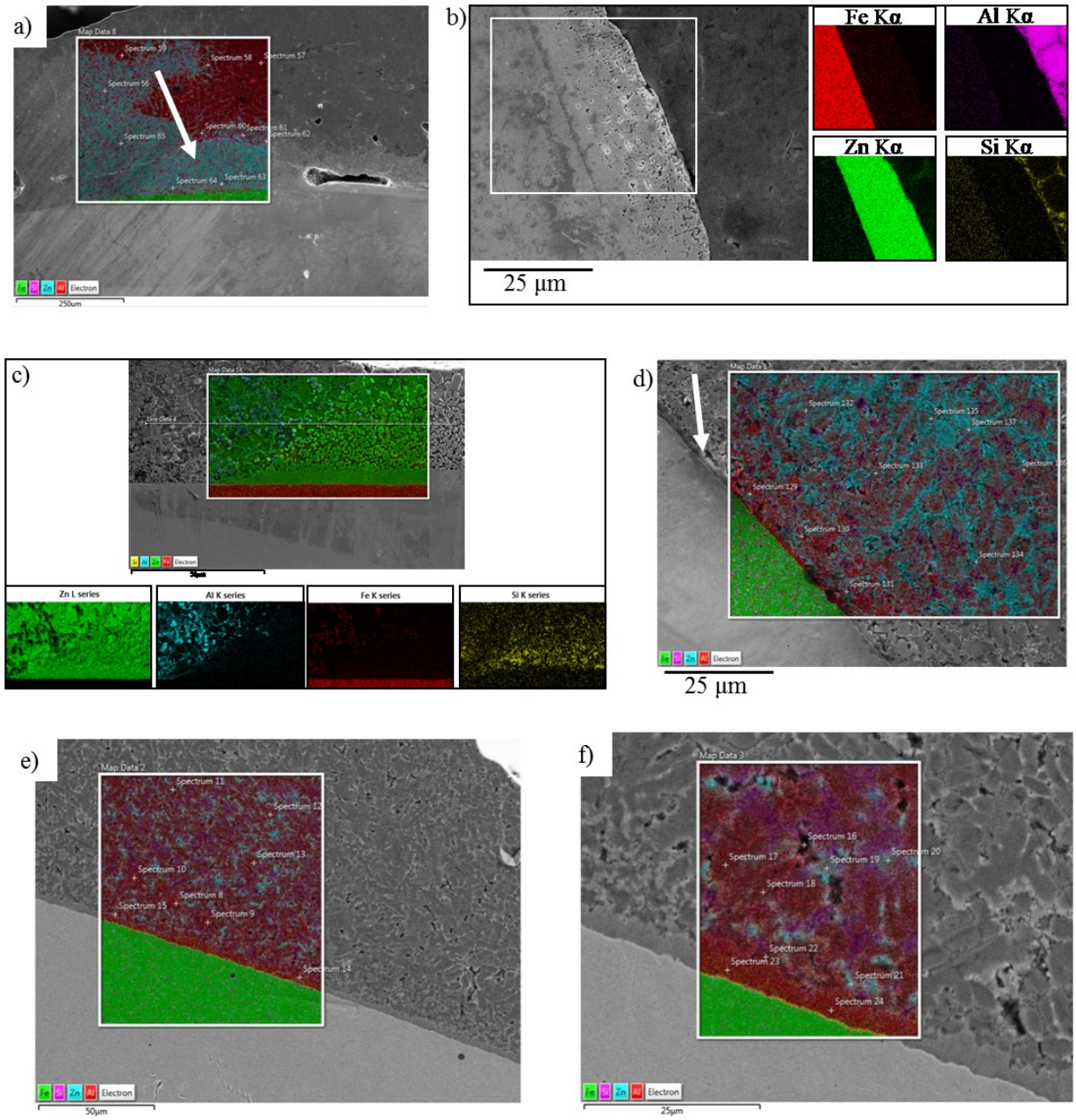


*Figure 3: SEM and EDS analysis of hot-dip galvanized steel samples dipped in liquid A356 for a) and b) 1s, c) and d) 3 seconds, e) and f) 5 seconds.*

*Hot-dipping of Sn Coated Steel in A356*

The micrographs shown in Figure 4 shows the difference in microstructure of the Sn coated specimen for dipping 1, 3, and 5 seconds. In Figure 4a the micrograph clearly shows that a reaction layer between the steel and the liquid aluminum has started to form. The EDS maps corresponding to the micrograph it can be seen that the layer consists of Al, Fe, and Silicon but very little Sn. It is too thin to get accurate quantitative point analysis using EDS and the average thickness of the reaction layer is measured to be 2 µm (standard deviation of 0.6 µm). The micrograph reveals that there is a relatively large quantity interdendritic segregation of Sn, see white arrows in Figure 4, in the aluminum matrix surrounding the steel insert.

After 3s of submersion in liquid aluminum alloy the microstructure is fairly similar to the 1s sample, see Figure 4b. The bond seems to have advanced slightly and the morphology is slightly irregular. The thickness of the formed metallurgical bond was measured to be 4 μm (standard deviation of 1 μm) and the irregular nature of the bond contributes to the slightly higher standard deviation. The composition of the phase contains on average 70 at%Al, and 21 at%Fe and 9 Si at% which corresponds to $\tau_5$-($Al_{7.4}Fe_2Si$). There are still significant interdendritic segregation of Sn in the aluminum matrix.

In figure Figure 4c the formed microstructure after 5 seconds of dipping is visible. Metallurgical bond is clearly visible with a thickness of 6 μm (standard deviation of 0.9 μm) and the EDS point analysis measures the composition to 1 at%Sn, 69 %Al, and 20 at%Fe and 10 Si at% which similar to the 3 second sample corresponds to $\tau_5$-($Al_{7.4}Fe_2Si$). There also seems to be significantly less interdendritic segregation of Sn.

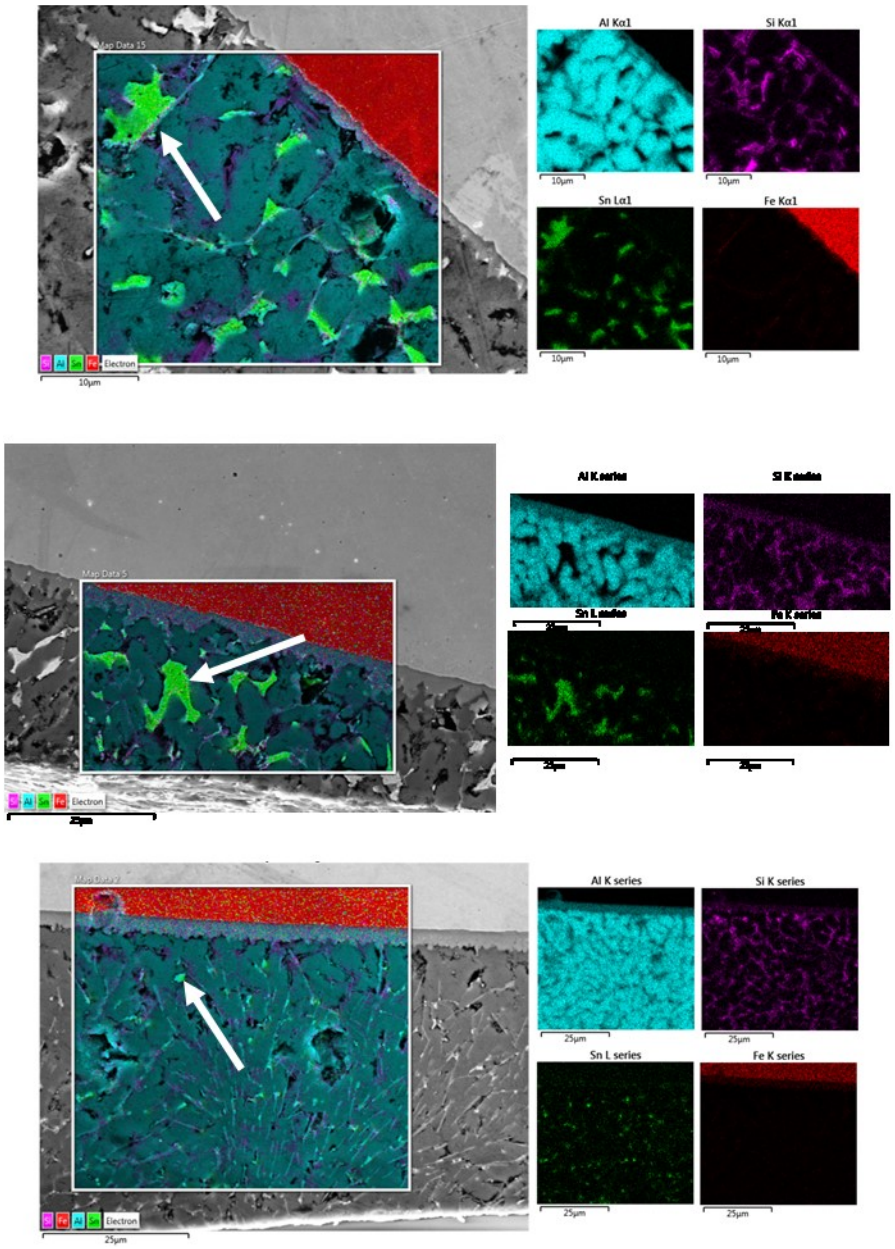


*Figure 4: SEM and EDS analysis of hot-dip galvanized steel samples dipped in liquid A356 for a) 1s, c) 3 seconds, e) 5 seconds.*

*Hot-Dipping of Titanium Coated Steel in A356 and Pure Al*

Three different experiments were performed with a titanium cold spray coating. The first experiment was dipping the substrate in A356, the second in pure Al, and the third in A356 but with a protective flux to prevent oxidation of the surface.

Overall the reactivity between the titanium and A356 is poor. There was no indication of interaction until 15 minutes of dipping time, see Figure 5a. The micrograph shows a that a thin reaction layer has formed with certain section more reacted than other indicated by the white arrow. To identify the formed phases this sample was investigated in the SEM and analyzed using EDS, see Figure 5b, and the EDS maps clearly indicate two phases. The thicker layer consists on average of 25 at%Ti, 64 at%Al,

and 11 at%Si and was identified to be $TiAl_3$ [17] with 10 at.% Si. The silicon rich needle shaped layer on the titanium interface had a measured composition of 28 at%Ti, 27 at%Al, and 45 at%Si and was identified to be $\tau_1$-($Al_2Fe_3Si_3$)[17].

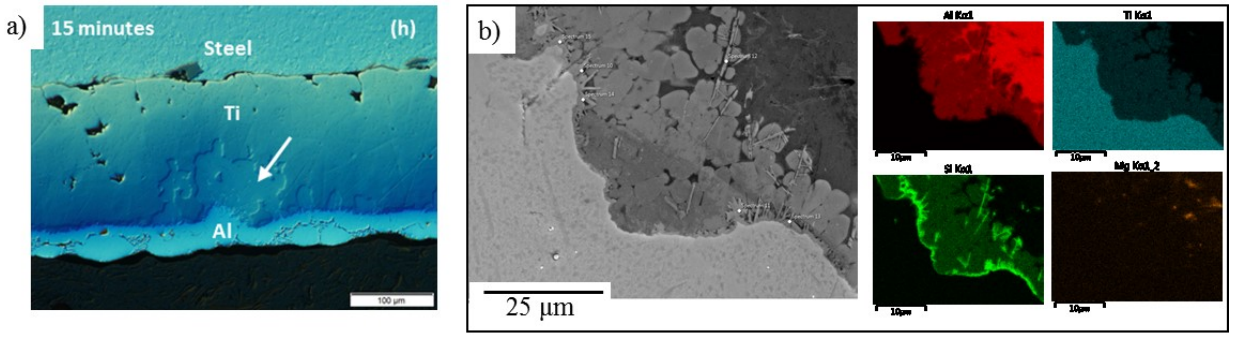


*Figure 5: a) Micrograph of a titanium coated steel sample dipped in A356 for 15 minutes. b) SEM micrograph and EDS analysis of the formed reaction layer.*

Pure aluminum initiated a reaction with the titanium at shorter interaction times. Small reaction zones are visible after five minutes, see the white arrow in Figure 6a. However, after five minutes only small zones mostly in crevices in the titanium coatings were visible. After 10 minutes of dipping time a substantial continuous reaction layer has formed between the aluminum and the titanium coating that is clearly visible in Figure 6b and was measured to have an average a thickness of 68 µm (standard deviation of 12 µm). The reaction layer is ragged and is visually similar to the reaction layer that forms between pure aluminum and steel[18]. To identify the phase formed between the aluminum and titanium the 10-minute sample was analyzed using EDS. Figure 6c shows the EDS maps and only two major elements were detected Al and Ti. Analysis of the reaction zone gives an average composition 24 at%Ti and 76 at%Al. This composition is a little high in aluminum but fits well with the binary $TiAl_3$ phase.

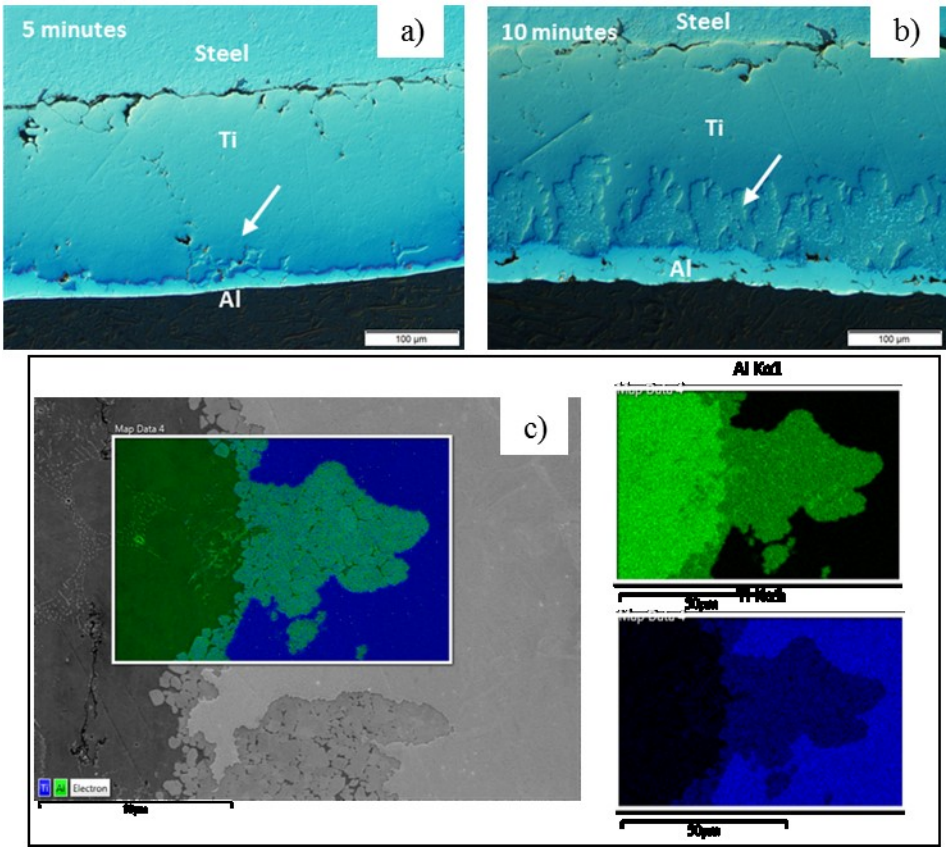


*Figure 6: Micrograph of a titanium coated steel sample dipped in pure aluminum for a) 5 minutes b) 10 minutes and c) SEM micrograph and EDS analysis of the formed reaction layer.*

For the third experiment a flux paste was applied to compare the effect of oxidation of the titanium and the effect of alloying elements in the liquid aluminum. To improve the efficiency of the flux had to be melted so samples had to be preheated to the melting point of the flux which is around 540-595°C. The flux had a profound effect on the time it takes to initiate a reaction between the Al and Ti. Figure 7 shows micrographs of the interface of the coating and the aluminum alloy and the white arrow indicates a formed reaction layer. The shortest dipping time this coating combination that was tried was 30 seconds which formed spots of reaction zones. After 1 minute a thin (~5 µm) continuous reaction layer has formed on the interface which has grown to approximately 8 µm after 5 minutes.

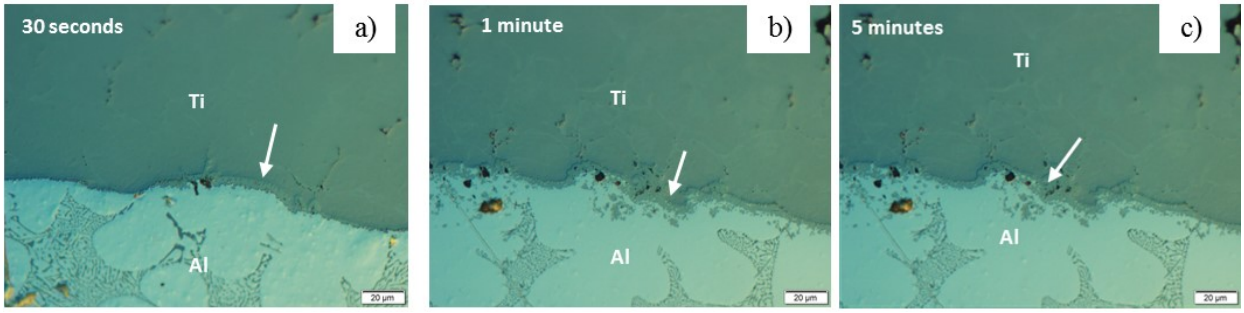


*Figure 7: Flux coated titanium sample dipped for a) 30 seconds b) 1 minute, and c) 5 minutes.*

**Discussion**

*Efficiency of Hot-Dip Zn and Sn Coatings*

Joining two metals does normally require a certain energy input and the available energy for the bond formation during casting is limited to the energy release during solidification and cooling. From the results shown in Figure 3a the segregation of Al and Zn makes it look like the zinc melts and starts mixing with the aluminum alloy. Similarly, Figure 3c also shows segregation of Al and Zn and it looks like the binary dissolution of the Fe-Zn δ-phase is progressing from left to right. The results indicate that the Zn coating seemingly melts and mixes with the Al and assuming this is true also for the Sn coating this is a phase transformation that requires energy. Studying the bond progression in Figure 3 and 4 it is clear that the formation of the metallurgical bond is initiated fast. These observations indicate that the limiting factor for metallurgical bond formation during multimaterial metal casting is not energy input.

The ternary A-Fe-Si IMC layer readily forms at the steel interface after short (3-7 seconds) liquid aluminum interaction time. The bond was identified to consist of $\tau_5$-($Al_{7.4}Fe_2Si$) which corresponds well with literature[5] and it is the phase that is in equilibrium with the A356 liquid composition. However, the binary $Fe_4Al_{13}$ and $Fe_2Al_5$ could not be detected and is normally accompanying the $\tau_5$-($Al_{7.4}Fe_2Si$) layer at the steel interface as in [3]. Aluminum is considered to be the fast diffuser and the short dipping time in combination with the fast cooling rate does allow enough time for the formation of the binary layers.

The lack of a reaction between the reference sample and the aluminum melt despite the fast reaction rate shows indicates very poor wetting. Wetting angle measurements of binary Al alloys performed by Fragner et al. [19] states a wetting angle of 59° between Al-7wt%Si alloy and mild steel which is considered to be partially wetting the substrate[20]. The formation of oxide layers reduces the wetting between aluminum and iron [19] which is likely one of the contributing factors to the poor wetting of the reference sample. In addition to the reduction in wetting an oxide film can act as an effective diffusion barrier.

When casting in steel into aluminum castings two oxide layers can form between the two metals. If the steel is improperly cleaned there will be an iron oxide layer on the surface and as aluminum flows alumina will instantaneously form on any newly exposed liquid. If air gets entrapped between the liquid Al and steel the oxygen will at the elevated temperature oxidize the exposed metal. The Zn and Sn coating will protect the steel from oxidation but the coating and thin oxide layer on the aluminum melt front as it covers the surface of the coated steel during insertion.

When aluminum is flowing, or surrounds an uncoated insert it could potentially be covered in a layer of aluminum oxide while a coated insert is covered in several layers, the innermost will be a layer of IMCs which bonds the coating to the steel, the metallic coating, a layer of coating oxide, a layer of alumina from the melt front and then surrounded by the aluminum melt, see Figure 8a and b. While the melting point of the Zn and Sn oxides are above 1500°C[21], alumina is above 2000°C[22], the Zn or Sn melts and the solid oxide layers become surrounded by liquid. During a casting operation, the velocity of the liquid during mold filling will exert shear stresses on the oxide layers. However, according to boundary layer theory these will be at a minimum close to a surface, see Figure 8c. But when the coating melts the solid-liquid interface moves which can destabilize the oxide layer and allow for mixing of the two liquid metals.

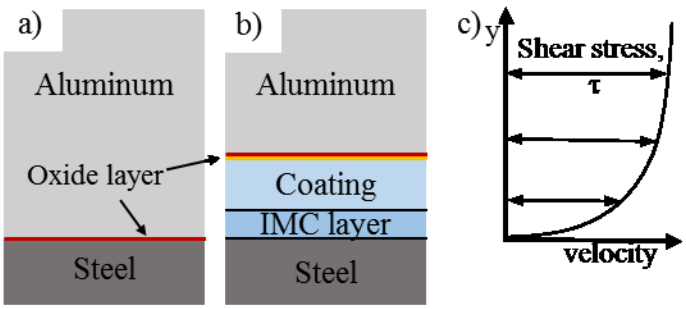

*Figure 8: Sketch of the suggested reason for wetting improvement.*

The mixing allows for the aluminum alloy to come in contact with the steel surface without any reactive wetting required. During dipping experiments, the sample exhibit slight different conditions compared to what a cast-in insert would experience with the biggest difference is during extraction of the sample. While the rate at which the samples were inserted to the melt is on the same scale as the velocity of a melt front the extraction step simply does not occur during casting. The effect will be of greater magnitude for short dipping times but is in a way self-counteracted for the shortest dipping time due to the instant solidification and extraction of a thick solid/semisolid layer around the steel. However, when this layer is not present the introduction of melt flow around the steel could affect the results and show greater efficiency of the coating than what it would during casting.

*Comparison: Zn and Sn*

In comparison, the Sn coating offers a faster formation of a metallurgical bond between the steel and the aluminum, a close to continuous ternary Al-Fe-Si layer on the steel surface after 1 second of dipping time. The higher melting point and thicker coating of zinc seems to slow down the initiation of the bond and there are still indications of a zinc layer present after 3 seconds of dipping time, see Figure 3c. To increase the efficiency of the zinc coating a common technique to reduce the IMC layer during hot-dip galvanizing is to add aluminum to the zinc bath. This creates a very thin layer of $Fe_2Al_5$ between the Zn and the steel which inhibits growth of the δ-phase[14]. Removal of the δ-phase could reduce the time for dissolution of the zinc layer. The Sn coating on the other hand is thinner and the formed reaction layer is also significantly thinner and has a lower melting point which allowed for faster metallurgical bond formation.

Quick dissolution of the coating metal is important to reduce the local concentration of coating element to avoid a macrosegregation within the casting. Elevated concentrations of Sn will as seen in Figure 4 cause interdendritic segregation which if thermally treated could cause incipient melting. Similarly, excessive amounts of zinc within the interdendritic space can also be seen in Figure 3. These problems could potentially be alleviated during casting by utalizing the melt flow for removal and dispersion of the coating material.

*Titanium Coating*

Generally, the wetting behavior of molten aluminum on the coldsprayed titanium coating was poor and it took several minutes to initiate any reaction between the two metals. In some cases, there was very little contact at all between the aluminum and the coating, see Figure 9 which is the interface after 10 minutes of dipping in A356 at 700°C. The inability to achieve continuous contact between the liquid and the solid could be due to the surface roughness of the titanium coating. Surface roughness does have an impact on the wetting and will be system dependent [20] and presence of an aluminum oxide

film at the liquid interface changes the surface tension [23] which could bridge the certain roughness magnitudes and prevent wetting.

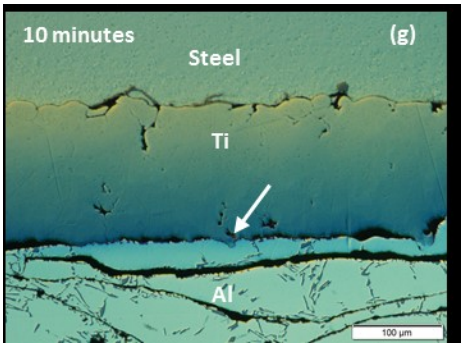


*Figure 9: Micrograph of titanium coated steel dipped in A356 for 10 minutes.*

Analysis of the reaction layer formed between A356 and the titanium coating revealed that there are two layers forming. A $TiAl_3$ layer with approximately 10 at.% of Si at on the aluminum which has been described by previous authors[17, 24, 25] and the second layer is much higher in silicon and EDS point analysis indicates an average composition of 28 at% Ti, 27 at% Al, and 45 at% Si In comparison with the results presented by Gupta [17] the composition and shape are in good accordance for the Tau1 phase but the location is different. Gupta report formation on the $TiAl_3$/Al interface while Figure 7c indicates that there is a thin layer forming on the Ti/$TiAl_3$ interface and some formation around the $TiAl_3$/Al interface. A similar silicon rich phase was not identified in [24, 25] which are experimentally more similar to this study. Differences could be due to higher silicon concentrations (~10-12 at.%) temperatures(750-900°C) in the previously mentioned studies and commercial A356 also contains Mg, Ti and Fe in small amounts. EDS is semi-quantitative and the large interaction volume of the electrons make accurate compositional analysis of small phases difficult and prone to relatively large errors and a more in depth analysis of the phase is required to confirm.

While phase determination is required the elevated Si concentrations at the titanium interface is interesting since the silicon concentration increases with increasing diffusion distance from the source, see Figure 12. The liquid aluminum contains ~7.2 at.% Si the $TiAl_3$ phase ~11 at.% and what is presumed to be Tau1 the average measured value is ~42 at.% Si. This layered structure would suggest that silicon is a faster diffuser through the $TiAl_3$ structure compared to aluminum which could be due to the high affinity between Al and Ti but further investigation is needed to determine the mechanism.

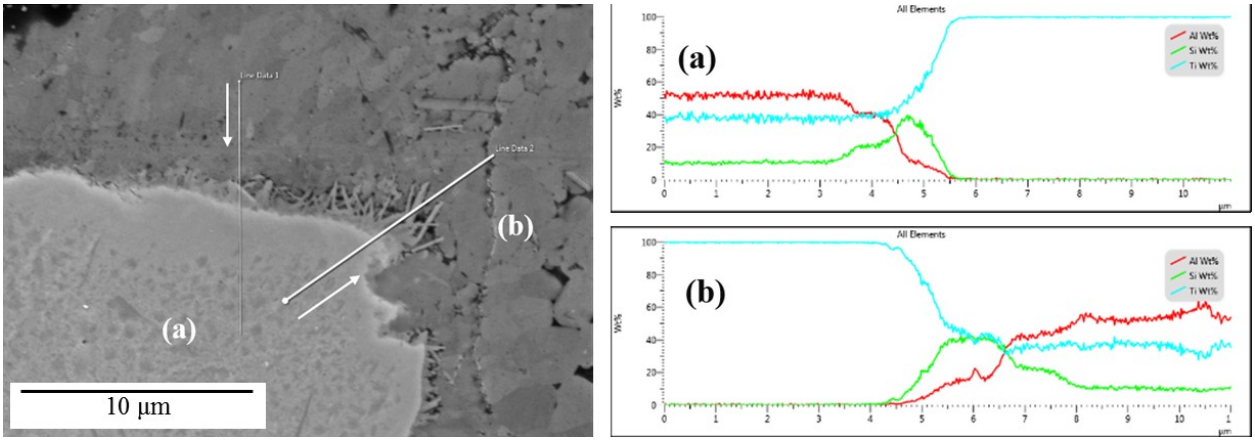

*Figure 10: a) SEM micrograph of the reaction layer of a titanium coated steel sample dipped for 15 minutes at 675°C b) EDS line scans across the interface.*

It was determined by Cammarota et al. [25] that silicon reduces the growth rate of the reaction layer. While there is not enough data within this study to collaborate these findings the reduction in growth rate could give insights to the difference in time it takes to form a continuous reaction layer between the Ti coating and pure aluminum vs A356. The time it took for the formation of a reaction layer was reduced from 15 to 10 minutes. Results from Harach and Vecchio[26] suggests that initially only aluminum is able to penetrate the oxide layers and during interaction and formation of $TiAl_3$ the oxide layer breaks down and more solid surface is exposed to aluminum. This type of reactive wetting or exposure of oxide free metal surface would be dependent of the growth rate of the $TiAl_3$ which is reduced by the additions of Si in the aluminum.

Pure aluminum allowed for faster reaction layer formation but the fluxed sample further reduced the time (10 minutes to 30 seconds). The flux enables preheating of the sample without oxidation of the titanium and could further improve wetting by breaking the aluminum oxides on the liquid metal. The significant improvement would suggest that the oxide layers has a greater effect on the timescale for metallurgical bond formation compared to the melt composition.
In accordance with [26] the reaction did not proceed upon cooling which would be an indication of self-propagating high-temperature synthesis coating. Which could be due to not reaching the adiabatic temperature (1245°C [27]) and if ignited such temperature could be hard to keep due to efficient heat transfer to the liquid aluminum.

The morphology of the reaction layer formed between the titanium and pure aluminum, see Figure 6b, is similar to the morphology between pure aluminum and iron. However, the formed $TiAl_3$ is looks to be more porous, similar to [17, 26, 28], in morphology, and islands of Ti isolated from the titanium coating is left behind the growth front, see Figure 11a. A magnification of the area within the white square of Figure 11a can be seen in Figure 11b where it can be seen that the liquid aluminum penetrates in between Ti powder particles (red lines in Figure 11a) that are not completely fused together. The islands of Ti within the reaction layer is larger Ti particles that has not yet been consumed by the aluminum to form $TiAl_3$.

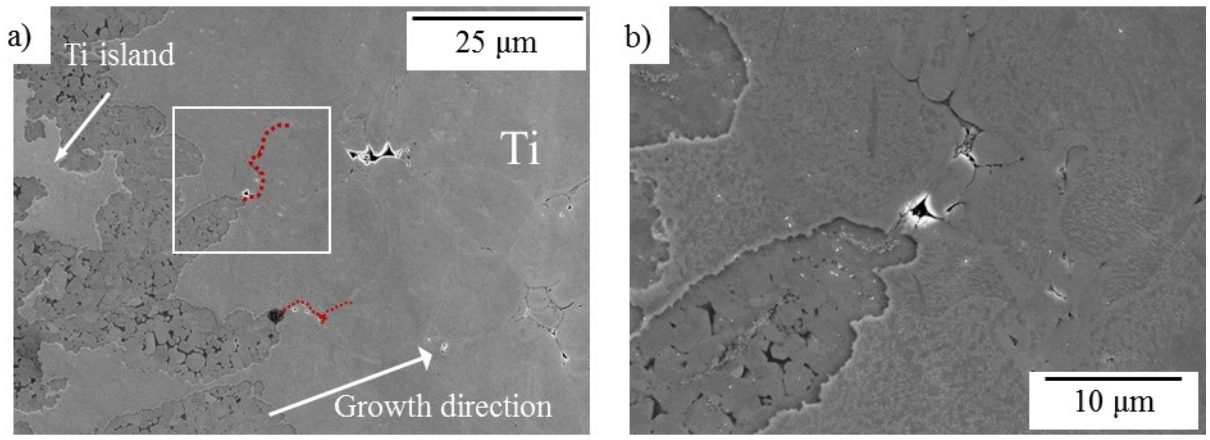


*Figure 11: Reaction layer of the Ti coated steel with pure Al. Growth direction of the $TiAl_3$ and the red lines indicate boundaries between powder particles.*

*Suitable coatings for multimaterial metal casting*

Tin is superior to zinc for accelerated metallurgical bond formation between both A356 and steel. In the case of industrial application, the price of the coatings, and tin is in today's metal prices over 7 times as expensive as zinc. There are on the other hand methods available to improve the hot-dip zinc coating. As mentioned before aluminum can be added to the zinc bath, so called galvalume coating, to change and significantly reduce the IMC layer formed between the zinc and the steel. Normally there are also excess zinc wiping techniques employed at continuous hot-dip galvanizing lines to reduce the zinc thickness. Electroplating is also an alternative to keep the zinc or tin coating thinner compared to hot-dipping processes. Springer et al [Springer zn] compared electroplated vs a galvanized (Zn with 2wt% Al) coating and reached the conclusion that the hot-dipped coating produced a more uniform bond to aluminum.

The titanium coating did not yield a metallurgical bond with A356 or pure Al during a reasonable timeframe for a casting process. However, in combination with a flux the reaction could be initiated fast enough to be more suitable. Use of this coating would however require further development to be useful in a bimetallic aluminum-steel component. The coating procedure needs to be optimized to produce a thinner coating that is consumed by both the steel and aluminum since titanium has coefficient of thermal expansion that is lower than steel [29]. The difference in thermal expansion could cause cracks during subsequent heat treatments. The apparent effect of slowing down the diffusion of aluminum is attractive due the formed Kirkendall porosity during isothermal holding at the aluminum alloy solutionizing temperatures.

**Conclusion**

The hot-dip low melting point metallic coatings offer a sacrificial coating that significantly improves the continuity of the metallurgical bond between aluminum and steel during hot-dipping making them prime candidates for use during casting. A thin coating with low melting point proved to be more efficient and instantly allows for a bond to form between the steel and aluminum alloy.

The results indicate that the formation of the metallurgical bond is not delayed due to insufficient energy input instead poor wetting and most likely poor contact due to oxide layers prohibit its formation. Sufficient aluminum melt flow is recommended around the insert during casting to facilitate mixing of aluminum and the sacrificial metallic coating. The flow will ensure transport of oxide layers away from the insert surface and reduce macrosegregation of coating material around the insert.

Cold sprayed titanium coating exhibits poor wetting of aluminum and is due to the presence of oxide layers. The wetting can be substantially improved by the application of a flux and a metallurgical bond can be quickly initiated. Presence of Si seems to further delay reaction and slow down the diffusion of aluminum through the reaction layer.

Acknowledgements

References

[1] Viala, J. C., Peronnet, M., Barbeau, F., and Bosselet, F., "Interface chemistry in aluminium alloy castings reinforced with iron base inserts," pp. 1417-1420.
[2] Durrant, G., 1996, "Squeeze cast aluminium reinforced with mild steel inserts," Journal of materials science, 31(3), pp. 589-602.
[3] Springer, H., Kostka, A., Payton, E. J., Raabe, D., Kaysser-Pyzalla, A., and Eggeler, G., 2011, "On the formation and growth of intermetallic phases during interdiffusion between low-carbon steel and aluminum alloys," Acta Materialia, 59(4), pp. 1586-1600.

[4] Shih, T.-S., and Tu, S.-H., 2007, "Interaction of steel with pure Al, Al–7Si and A356 alloys," Materials Science & Engineering A, 454, pp. 349-356.
[5] Zhe, M., 2011, "Chemical Changes at the Interface Between Low Carbon Steel and an Al-Si Alloy During Solution Heat Treatment," Journal of phase equilibria and diffusion, 32(6), pp. 486-497.
[6] Aguado, E., 2013, "Comparative Study of Different Interfaces of Steel Inserts in Aluminium Castings," Materials Science Forum, 765, pp. 711-715.
[7] Choe, K., Park, K., Kang, B., Cho, G., Kim, K., Lee, K., Kim, M., Ikenaga, A., and Koroyasu, S., 2008, "Study of the interface between steel insert and aluminum casting in EPC," JOURNAL OF MATERIALS SCIENCE & TECHNOLOGY, 24(1), pp. 60-64.
[8] Bouayad, A., 2003, "Kinetic interactions between solid iron and molten aluminium," Materials science & engineering. A, Structural materials : properties, microstructure and processing, 363(1-2), pp. 53-61.
[9] Bouayad, A., Gerometta, C., Radouani, M., and Saka, A., 2010, "Interface Characterization in Aluminum Alloy Casting Reinforced with SG Iron Inserts.," 1(4), pp. 226-231.
[10] Whitfield, M. G., and Victor, S., 1946, "Coating metal," Al Fin Corp.
[11] Dezellus, O., Digonnet, B., Sacerdote-Peronnet, M., and Bosselet, F., 2007, "Mechanical testing of steel/aluminium–silicon interfaces by pushout," International journal of adhesion and adhesives, 27(5), pp. 417-421.
[12] Jiang, W., 2015, "Improved steel/aluminum bonding in bimetallic castings by a compound casting process," Journal of materials processing technology, 226, pp. 25-31.
[13] Liu, Y., and Bian, 2013, "An investigation of metallurgical bonding in Al-7Si/gray iron bimetal composites," Journal of materials research, 28(22), p. 3190.
[14] Springer, H., Szczepaniak, A., and Raabe, D., 2015, "On the role of zinc on the formation and growth of intermetallic phases during interdiffusion between steel and aluminium alloys," Acta Materialia, 96, pp. 203-211.
[15] Moridi, A., Hassani-Gangaraj, S. M., Guagliano, M., and Dao, M., 2014, "Cold spray coating: review of material systems and future perspectives," Surface Engineering, 30(6), pp. 369-395.
[16] Krendelsberger, N., Weitzer, F., and Schuster, J. C., 2007, "On the Reaction Scheme and Liquidus Surface in the Ternary System Al-Fe-Si | SpringerLink," Metallurgical and materials transactions A, 38(8), pp. 1681-1691.
[17] Gupta, S. P., 2002, "Intermetallic compounds in diffusion couples of Ti with an Al–Si eutectic alloy," Materials Characterization, 49(4), pp. 321-330.
[18] Takata, N., 2015, "Crystallography of Fe2Al5 phase at the interface between solid Fe and liquid Al," Intermetallics, 67, pp. 1-11.
[19] Fragner, W., Zberg, B., Sonnleitner, R., Uggowitzer, P. J., and Loftier, J. F., 2006, "Interface reactions of al and binary Al-alloys on mild steel substrates in controlled atmosphere," Materials Science Forum, 519-521, pp. 1157-1162.
[20] Kumar, G., and Prabhu, K. N., 2007, "Review of non-reactive and reactive wetting of liquids on surfaces," Advances in colloid and interface science, 133(2), pp. 61-89.
[21] Ellmer, K., and Klein, A., 2008, "ZnO and Its Applications," Transparent Conductive Zinc Oxide: Basics and Applications in Thin Film Solar Cells, K. Ellmer, A. Klein, and B. Rech, eds., Springer Berlin Heidelberg, Berlin, Heidelberg, pp. 1-33.
[22] Schneider, S. J., and McDaniel, C. L., 1967, "Effect of environment upon the melting point of Al2O3," J. Res. Natl. Bur. Stand., Sect. A, 71, p. 317.
[23] Bainbridge, I. F., and Taylor, J. A., 2013, "The surface tension of pure aluminum and aluminum alloys," Metallurgical and Materials Transactions A, 44(8), pp. 3901-3909.
[24] Xiong, H.-P., Mao, W., Ma, W.-L., Xie, Y.-H., Chen, Y.-F., Yuan, H., and Li, X.-H., 2006, "Liquid-phase aluminizing and siliconizing at the surface of a Ti60 alloy and improvement in oxidation resistance," Materials Science and Engineering: A, 433(1), pp. 108-113.

[25] Cammarota, G. P., Casagrande, A., and Sambogna, G., 2006, "Effect of Ni, Si and Cr in the structural formation of diffusion aluminide coatings on commercial-purity titanium," Surface and Coatings Technology, 201(1), pp. 230-242.
[26] Harach, D. J., and Vecchio, K. S., 2001, "Microstructure evolution in metal-intermetallic laminate (MIL) composites synthesized by reactive foil sintering in air," Metallurgical and Materials Transactions A, 32(6), pp. 1493-1505.
[27] Yi, H. C., Petric, A., and Moore, J. J., 1992, "Effect of heating rate on the combustion synthesis of Ti-Al intermetallic compounds," Journal of materials science, 27(24), pp. 6797-6806.
[28] Mackowiak, J., and Shreir, L. L., 1959, "The nature and growth of interaction layers formed during the reaction between solid titanium and liquid aluminium," Journal of the Less Common Metals, 1(6), pp. 456-466.
[29] Brandes, E. A., and Brook, G. B., 1992, Smithells Metals Reference Book, Butterworth-Heinemann.

# Appendix F

## From Theory to Practice: Specimens for Mechanical Testing

### A Practical Guide to Multi-Material Metal Casting of Aluminum and Steel

## Introduction

The theoretical aspects of multi-material metal casting are quite well known with to the assumption that hot-dipping experiments of steels into liquid aluminum equates the casting procedure. While this is true for many aspects in terms of liquid-solid interaction between aluminum and the steel. Hot-dipping experiments show good correlation with several aspects of the casting procedure such as poor wetting, the formation and growth of the metallurgical bond. In other cases such as heat treatment of components there seems to be a distinct difference between a dipped structure and a casting, see Appendix D and [1]. However, there is limited information on the potential defects that can occur as a result of different casting process parameters.

As part of the "Multi-Material Metal Casting" project for the Advanced Casting Research Center (ACRC) new testing methods for the metallurgical bond strength were investigated. Since accurate strength measurements are needed to be able to model the stress distribution in bimetallic components upon loading. If cast-in inserts are bonded to the casting by both a mechanical and metallurgical bond the resulting strength will be a combination between the two. It can therefore be complicated to determine how much of the strength that is contributed by the metallurgical bond and what part is due to the mechanical bond.

A common test method for bond shear strength of bimetallic samples is the push-out method. A round steel rod is cast-in and then pushed out. In literature, the shear strength measurements show results ranging from 13 – 114 MPa, see Table 1. The data available shows that there is a wide spread in the reported numbers. Looking within the experiments of the individual authors there is a strong correlation between the insert roughness and high strength, with and without a metallurgical bond present. Using this method makes it difficult to measure the strength of the metallurgical bond by itself and therefore new testing methods for the metallurgical bond were investigated.

*Table 1*

| Authors | Test type | Alloys | Insert | Manufac. Conditions | Layer thickness | Strength (MPa) |
|---|---|---|---|---|---|---|
| Durrant et al 1996[2] | Push-out | Al-7Si | Steel | Preheat 300 °C | - | 30.5 |
| | | | | Preheat 900 °C | - | 44.5 |
| | | | | Al-coat, preheat 300 °C | ~50-80 µm | 114 |
| | | | | Al-coat, preheat 900 °C | ~50-80 µm | 112 |
| | | | | Ti-coat, smooth, preheat 300 °C | - | 5 |
| | | | | Ti-coat, rough, preheat 300 °C | - | 150 |
| | | | | Ti-coat, smooth, preheat 900 °C | - | 34 |
| | | | | Ti-coat, rough, preheat 900 °C | - | 126 |
| Pan et al 2000[3] | Push-out | A356 | Steel | Ultrasound vibration | 5~8 µm | 60 |
| Han et al 2003[4] | Push-out | A354 | Steel | Ni/Cu coating, preheat 120 °C | ~10 µm | 65 |
| Dezellus et al 2007[5] | Push-out | A413 | Steel | Al-coat, preheat 735 °C | 12~14 µm | 92 |
| Li et al 2012 [6] | Push-out | Al-2Si | Aust-Cast-iron | Al-coat, preaheat 700 °C | - | 3.6 |
| | | Al-6Si | Aust-Cast-iron | Al-coat, preaheat 700 °C | - | 8.8 |
| | | Al-11Si | Aust-Cast-iron | Al-coat, preaheat 700 °C | ~20 µm | 13.6 |
| | | Al-16Si | Aust-Cast-iron | Al-coat, preaheat 700 °C | - | 4.8 |
| Aguado et al 2013[7] | Push-out | AlSi7Mg0.6 | Steel | Degrease | - | 13 |
| | | AlSi7Mg0.6 | Steel | Pickling | - | 12 |
| | | AlSi7Mg0.6 | Steel | Pickling, preheat 100 °C | - | 14 |
| | | AlSi7Mg0.6 | Steel | Pickling, preheat 300 °C | - | 12 |
| | | AlSi7Mg0.6 | Steel | Shot blast | - | 31 |
| | | AlSi7Mg0.6 | Steel | Pickling, Al-coat | * | 2 |
| | | AlSi7Mg0.6 | Steel | Zinc coat (hot dipped) | * | 14 |
| | | AlSi7Mg0.6 | Steel | Zinc coat (plated) | * | 14 |
| | | AlSi7Mg0.6 | Steel | Cu/Ni coating | * | 19 |
| | | AlSi7Mg0.6 | Steel | Shot blast, Al-coating | * | 22 |
| | | AlSi7Mg0.6 | Steel | Shot blast, Cu/Ni coating | * | 27 |
| Salimi et al 2017[8] | Push-out | 1035 | Steel (Mo40) | Al-coating | ~21 µm | 23 |
| | Push-out | 1035 | Steel (Mo40) | Cu-coating | ~39 µm | 31 |

## Objective

The purpose of this guide is to give general design and processing guidelines to successful metallurgically bond ferrous inserts to aluminum during multi-material metal casting. Two components, for testing shear and tensile strength of the metallurgical bond as part of the project "Multi-Material Metal Casting" for the Advanced Casting Research Center (ACRC) will be used as an example.

It will give suggestions on the following steps for making a successful casting:

- Component design
- Materials selection
- Mold and tooling design
- Insert design
- Casting procedure

## Component design

Investigating the strength of the metallurgical bond requires that it is separated from the influence of a mechanical bond that forms due to internal residual stresses. Trials with a simple geometry for tensile test specimen, see Figure 1a, showed a lot of scatter in the data from samples collected from the same casting, see Figure 1b.

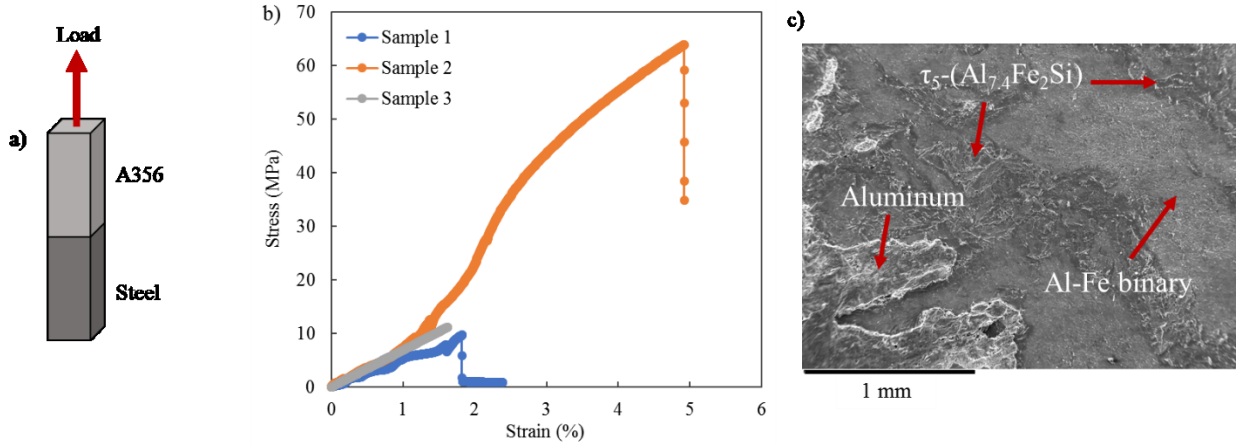


*Figure 1: a) Test specimen of simple geometry. b) Stress vs strain curve for 3 samples taken from the same casting.*

The large scatter in the data is likely due to the difficulty in aligning the sample so that the stresses are perpendicular to the bond. If the sample is slightly of center then stress will be concentrated in one of the corners of the sample and the effect of small edge defects are exagerated. This in combination with the fact that the brittle layer has little resistance to the crack propagation. Figure 1c shows the fracture surface of the which indicates that the fracture occurs between the binary and the ternary layer as well as through the ternary $\tau_5$-($Al_{7.4}Fe_2Si$) layer. The sharp edges of the the $\tau_5$-($Al_{7.4}Fe_2Si$) phase has a cleavage plane that it preferetially fails at.

Instead of following an ASTM standard a military specification (MIL-J-24445A) was suggested to ease alignment during testing. The tensile test specimen and testing procedure can be seen in Figure 2. To quantify the shear strength a shear lug test will be performed the specimen and the setup can be seen in Figure 3.

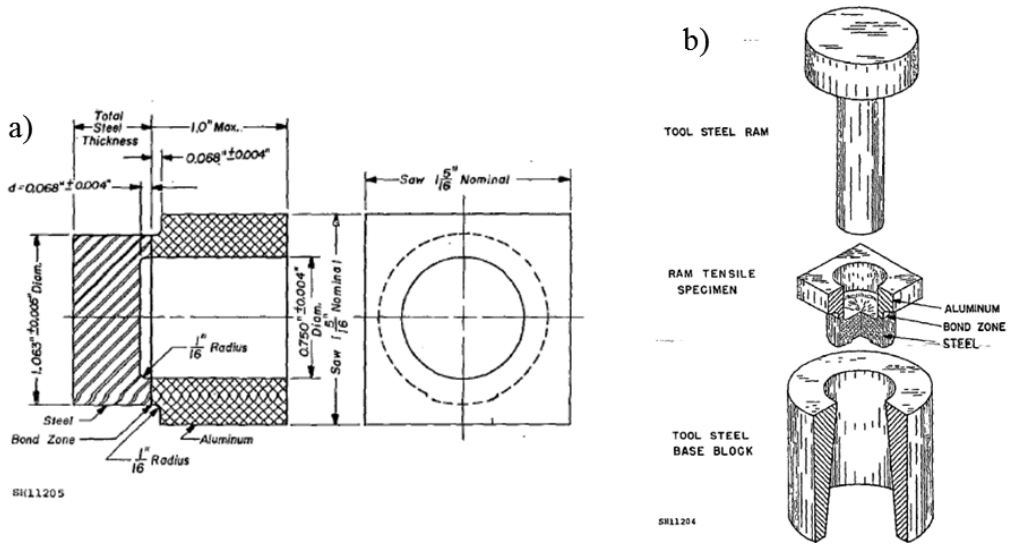


*Figure 2: a) Specification for the tensile strength specimen. b) Method for testing the tensile strength of the metallurgical bond.*

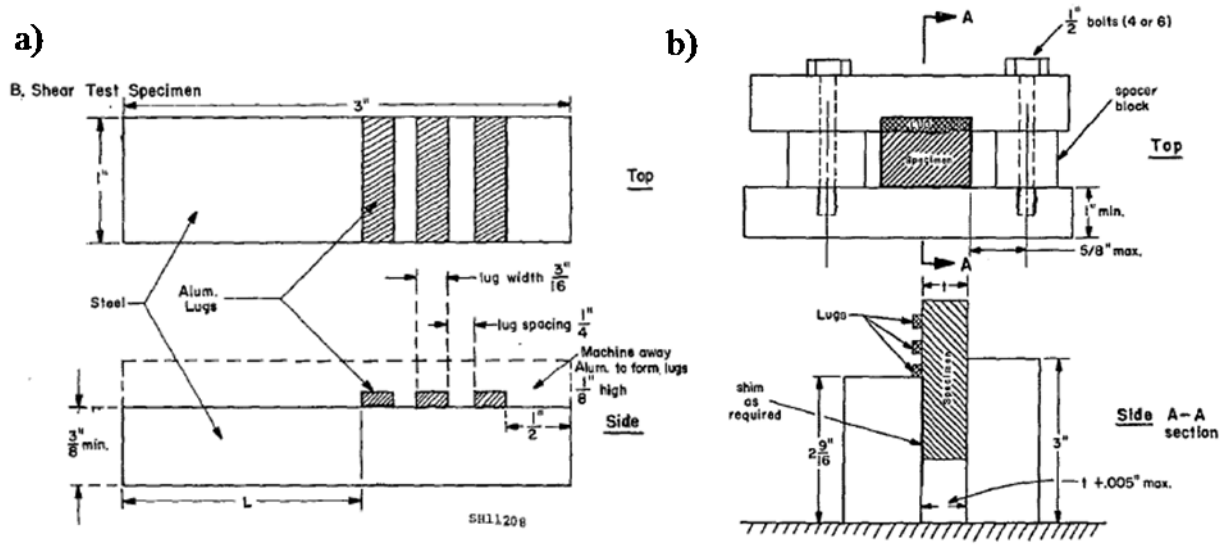


*Figure 3: a) Shear test specimen for the triple lug shear test. b) Test setup for the shear strength tests.*

**Casting Design**

*Cast-in the Insert*

Initial trials at the ACRC showed that it is very difficult to make the samples without the cast-in approach. If the melt is cast over steel then due to insufficient wetting of liquid on the mold wall a sharp angle tends to form at the aluminum/steel interface, see Figure 4a. Figure 4b shows cracks that formed during a sessile drop wetting experiment. The sharp angle acts as a stress raiser and the bond tends to crack along the brittle interface during solidification due to shrinkage of the liquid aluminum.

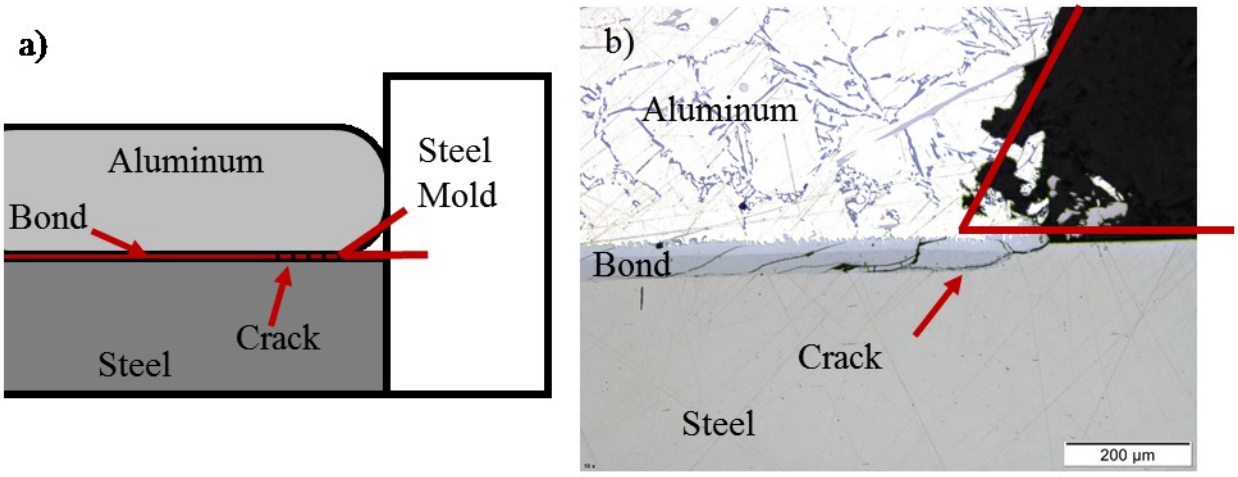


*Figure 4: Sketch of sharp angle created due to insufficient wetting.*

Two different castings were designed with geometries that would make them suitable for machining, allow for shrinkage around the insert, see Figure 5. They provide a small insert to cavity ratio providing time for solidification and a relatively long fill time which allows for a lot

of flow around the insert. The molds, see Figure 6 were designed to have a very even flow during filling. The importance of shape and flow will be discussed in the next section.

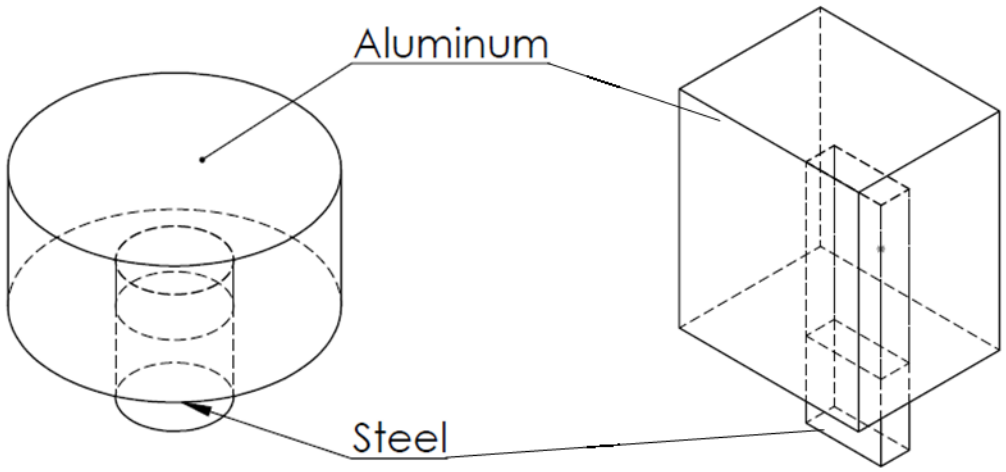


*Figure 5: Dissimilar metal castings that are to be machined to the mechanical testing specimens. Left is the casting for the tensile strength and right for the shear strength.*

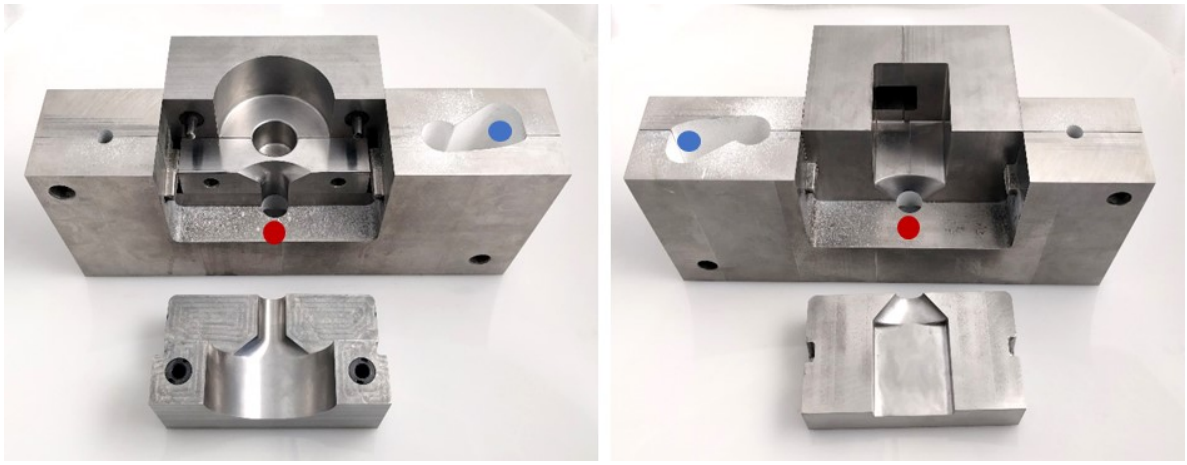

*Figure 6: Molds to make the castings for the mechanical properties. Left is the casting for the tensile strength and right for the shear strength.*

**Mold Design**

The diffusional nature of the metallurgical bond requires both time and temperature to form and grow. It is also very likely that there is going to be a need to do some form of interfacial engineering on the insert to speed up the bond formation. These requirements influence many aspects of the design process of a mold that is designed to make bimetallic castings and a few considerations is worth discussing.

*1. Melt flow*

Melt flow around the insert will determine the supply of hot liquid metal without impurities. The formation and growth of the bond relies on both the temperature of the melt as well as the

diffusional transport of iron. High flow will assist in removing impurities from the surface and provide fresh aluminum which speeds up the bond development. However, dissolution of iron also means that too much flow will reduce the size of the insert. Iron only provides strength within the steel and reduces strength for aluminum, see the effect of dissolution in Appendix C.

If a coating is utilized to initiate the bond formation the flow around the insert is necessary to transfer the residues of the coating away from the bond area. While metallic coatings are dissolved in liquid aluminum other methods for improving wettability like a flux (will be discussed in more detail below) needs to be transported away and out of the casting, see Appendix E.

*2. Heat transfer*

The volume ratio between the insert and the casting cavity is also important to consider. Especially if the insert will be of a different temperature compared to the aluminum alloy since this will establish the amount of heat and time the solid surface will be in contact with the liquid aluminum.

There can only be *one* solidification front operating during solidification. If the solidification starts at both the insert and the mold wall the shrinkage will not center around the insert. This will cause residual stresses away from the insert, see red arrows on the right side of Figure 7a. Depending on the direction of the solidification front (from the insert out to the mold or from the mold to the insert there will be more or less residual stresses holding the insert in place. For maximum mechanical bonding the solidification front should start at the insert interface as in the left side of Figure 7a. Figure 7 b and c shows worst case scenario when two solidification fronts are operating which causes no mechanical bond which in turn prevents any metallurgical bond.

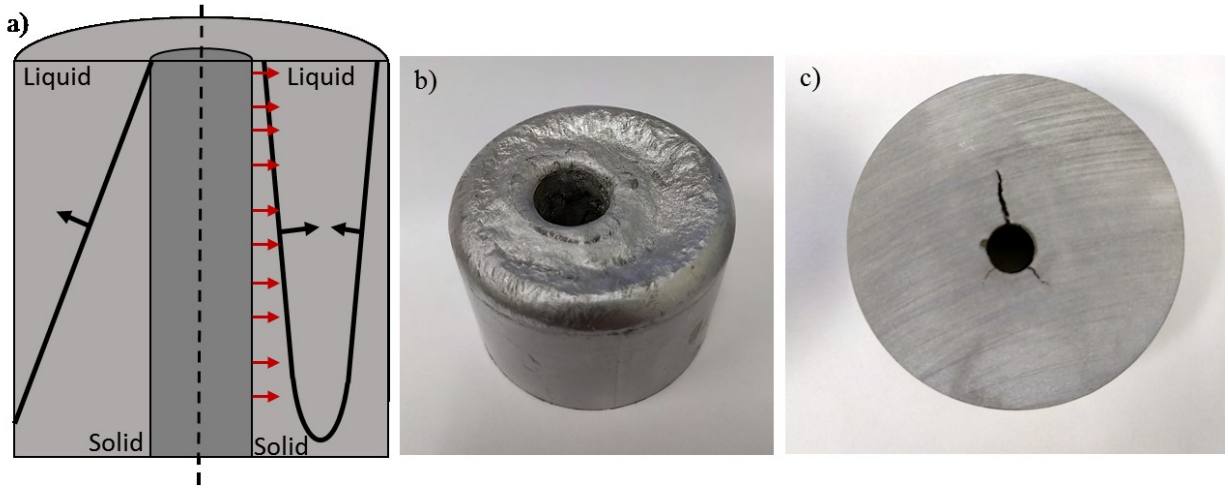


*Figure 7: a) Sketch of the solidification fronts (black arrows) in a bimetallic casting. The red arrows represent stress that is induced to the shrinkage during solidification. b) Casting in which there were two operating solidification fronts which can be seen at the top resulting in no mechanical or metallurgical bond. c) Cracks which are likely due to the induced stresses due to residual stress as a result of multiple moving solidification fronts.*

**Design of Insert**

The design of the insert needs of course to be optimized for the final applications but there are a few things that needs to be considered for the casting part. The shape and size of the insert needs to be well thought through if the casting is going to be heat treated. Difference in thermal expansion and the low strength of aluminum at elevated temperatures can cause cracking and distortion. The system appears to be size dependent which could change the diffusional behavior during solid state diffusion, see [1] and Appendix D. The sharp edges and corners needs to be made with a curvature to minimize any risk of cracking, see Figure 8 and 9. The shape also has to be optimized to allow for proper filling of the mold so that contact between the molten aluminum and insert is secure, see Figure 9 and 10.

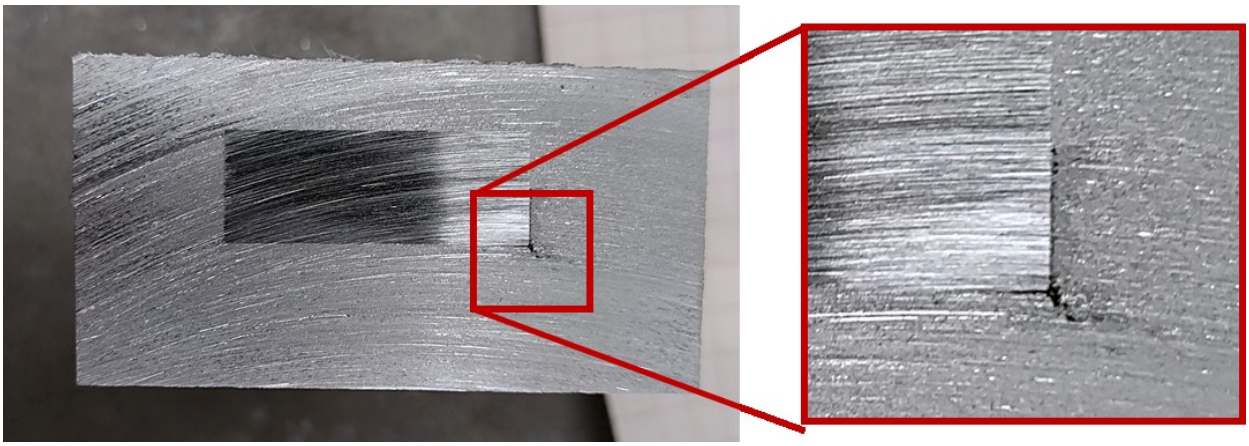

*Figure 8: Crack formed at the corner of the insert.*

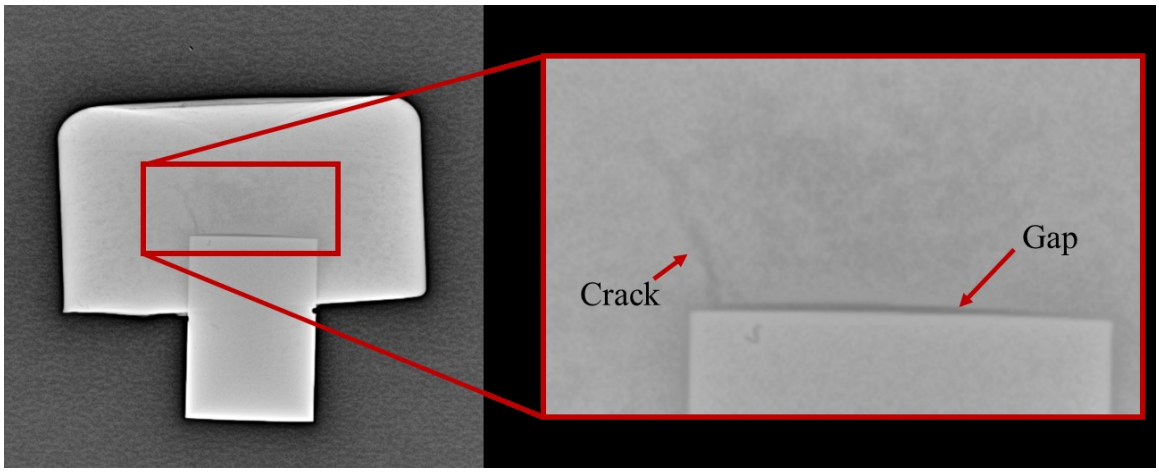


*Figure 9: X-ray image of the tensile specimen were a crack formed at the edge of the round insert and a gap which could be due to improper filling.*

*Figure 10: Incomplete filling due to the insert is blocking the flow of the molten aluminum.*

**Materials Selection**

While this is not applicable to the Multi-Material Metal Casting project since it had predefined aluminum alloys of interest there are still some considerations that are of importance. Mild steel (1015) rods with the diameter of 0.125'' were cast into the tensile bars in the ASTMB108 mold as depicted in Figure 11, centering proved very difficult so many were of centered but were tested for mechanical properties. The resulting stress vs. strain curve can be seen in Figure 12. While the stiffness and yield strength showed a marginal improvement the UTS showed very little improvement from which a couple of conclusions can be made regarding the materials selection.

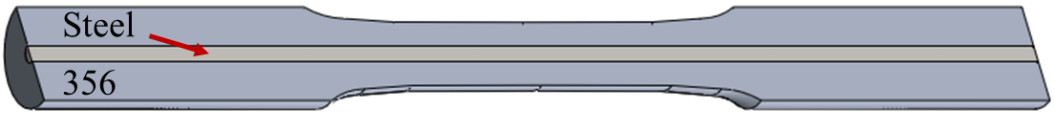


*Figure 11: Ideal specimen geometry but centering was difficult so most steel rods were slightly off-center.*

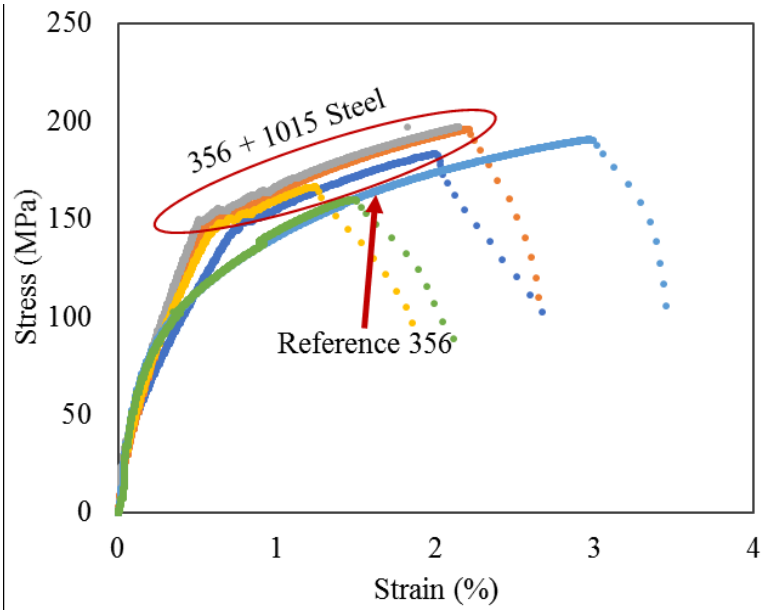


*Figure 12: Ideal specimen geometry but centering was difficult so most steel rods were slightly off-center.*

*Aluminum alloy*

1. *Ductility equal to insert* – Ductility of the aluminum alloy needs to higher or equal to the insert. Otherwise cracks can initiate and failure occur before the steels strength has been utilized.

2. *Minimize heat treatment* requirements – Avoid alloys that requires T6 heat treatments due to the crack formation within the bond during quenching. If a solutionizing step is required, it needs to be minimized since it activates diffusion along the bond interface and voids are created, see Appendix D.

3. *Composition changes thermal stability* – Composition matters. Both during the liquid-solid interaction and the solid-solid interaction which influences growth rates of the metallurgical bond. Silicon has a good tendency to reduce the overall thickness of the bond and showed very little change during thermal holding at 180°C, see Appendix D.

*Insert Alloy*

1. *Stiffness and Strength greater than aluminum alloy* – Since the steel will experience elevated temperatures during the processing it is important to pick an alloy that is not dependent on cold-working or other heat treatments to achieve good properties. More obviously, a ferrous alloy that has a much greater strength and stiffness compared to the aluminum casting is desired and considering the low ductility of many aluminum casting alloys there is a lot of choice.

2. *Composition changes growth* – The composition of the ferrous alloy can be selected to reduce growth of the intermetallic layer formed. This is however also going to affect the ability of the system to form a metallurgical bond, see Appendix A and Figure 13. Figure 13 shows the difference in the amount of metallurgical bond formation of a nitride steel dipped in aluminum and is from Masters' Thesis by Chiara Bertuccioli. A protective white layer completely prevents a reaction while the diffusional layer inhibits growth compared to the reference material.

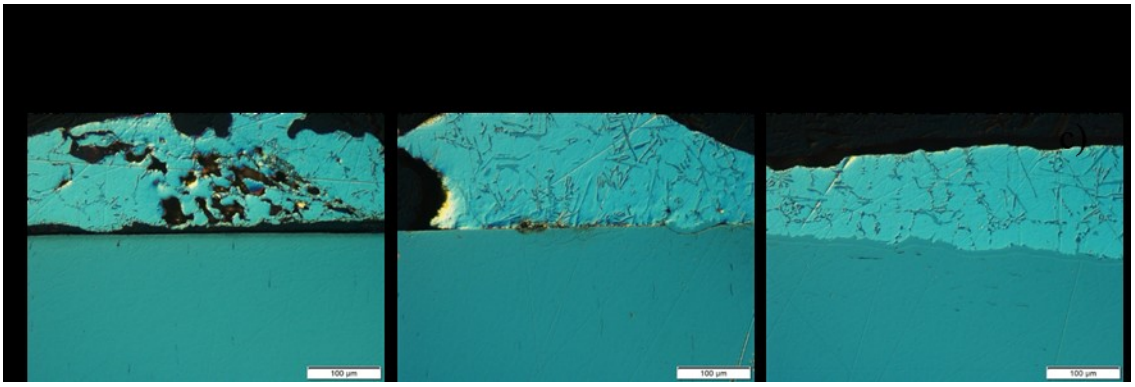

Figure 13: Different parts of a nitride steel hot-dipped in liquid A356 for 1 minute at 700°C. a) White a white layer. b) No white layer but a diffusional zone of N. c) Reference material without white layer.

**Coatings**

To initiate a metallurgical bond, it is recommended to use a coating. A coating will improve the wetting of the liquid aluminum and at the same time keeping the interface clean providing an

opportunity for a defect free bond. The type of coating will depend on the casting process and the restriction of only allowing one moving solidification front. Two examples will be discussed, a sand casting and a permanent mold casting.

Sand casting – The low heat transfer to the sand casting mold provides the possibility to start the solidification front at the insert interface essentially utilizing it as a chill. This requires a relatively cold insert and thus the low-melting point coatings discussed in Appendix E can be utilized. Initiation of the solidification at the insert should maximize the mechanical bond.

Permanent mold – It could be very difficult to initiate the bond at the insert interface due to the high heat transfer into the steel mold but if the insert is preheated to a high temperature dual solidification fronts can be avoided. However, the low-melting point coatings will not be able to withstand the elevated temperatures needed for preheating.

**Machining**

The final step before testing the mechanical properties of the metallurgical bond is to machine the samples out of the castings. Transforming them from what is seen in Figure 5 to the dimensions in Figure 2a and 3a. Due to excessive forces and impacts it proved extremely difficult to machine out the specimen from the casting using traditional machining. Out of 5 shear samples only one lug stuck to the steel, see Figure 13, the red arrows indicate the lug that remained attached to the steel.

The fracture surfaces were examined, see Figure 14, and the fracture appears to proceed through between the binary Al-Fe phase layer and the $\tau_5$-($Al_{7.4}Fe_2Si$) phase. The flat surfaces present at the break indicates that there are certain cleavage planes that facilitates the failure through this phase.

Figure 13: Machined shear samples with the red arrow indicating the only lug that stuck to the steel after machining operation finished.

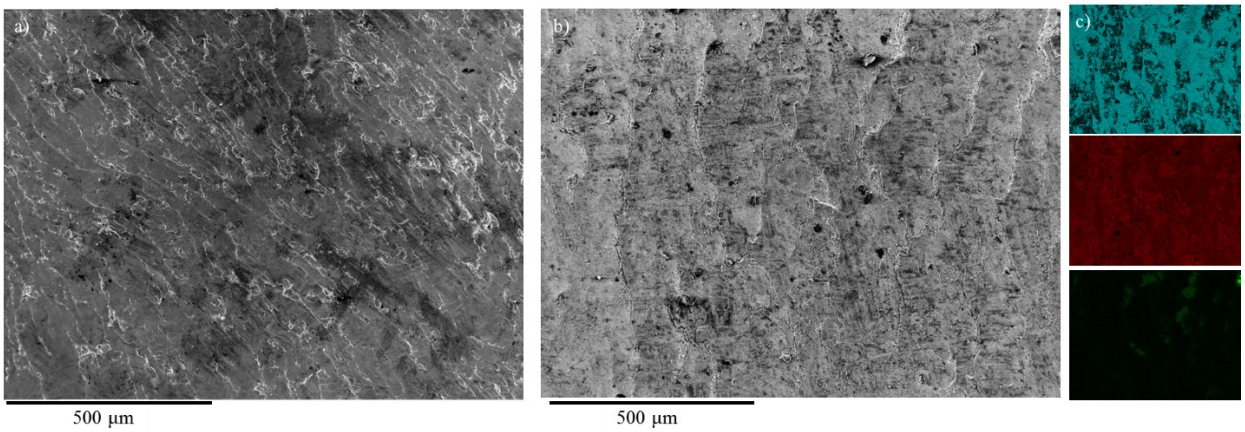


Figure 14: SEM micrograph of the fracture surface on a) aluminum side, b) steel side and c) with the corresponding EDS maps for the steel side.

**Conclusion**

While some of the presented discussion above is more practical and in a way common sense there are certain conclusions that can be drawn. For example, the bond between the ferrous alloy and aluminum will be dependent on the casting process and how it is solidified. The solidification will determine the internal residual stresses around the insert which seems to be affecting not only the mechanical bond but can also alter the diffusional behavior during heat treatment. As a result of this the available data from literature can be difficult to trust since it is hard to estimate the specific conditions for each data point in literature.

For inserts that requires a high preheating temperature a liquid flux coating would be suggested. By preheating the insert in a liquid flux bath and the quickly placing it in the mold an oxide free preheated steel insert can be cast-in. For a high integrity casting this need to be combined with properly designed mold to transport away flux residues from the casting out to a riser or a part that is going to be machine away.

In conclusion, the following guidelines for successful metallurgical bonding during multi-material metal casting with aluminum and ferrous inserts are proposed:

1. Component and Casting Design – The metallurgical bond should in the extent possible be cast-in so it is surrounded by aluminum to prevent failure along the brittle intermetallic layer.
2. Mold Design –
    - Melt flow – Generally a higher flow rate is better around the insert to promote bond formation and to remove any eventual coating residues.
    - Heat transfer – The volume ratio of insert to mold cavity will determine the amount of heat available for bond formation and thus should rather be lower than higher. There can be only one solidification front to avoid formation of counterproductive residual stresses.
3. Insert Design – Large complex insert could be difficult to predict the behavior during heat treatment in manners of both diffusion within the metallurgical bond and distortions due to difference in thermal expansion. The edges of the insert need to have a curvature to prevent crack initiation and propagation.
4. Materials Selection –

- Aluminum alloy – Should be selected to have a higher ductility than the ferrous alloy and should preferably not require extensive heat treatments. Composition of the aluminum alloy can change the thermal stability of the bond.
- Ferrous alloy – Should have greater stiffness and strength than aluminum to maximize the benefits of the bimetallic component. The composition of the ferrous alloy can change the growth of the metallurgical bond.

5. Coatings – The coating is necessary to form a defect free continuous metallurgical bond and needs to be selected based on the casting process.
6. Machining – The metallurgical bond is brittle and it is not recommended to machine the components in a manner where it is completely exposed.

**References**

[1] Zhe, M., 2011, "Chemical Changes at the Interface Between Low Carbon Steel and an Al-Si Alloy During Solution Heat Treatment," Journal of phase equilibria and diffusion, 32(6), pp. 486-497.

[2] Durrant, G., 1996, "Squeeze cast aluminium reinforced with mild steel inserts," Journal of materials science, 31(3), pp. 589-602.

[3] Pan, J., Yoshida, M., Sasaki, G., and Fukunaga, H., 2000, "Metal pipe joining with aluminum alloy by ultrasonic insert casting," MATERIALS AND MANUFACTURING PROCESSES, 15(6), pp. 867-881.

[4] Han, Q., More, K. L., Myers, M. R., Warwick, M. J., and Chen, Y. C., 2003, "Reinforcement of Aluminum Castings with Dissimilar Metals," U.S. Department of Energy (DOE).

[5] Dezellus, O., Digonnet, B., Sacerdote-Peronnet, M., and Bosselet, F., 2007, "Mechanical testing of steel/aluminium–silicon interfaces by pushout," International journal of adhesion and adhesives, 27(5), pp. 417-421.

[6] Li, C. A., 2012, "Effect of Si content in hot dipping aluminium bath on Al–Fe bonding layer of aluminium piston with reinforced cast iron ring," Materials science and technology, 28(8), pp. 953-958.

[7] Aguado, E., 2013, "Comparative Study of Different Interfaces of Steel Inserts in Aluminium Castings," Materials Science Forum, 765, pp. 711-715.

[8] Salimi, M., Malekan, M., Nami, B., and Hoseiny, H., 2017, "Microstructure characteristics and mechanical properties of the interface layer of coated steel insert-aluminum bimetals," Journal of Materials Research, 32(4), pp. 874-882.